

2014•2015
FACULTEIT INDUSTRIËLE INGENIEURSWETENSCHAPPEN
master in de industriële wetenschappen: elektromechanica

Masterproef

Selective Laser Melting for production of injection moulds

Promotor :
Prof. dr. ir. Albert VAN BAEL

Promotor :
BSc(Hons) PgCert FHE DAN GARNER

Copromotor :
Prof. dr. ir. FREDERIK DESPLENTERE

Gezamenlijke opleiding Universiteit Hasselt en KU Leuven

Christiaan Vanbergen

Scriptie ingediend tot het behalen van de graad van master in de industriële wetenschappen: elektromechanica

2014•2015

Faculteit Industriële

ingenieurswetenschappen

master in de industriële wetenschappen: elektromechanica

Masterproef

Selective Laser Melting for production of injection
moulds

Promotor :
Prof. dr. ir. Albert VAN BAEL

Promotor :
BSc(Hons) PgCert FHE DAN GARNER

Copromotor :
Prof. dr. ir. FREDERIK DESPLETERE

Christiaan Vanbergen

*Scriptie ingediend tot het behalen van de graad van master in de industriële
wetenschappen: elektromechanica*

Preface

This master thesis is the result of a full year of hard work, of which 4 months were spent on Erasmus internship in England at the University of Derby. The first steps in a real engineering project were not always easy and being in another country enhanced the challenge, but through persistence and good guidance, I managed to deliver this thesis of which I am proud.

I could never have made this thesis without the help of my promotors. Foremost I would like to thank Prof. dr. ir. Albert Van Bael, Director of the polymer research group *Cel Kunststoffen* on the Technology Campus Diepenbeek of KU Leuven in Belgium and Prof. Richard Hall, University Director of Research, Innovation and Impact at the university of Derby in England, for giving me the opportunity to go on an Erasmus internship and allowing me to perform experiments with their equipment.

I would also like to thank ing. Raf Appermont for assisting me through the whole process concerning injection moulding, M.Eng. Michal Mis for his support in matters of additive manufacturing with the selective laser melting process and BSc(Hons) PgCert FHE Daniel Garner for his supervision of my project. I thank Koen Libens for his support in material tests and analysis. They were very involved in my project and were an invaluable source of guidance and information.

I would also like to thank assistant Prof. dr. ir. Frederik Desplentere and ing. Wim Six from Propolis for their support in matters of simulations.

Mrs. Ing. Mertens, PhD student at KU Leuven supported me with her expertise in Selective Laser Melting.

Furthermore I would like to thank my parents for their continued support, my flatmates and the member of the World Wide Derby Society for an amazing experience in England.

Table of contents

List of Tables.....	5
List of Figures.....	7
List of Graphs.....	9
Glossary.....	11
Abstract.....	13
Abstract in het Nederlands.....	15
1 Introduction.....	17
2 Literature study.....	19
2.1 Injection moulding.....	19
2.2 Conventional cooling.....	21
2.3 Conformal cooling.....	23
2.3.1 Properties.....	23
2.3.2 Design.....	26
2.4 Selective laser melting.....	28
2.4.1 Process properties.....	30
2.4.2 Limitation.....	34
2.4.3 Influence of process parameters on material properties.....	38
3 SLM Experiment setup.....	49
3.1 Goal.....	49
3.2 Product design.....	50
3.3 Setup.....	52
3.4 SLM Parameters.....	55
3.4.1 Constant parameters.....	55

3.4.2	Variable parameters	57
3.5	Test design.....	60
4	Experiment execution	63
4.1	Execution	63
4.2	Visual inspection	66
4.2.1	Analysis	66
4.2.2	Summary.....	73
4.3	Density	74
4.3.1	Method.....	74
4.3.2	Results and discussion	77
4.3.3	Conclusion	87
4.4	Strength.....	88
4.4.1	Method.....	88
4.4.2	Results and discussion.....	91
4.4.3	Conclusion	99
4.5	Overall Discussion.....	100
4.6	Conclusion	104
5	Mould design	105
5.1	Product design.....	105
5.2	Printed mould design.....	111
5.3	Milling.....	113
5.4	Mould assembly design	115
6	Conclusion.....	119
	List of used sources	121
	Appendix.....	125

List of Tables

Table 1 : Advantages and disadvantages of conformal cooling.....	23
Table 2 : Characteristics of tool steels and stainless steel currently offered by Layerwise	33
Table 3 : Effects of heat treatment at different temperatures on the hardness and yield strength and ultimate tensile strength seen by K. Saedi [30].	47
Table 4 : The shapes and the sizes of the important features in the experimental design	51
Table 5 : Technical specification Renishaw AM250	52
Table 6 : Properties of 316L stainless steel produced with SLM from Layerwise.....	54
Table 7 : Composition of 316L stainless steel powder by LWP technologies [32].....	54
Table 8 : Overview constant SLM parameters	55
Table 9 : Standard Renishaw parameters for checkerboard and 50 ×m layer thickness.....	57
Table 10 : Top Left: the parameters for laser power and scan spacing used in this experiment. Top Right: the parameters used by A. Cherry in her experiment, each table contains the energy density belonging to each parameter set. Down middle: the setting of the other parameters for this experiment and for the experiment by A. Cherry	58
Table 11 : The coding corresponding to each parameter set.....	61
Table 12 : Important parameters over different layers	63
Table 13 : Scan spacing compared to print time of 1 layer of 1 test piece	65
Table 14 : Table with results from the Archimedes test	77
Table 15 : Table with the results for T6 and T10.....	83
Table 16 : 2D Graph of the code, parameters (power, scan spacing and energy density in J/mm ³) for each piece in their respective position	85
Table 17 : 2D graph with the density of every piece in their respective position.....	86
Table 18 : The settings used in the tensile tests and their explanation	89
Table 19: Compiled results of the tensile test.....	91
Table 20 : The values to compare T5 and T6.....	102
Table 21 : Parameters used in the literature and my experiment	103
Table 22 : The changes made in the model for simulations.....	106
Table 23 : Forces on the simulation model	107

List of Figures

Figure 1: Cross section of the screw injection moulding process	19
Figure 2 : Schematic overview of mould build up [2]	20
Figure 3 : Conventional straight drilled cooling channels versus conformal cooling channels.....	21
Figure 4: Example of a baffle in the core of a mould [6]	22
Figure 5 : Test product and Cooling channels in the research by E. Sachs [4], Top: moulded product, Middle: conventional cooling channels, Bottom: conformal cooling channels, Right: moulded product	24
Figure 6: Channels simulated in [9]	25
Figure 7 : Design rules for conformal cooling by EOS [10], Image edited by L. Frick [5]	26
Figure 8 : Left : Example of a spiral made over a straight trajectory with a sweep, Right ; example of the possibilities with a swept blend in PTC Creo Parametrics	26
Figure 9 : Different shapes of cooling channels possible with conformal cooling channels.....	27
Figure 10 : Visualization of the principle of an SLM-machine [11]	28
Figure 11 : Schematic representation of a single track being produced by the SLM process, in the top left corner a section of a good single track is seen [13].....	30
Figure 12 : front view of a sectioned laser track, figure by V. E. Beal [19] (P. 5)	31
Figure 13 : An example of bad porosity due to low energy density. Left is shown the porosity seen from the side and right is the porosity seen from te top. [16]	32
Figure 14: Left: Representation of curling [21], Right: Cracking due to residual stress in M2 Tool steel [22]	34
Figure 15 : Cause of balling in the SLM process image from [13].....	35
Figure 16 : An extreme case of balling seen in [13].	35
Figure 17 : Stair effect in sloped surfaces. Taken from a presentation by Layerwise	36
Figure 18 : A 5 mm long horizontal overhang made in 316L with SLM [18]	36
Figure 19 : Left: Sagging of the ceiling of holes with a diameter of 1 mm, 3 mm and 7 mm, Right; Horizontal circular holes with diameters from 1 mm to 10 mm [21].....	37
Figure 20 : Sink mark caused by curling in a horizontal hole on the side of a part of 20x20x20 mm (part is placed on its side).....	37
Figure 21: Relative density for 361L using different inert gasses by B. Zhang [19].....	38
Figure 22 : Schematic representation of the effect of higher point distance on the roughness	41
Figure 23 : Scan strategies available in the Renishaw software	44
Figure 24 : Solution annealing (a) and stress relieve (b)	46
Figure 25 : The experimental design with indication of the position of the different shapes	51
Figure 26 : The design of the tensile test pieces used in this experiment.....	52
Figure 27: The Renishaw AM250 at the IISE in Derby	53
Figure 28 : An image from the Renishaw AutoFab software showing the different areas.....	56
Figure 29 : Representation of the theory behind lower scan spacing.....	58
Figure 30 : Experimental setup of print job.....	60
Figure 31 : The base plate after printing in the position it was printed	61
Figure 32 : Explanation of the tensile pieces coding	62
Figure 33 : Picture of the powder depleted zones at layer 9, the left piece is part number 4 and the right piece is part number 7	64

Figure 34 : Top: A protruding piece caused by a cut in the soft coater. Bottom: The consequence of the protruding piece a clear line across pieces 1, 2 and 3.....	66
Figure 35 : The baseplate after the finished print job	67
Figure 36 : Top view of a piece number 6.....	68
Figure 37 : Comparison of the 0,5 mm and 1 mm diameter vertical holes.....	69
Figure 38 : Example of the balling seen on the top surface, piece number 6 in this example	69
Figure 39 : Top comparison of the deformation around the horizontal circular tube of 9 mm diameters, below: side view of the deformation of piece number 5	70
Figure 40 : Comparison of the triangular tubes, the angle values at piece 1 show the value for the green marked corner	71
Figure 41 : Comparison of the square tubes.....	72
Figure 42 : Side holes of the upwards turn.....	72
Figure 43 : Example of the stalactites on the overhang of the tensile pieces	73
Figure 44 : Close up of the setup	74
Figure 45 : Tensile pieces in the ultrasonic bath,	75
Figure 46 : Corrosion of the tensile piece after minutes in deionized water	75
Figure 47 : Top view of the finished print job.....	84
Figure 48 : Left: Tensile test bench Zwick Z050, Right: Example of how a horizontal piece is clamped in the machine.....	88
Figure 49 : Removal of the support structure, top: before removal of support structure, bottom: after removal of support structure.....	89
Figure 50 : Stress-strain curves until 300 N/mm ² of 3 successive tests on piece T3.1.....	90
Figure 51 : Break lines of the pieces of parameter set T1, T3 and T7.....	92
Figure 52 : The final product with some of its dimension in mm	105
Figure 53 : The simulation setup: left : the mechanical forces and fixtures, right : the thermal forces and fixtures	107
Figure 54 : Simulation results of the cup holder	108
Figure 55 : Ergonomic test of the first product; left: side view with empty cup, middle: top view with empty cup, right: side view with full cup	110
Figure 56 : Left: Results of the gate location analysis, Right: Filling times with the gate in the middle of the best gate location	111
Figure 57 : Left: the cavity insert on the smaller base plate. Right: the core on the smaller base plate	112
Figure 58 : Parting line of window feature	113
Figure 59 : The mould assembly for the cavity part (Stationary).....	115
Figure 60 : Placement of ejectors in the core of the mould.....	116
Figure 61 : The section of the assembled mould.....	117

List of Graphs

Graph 1 : The quality of a surface printed on loose powder at different laser powers (P_L) and different scan speeds (V) [14].	40
Graph 2 : Different quality zones for the 10x10 plates on loose powder dependent on the scan spacing (S_s) and the scan speed (V).	43
Graph 3 : Pieces in the horizontal direction and perpendicular to the spreader (T0.1): density vs scan spacing	78
Graph 4 : Pieces in a horizontal plane parallel to the spreader (T0.2): density vs scan spacing	79
Graph 5 : Pieces in vertical direction (T0.3): density vs scan spacing	79
Graph 6 : Pieces in the horizontal direction and perpendicular to the spreader (T0.1): density vs laser power	80
Graph 7 : Pieces in a horizontal plane parallel to the spreader (T0.2): density vs laser power	81
Graph 8 : Pieces in vertical direction (T0.3): density vs laser power	81
Graph 9 : Density vs Energy density per direction	82
Graph 10 : Graph of porosity (density) and energy density made by A. Cherry [17].	82
Graph 11 : Yield strength per print direction per tensile piece set	93
Graph 12 : Ultimate tensile strength per print direction per tensile piece set	93
Graph 13 : Elongation at Rm per print direction per tensile piece set	94
Graph 14 : Elongation at break per print direction per tensile piece set	95
Graph 15 : The post uniform elongation per print direction	95
Graph 16 : The yield strength, ultimate tensile strength, elongation at Rm and elongation at break versus the energy density for the horizontal pieces perpendicular to the spreader directions. (T0.1)	96
Graph 17 : The yield strength, ultimate tensile strength, elongation at Rm and elongation at break versus the energy density for the horizontal pieces parallel to the spreader directions. (T0.2)	96
Graph 18 : The yield strength, ultimate tensile strength, elongation at Rm and elongation at break versus the energy density for the vertical pieces (T0.3)	97
Graph 19 : Yield strength (R_p) and ultimate tensile strength (R_m) versus scan spacing for a laser power of 200 W	98
Graph 20 : The relative density, the yield strength (R_p) and the ultimate tensile strength versus the energy density for the horizontal pieces perpendicular to the spreader directions (T0.1)	100
Graph 21 : The relative density, the yield strength (R_p) and the ultimate tensile strength versus the energy density for the horizontal pieces parallel to the spreader directions (T0.2)	101
Graph 22 : The relative density, the yield strength (R_p) and the ultimate tensile strength versus the energy density for the vertical pieces (T0.3)	101
Graph 23 : Yield strength (R_p) and ultimate tensile strength (R_m) versus Density	102
Graph 24 : Top: relation between stresses caused by the water mass versus the wall thickness. Bottom: relation between the deformation in Y-direction caused by the water mass versus the wall thickness	109

Glossary

Laser spot is the light spot on the powder surface made by the laser containing 86 or 96% of the laser powder dependent on the machine type.

Scan speed is the speed at which the laser spot moves across the powder surface

Scan track is the track followed by the laser

Point distance is a parameter of a pulsed laser that describes the distance between each point divided across the scan track.

Single track test is a test where one track is printed either on loose powder or on one layer on a baseplate

Track width is the width of the melt pool in a single track test

Laser spot is the spot of energy on the powder surface made by the laser

Overlap is percentage of overlap between two laser spots with the same spot size with their centers one scan spacing removed from each other.

Parameter set refers to one complete set of parameters to run a printjob in this project nine different parameter sets were used.

Extensometer is a device mounted on a tensile bench to enable an accurate measurement of the elongation of the tensile test piece

Original gauge length (S_0) is the distance between the clamps of the extensometer at the beginning of a tensile test

Contact angle is the angle indicating the contact surface of the melt pool with the underlying substrate.

Substrate is the solid material upon which a melt pool is attached.

Balling describes the splitting of an unstable melt pool into balls

Mill bit is the drill shaped replaceable head doing the actual cutting in a milling machine

Injection moulding: This technique involves melting granules of a particular plastic to a viscous melt and proceeding to push it into a metal mould.

Selective laser melting (SLM): This technique utilises metal powders and a laser to enable the creation of more complex structures that cannot be made with conventional production methods.

Selective laser sintering (SLS): Powder is sintered together instead of fully melted.

Variotherm injection moulding: The dynamic temperature control of the mould, during each cycle.

Conformal cooling channels: Cooling channels designed to follow the cavity surface.

Quenching: Cooling down very fast from a high temperature.

Sensitisation: The forming of chrome carbides that deplete stainless steel of chrome, reducing its corrosion resistance.

Abstract

Cell Kunststoffen at KU Leuven is cooperating with the Institute for Innovation in Sustainable Engineering (IISE) at the University of Derby, England to study the production of injection moulds with conformal cooling channels by means of selective laser melting (SLM). Because drilled cooling channels often cool inefficiently, this master's thesis aims to investigate which opportunities the design freedom of the SLM process can provide to improve cooling.

With a Renishaw AM 250 3D-printer several test channels and geometries in stainless steel (316L) were printed, using different laser power, print direction and scan spacing. The results are examined on strength, density and geometrical quality. Secondly, a test product and an injection mould to be produced with SLM are designed by means of numerical simulations and 3D-printing of prototypes.

The research proves that the SLM 3D-printing technique provides the possibility to print different shapes of conformal cooling channels in high density materials. The research delivers an overview of the properties of stainless steel (316L) produced with SLM. It also distinguishes the relevant from the irrelevant parameters. The best parameters for the production of conformal cooling channels with SLM are defined.

A test product in the shape of a cup holder and its injection mould are designed. Further research can include complex conformal cooling channels within this mould to improve product quality and efficiency.

Abstract in het Nederlands

De Cel Kunststoffen aan de KU Leuven werk samen met het Institute for Innovation in Sustainable Engineering (IISE) aan de universiteit van Derby, Engeland om de productie van spuitgietmatrijzen met conformal koelkanalen door middel van selective laser melting (SLM) te bestuderen. Omdat geboorde koelkanalen vaak inefficiënt koelen, richt deze masters thesis zich op de opportuniteiten die de design vrijheid van het SLM proces biedt om de koeling te verbeteren.

Met een Renishaw AM 250 3D-printer worden verschillende proefkanalen en geometrieën in roestvrij staal (316L) geprint met variërende laserkracht, richting en scan afstand. De resultaten worden onderzocht op sterkte, dichtheid en geometrische kwaliteit. Een testproduct en een spuitgietmal voor productie met SLM worden ontworpen door middel van numerieke simulaties en het 3D-printen van prototypes.

Het onderzoek bewijst dat de SLM 3D-printtechniek de mogelijkheid biedt om verschillende vormen van conformal koelkanalen te printen in materialen met een hoge dichtheid. Dit levert een duidelijk beeld van de kenmerken van roestvrij staal geproduceerd met SLM, alsook de relevante en irrelevante parameters. Hieruit konden de beste parameters om conformal koelkanalen met SLM te produceren bepaald worden.

Een bekerhouder als testproduct en zijn spuitgietmatrijs werden ontwikkeld. In verder onderzoek kunnen hier complexe conformal koelkanalen in verwerkt worden om de productkwaliteit en efficiëntie te verbeteren.

1 Introduction

This master thesis was performed at the Cell Kunststoffen in cooperation with the Institute for Innovation in Sustainable Engineering (IISE) and supported by ProPoLiS.

The polymer research group *Cel Kunststoffen* on the Technology Campus Diepenbeek of KU Leuven, Belgium [1] works together with companies to develop special injection moulding techniques and thermoforming techniques. The Cell offers services to companies such as product and material tests and test setups for new production techniques. Earlier projects include a research into water injection during injection moulding, injection moulding of long fibres and intelligent thermoforming. They supported me in matters of mould and product design. Prof. dr. ir. Albert Van Bael and ing. Raf Appermont are part of this organisation and acted as my main supervisors.

The Institute for Innovation in Sustainable Engineering (IISE) [2] is a research group connected to the University of Derby in England. Just like the Cell Kunststoffen, their goal is to cooperate with companies to support the innovation of advanced production techniques. Apart from advanced production techniques their working field ranges from embedded systems to energy and environment. Their list of partners contains large companies like Rolls Royce, Toyota and Bombardier. They have helped me with everything concerning selective laser melting. The 3D-printing was done at their facility during my four months Erasmus internship at the University of Derby. My supervisors from this organisation are Prof. Richard Hall, BSc(Hons) PgCert FHE Daniel Garner and M.Eng. Michal Miss.

Propolis [2] is also a research group at Oostende in Belgium and is a part of the Catholic University of Leuven (KU Leuven). Their specialties lay in 4 areas: material characterization, polymer processing, numeric simulations and application testing. They have helped me in matters of numeric simulation of the injection moulding process but they also supported me in mould and product design. Prof. dr. ir. Frederik Desplentere and Mr. ing. Wim Six are my supervisors at ProPoLiS.

One of the most frequently-used production techniques for producing plastic parts is injection moulding. This technique involves injecting viscous plastic into a mould cavity, then cool it down, eject the part and start over again. This permits high-speed production of plastic parts with a great variety in shapes with good quality. Although this technique is already used for more than half a century, it is not yet fully optimised and there is constant research done for ways to improve quality, defect rates, cycle times and shape possibilities. A way to improve the process is to improve the temperature control of the surface of the cavity. Additive manufacturing of the mould can provide a real improvement in this area.

The additive manufacturing technique studied in this thesis is selective laser melting (SLM). This is a relatively new technique, currently it is primarily used in the production of prototypes, called Rapid Prototyping. This technique utilises metal powders and a laser to enable the creation of more complex structures that cannot be made with conventional production methods. This gives the opportunity to make complex cooling channels within a mould. The full melting of the powder with this technique causes the finished product to have an almost full density and thereby

all the properties of the base material. This fact makes it more interesting to create injection moulds than a similar process called selective laser sintering (SLS), here the powder is sintered together instead of fully melted. To obtain a full density an extra infiltration step is needed in which the pores between the sintered powders are filled with bronze resulting in a low surface hardness which is undesirable when making injection moulds.

The first problem is that conventional production methods, such as milling and drilling, cannot produce the optimal cooling channels in injection moulds. This is because holes can only be drilled straight, which means the shape of the cavity cannot be followed and the drilling forces make it necessary to position the channels further from the cavity. In many cases, this results in a non-uniform cooling of the plastic product which causes internal stresses that can lead to early failure of the product, longer cycle times, warpage of the product after ejection and other problems as well. This also causes problems when trying to use variotherm temperature control. In variotherm temperature control the cavity surface is heated before the injection of the plastic, this keeps the plastic fluid during the injection enabling more complex shapes and diminishing the effects of various defects like welding lines. To realize this, only the cavity surface needs to be heated to the desired temperature. The rest of the heated mass is lost energy, it even counteracts the cooling of the mould after injection because a larger mass needs to be cooled. The fact that drilled cooling channels are positioned so far from the cavity decreases the positive effects the variotherm temperature control can give.

A possible solution is the inclusion of conformal cooling channels through means of 3D-printing with SLM. The principle of this technique is to design the cooling channels so that they follow the cavity surface and lay as close to this surface as possible without compromising the integrity of the mould. This would mean the bulk of the product can be uniformly cooled or heated, enabling the full use of the positive effects that the variotherm temperature control has to offer, but also permits the cooling of the cavity surface with the lowest possible energy and in as little time as possible.

Finding out the size of these benefits and how the conformal cooling channels can be optimally designed for both the injection moulding process and for production with the SLM-process was the main subject of the first part of this master thesis. The intention was to design a test product, a mould with conformal cooling and one with conventional cooling and have them both produced and perform injection moulding tests with variotherm temperature control on both. But due to complications in the product design and cooling channel simulations only the basic design of the mould was finished.

The SLM machine has a set of parameters which need to be adjusted to the currently used material. The second part of the master thesis looks at the effects of variations on the scans pacing and laser power around the original parameters. For this purpose the most interesting material for injection moulds is maraging steel, though that material was not available for our SLM machine at the University of Derby and to reduce the costs the material that was available at the institute was used. This is a 316L stainless steel material, the geometries, density and strength were studied in this thesis.

2 Literature study

2.1 Injection moulding

Injection moulding works by melting granules of a particular plastic to a viscous melt and proceeding to push this into a metal mould. There exist different types of injection moulding machines but currently the most used type is the screw injection moulding machine as schematically shown in Figure 1. This machine has a screw within a cylinder, granules of plastic enter the screw at the back. The screw rotates, pushing the granules to the front whilst the heat from heaters around the cylinder and the shear heat of the movement turn the plastic into a viscous melt. During rotation, the screw is moved backwards creating room for the molten plastic to collect at the tip of the cylinder [1]. When enough material is collected, the screw stops turning and is moved forward injecting the melt into the mould. This mould consists of two or more metal blocks that form the shape of a product when held together, after the melt has cooled and solidified the mould opens and the part is ejected, the cycle starts again.

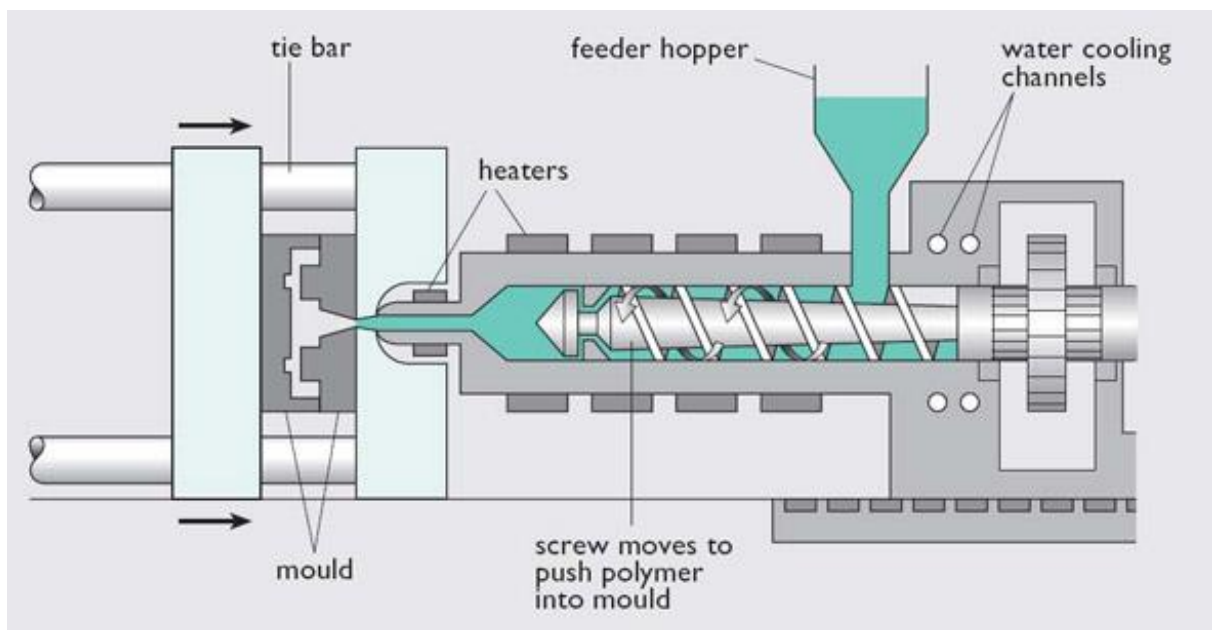


Figure 1: Cross section of the screw injection moulding process

Figure 2 shows a schematic overview of the mould build up, going from right to left, the stationary plate (e) is attached to the side with the injection screw. Attached to this is the stationary insert containing the sprue (d) through which molten plastic is injected into the cavity (c). The moving part of the mould starts at the parting line, with the moving insert, in this instance, containing the full cavity (c). Through the moving inserts pins from an ejector system (b) reach up to the surface of the mould. When the cavity is filled with plastic and cooled down, so that the product is sufficiently solid, the mould will open at the parting line and the injector pin will push the ejector system forwards which in turn will push the plastic product out of the mould. Besides ejecting the product, ejector pins also serve as air vents to remove air from the cavity, though sometimes extra air vents are needed to let all the air escape. In this thesis the focus is on the production of the stationary insert and the moving insert and the cooling channels that are included in most moulds to reduce cooling times and improve the uniform shrinkage.

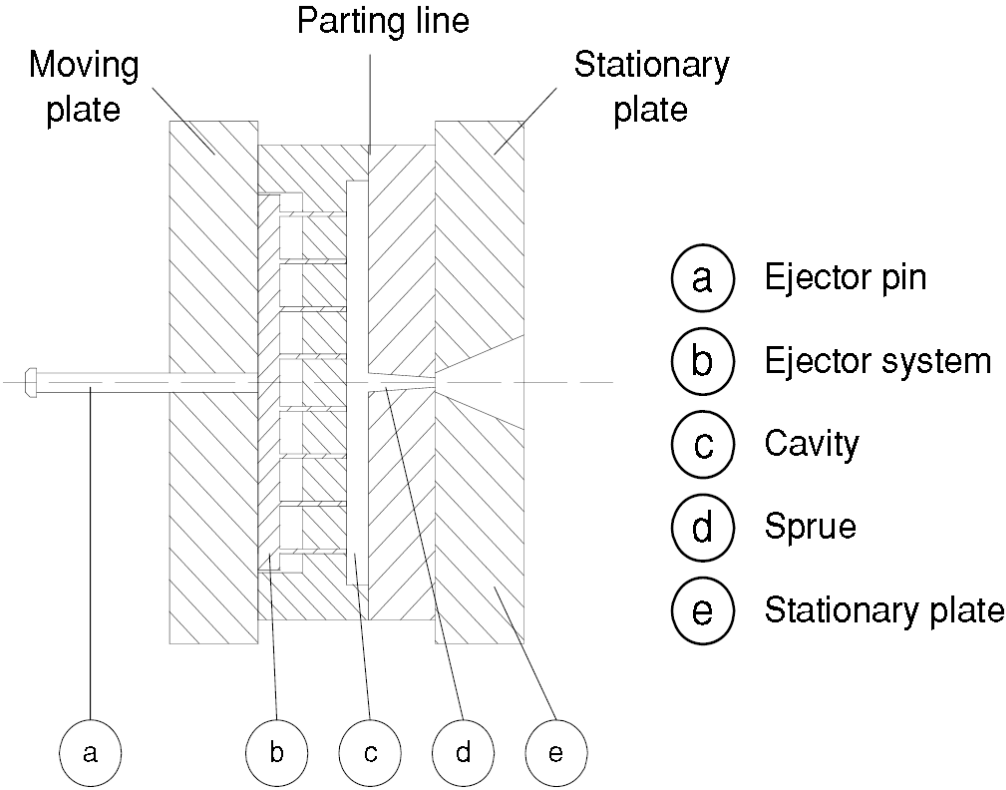


Figure 2 : Schematic overview of mould build up [2]

In moulds for production of high volumes the hardness of the cavity surface is an essential property. The viscous nature of molten plastic combined with high flowrates and high pressures cause the cavity surface to be subjected to high level of shear forces. Moulds made with SLS or other low hardness materials erode very fast under these forces. Looking at conventional steels used by the mould producer DME in their 2015 catalog [3] one of the high grade steels used is an AISI 420 steel able to reach a hardness of 55 HRC (600 HV).

2.2 Conventional cooling

Conventionally cooling channels are made by drilling straight channels through the mould block. This method has a number of disadvantages. First of all, the force accompanied by the drilling of the cooling channels, this could potentially deform the thin layer of steel present between the channels and the mould cavity or between the channels themselves. This limits how close the cooling channels can be placed to the cavity and other channels. Secondly these holes are in most cases very long, longer drills need larger diameters to avoid deformation of the drill due to the forces. This limits the minimum size of the holes that can be created. The combination of point one and two will in most cases impair the creation of the optimal distance/size proportion for an optimal cooling distribution and cooling time. Thirdly a very important consequence of drilling cooling channels is the fact that holes can only be drilled straight. Complex geometries of products cannot be followed and ejector pins must be avoided, giving an inherent uneven cooling of the part [4]. This will cause hot spots in the mould that will take longer to cool, increasing the cooling time and reducing the quality of the part [5].

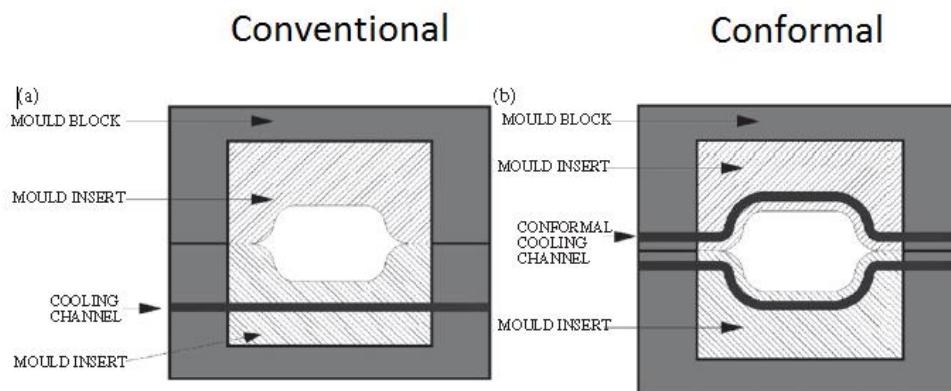


Figure 3 : Conventional straight drilled cooling channels versus conformal cooling channels

Cooling of round cores can be done with special inserts like baffles, bubblers or spirals. All of these types are inserted into a blind hole in the core of the mould. A baffle (Figure 4) is basically a plate splitting the hole in two sides with an opening at the top forcing the flow of coolant to the tip of the core. A bubbler is a tube within the core, the coolant flows to the top of the core through the tube and flows back down around the tube. A spiral is similar to a bubbler but instead of flowing straight down a spiral is made around the tube forcing the coolant to take the spiral path creating more contact between core and coolant. The only real problem with this technique is again the drilling forces and the fact that a large cavity in the core reduces its strength significantly [4].

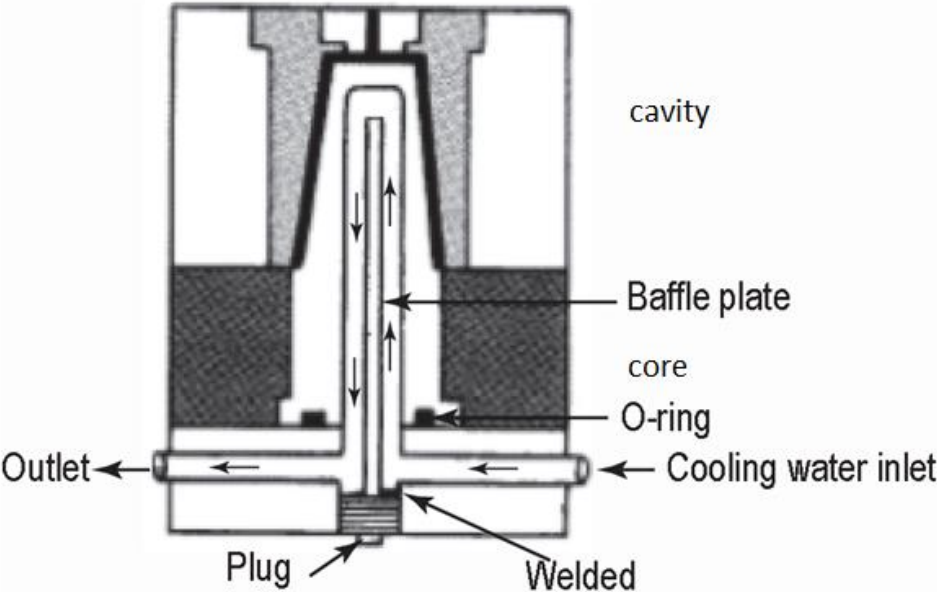


Figure 4: Example of a baffle in the core of a mould [6]

Only for a cavity with separate inserts, slightly more complex cooling channels can be applied. They contain cooling channels connected to the main channels in the main inserts. These inserts have a very complex construction and need to fit perfectly in the mould demanding expensively tight tolerances and the fitting between the two channels has to be water tight. They also take a lot of space, making them unsuitable for all areas.

2.3 Conformal cooling

2.3.1 *Properties*

Conformal cooling is the term used to describe a uniform cooling of the moulded product. The only way to achieve this is to create cooling channels that lay at an equal distance from the cavity throughout the whole mould. In the past this was done by milling channels into steel plates stacking those plates to create a full insert and vacuum welding them together. Nowadays Selective Laser Melting and Selective Laser Sintering are gaining popularity.

There has already been done plenty of research into this topic, though until now it was done primarily with SLS, which has a better geometrical accuracy but less hardness. EOS already has a few cases in which conformal cooling made with SLM was applied with impressive results [7]. Table 1 shows the advantages and the drawbacks of conformal cooling channels within a mould.

Table 1: Advantages and disadvantages of conformal cooling

Advantages	Disadvantages
Reduced cooling time => improving the productivity. [6]	Design is complex
Improved surface quality. [6]	Expensive simulation software to simulate the effect of the conformal cooling channels and the mechanical strength are needed
Stabilizing product quality by keeping the mould temperature constant. [6]	The design of the mould and conformal cooling channels has to keep into account the limitations of the SLM process.
Better control over the shrinkage of the product and control over the crystallization to ensure the same mechanical strength over the whole product. [6]	The SLM-machine is very complex and expensive
Less shrinkage leads to less failed products providing a better quality control and less material wastage. [8]	Due to the high surface roughness, milling of the cavity is still necessary so that milling machines and operators are still necessary.
Allows more complex moulded products.	

E. Sachs [4] used the test product and cooling channels shown in Figure 5 to inject PS plastic at 215°C, 1000 Psi (70 bar) injection pressure and 1,8 inch/sec (46 mm/sec) injection speed, into a moulds cooled with water at a flowrate of 1,3 gal/min (5 l/min). Conformal cooling was found to reduce the temperature fluctuation at the cavity surface during one cycle with 33 %. The average mould temperature did not rise more than 15°C, while with the normal cooling it rose 60°C above room temperature. The gap in the moulded test product fluctuated until the average temperature was stable. The conformal cooling mould reached his equilibrium much earlier resulting in less defective products at start up.

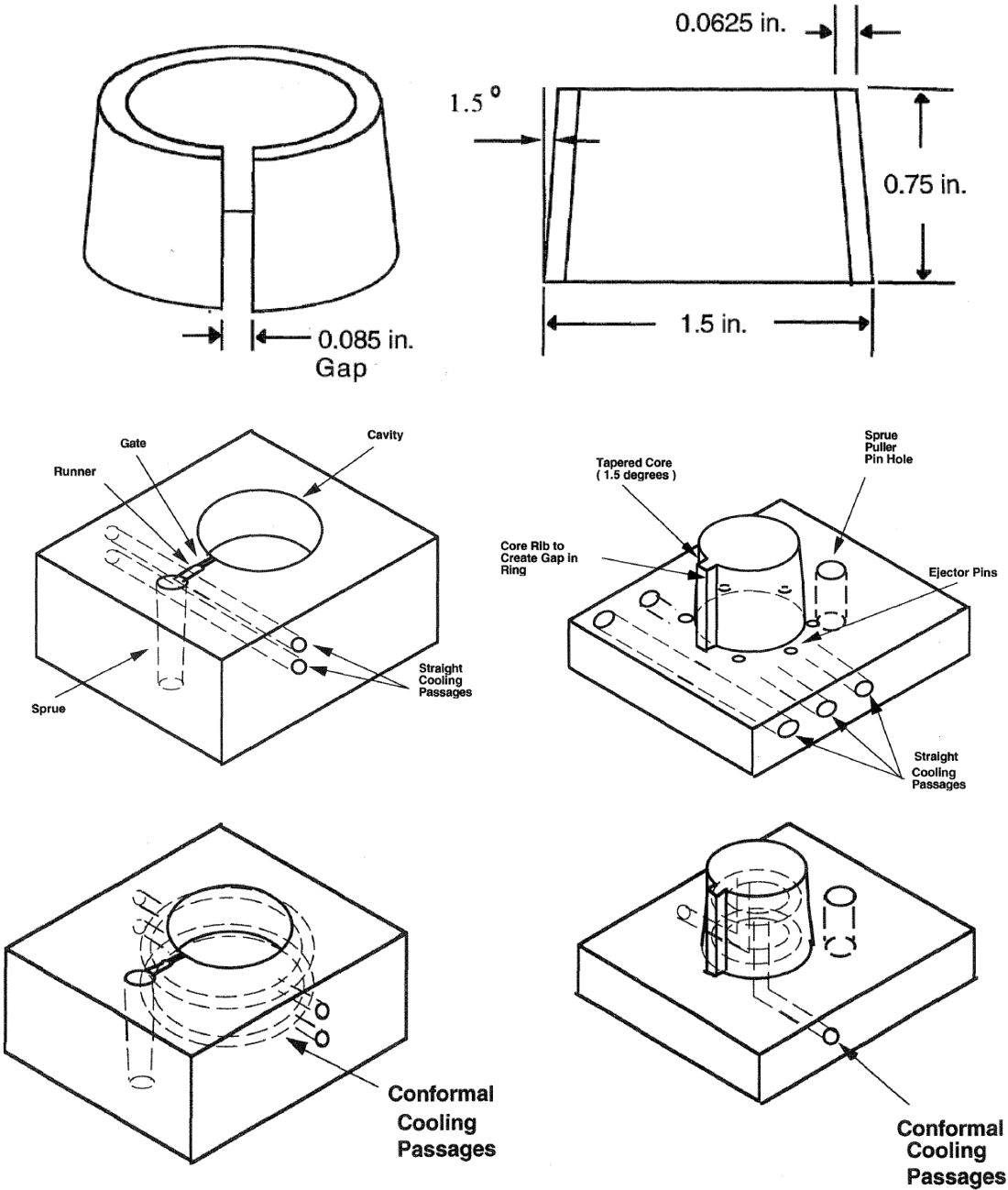


Figure 5: Test product and Cooling channels in the research by E. Sachs [4], Top: moulded product, Middle: conventional cooling channels, Bottom: conformal cooling channels, Right: moulded product

Simulations with conventional and conformal cooling channels on a round pitcher in [9] using PP plastic at an injection temperature of 225°C using water as coolant (Figure 6). The best improvements were seen in the cycle time (75 s – 37s) and the maximum temperature (220°C to 141,5 °C). Only slightly lower volume shrinkage (17 % - 15,7%) and slightly improved sink marks (3,9% - 3,58 %) were seen. In this particular instance the warpage rose from 1,481 mm to 1,587 mm. Though in this study conventional cooling combined with baffles was not used.

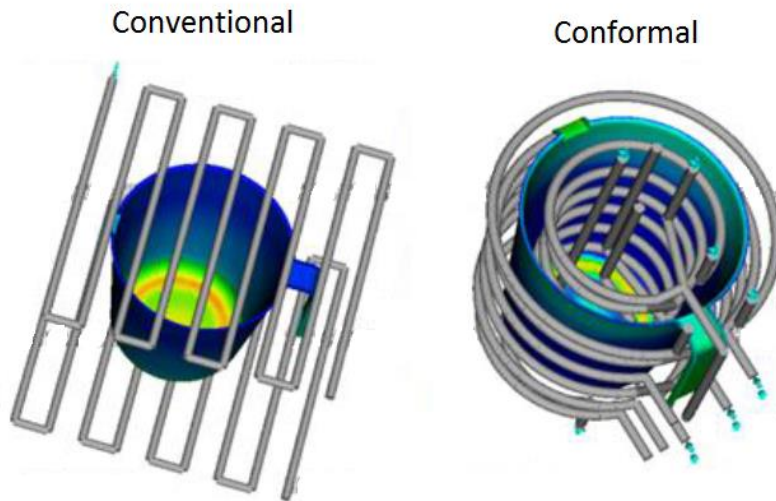


Figure 6: Channels simulated in [9]

Another issue in the production of conformal cooling channels is the removal of the powder within the channels. Not too complex channels can be cleaned with air jets but more complex parts might need different methods or a simpler design all together. [4]

2.3.2 Design

S. Mayer [10] from EOS, a company invested in the SLS and SLM processes, sets a number of design rules for the design of circular conformal cooling channels in moulds. The distance from the cavity and diameter of the channels is dependent on the wall thickness of the product as shown in Figure 7, with the grey area representing the cavity and the blue areas the cooling channels.

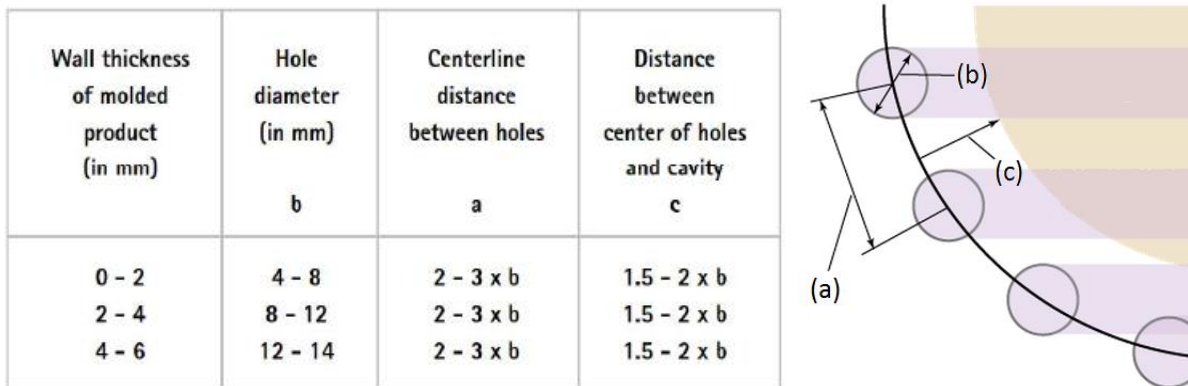


Figure 7: Design rules for conformal cooling by EOS [10], Image edited by L. Frick [5]

To design conformal cooling channels an advanced 3D modelling program, such as PTC Creo Parametric, is needed to model the complex channels at accurate distances from the cavity. This process starts by sketching a track representing the centre of the channel on a sketch plane at the required height and drawing the track to follow the cavity as required. In this manner tracks in sketch planes with different orientations can be connected to create smooth channel tracks. Spirals can be created using the sweep function. This function allows a spiralling surface to be created by extruding a line over a trajectory combined with a rotation of this line around the trajectory. The edges of this spiral are used as channel tracks. To create the actual channels the same sweep function is used to extrude the preferred channel section over previously created channels tracks. In Figure 8 (Left) an example of a swept spiral track and a circular tube swept over the spiral channel track can be seen. With the swept blend function in Creo parametric, channels with different sections and smooth transitions between these sections can be created over the previously mentioned channel tracks, Figure 8 (Right) shows an example of the possibilities with the swept blend function.

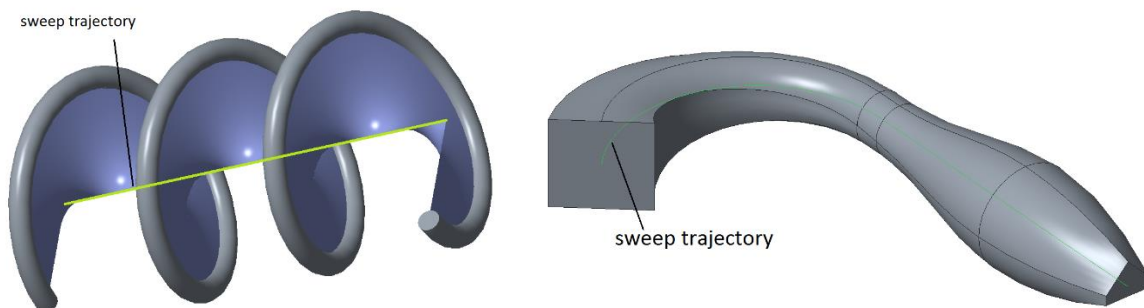


Figure 8: Left: Example of a spiral made over a straight trajectory with a sweep, Right; example of the possibilities with a swept blend in PTC Creo Parametric

Typically classic circular cooling channels are used in conformal cooling channels but there is the possibility to create cooling channels with different shapes to better fit the cavity surface (Figure 9 (a and b)) or to increase the turbulence of the coolant stream (Figure 9 (c)) [10]. Though the limitation of the production process should be observed to create channels of good quality. Figure 9 (a and b) show which cooling channels geometries are better to be created with SLM and SLS.

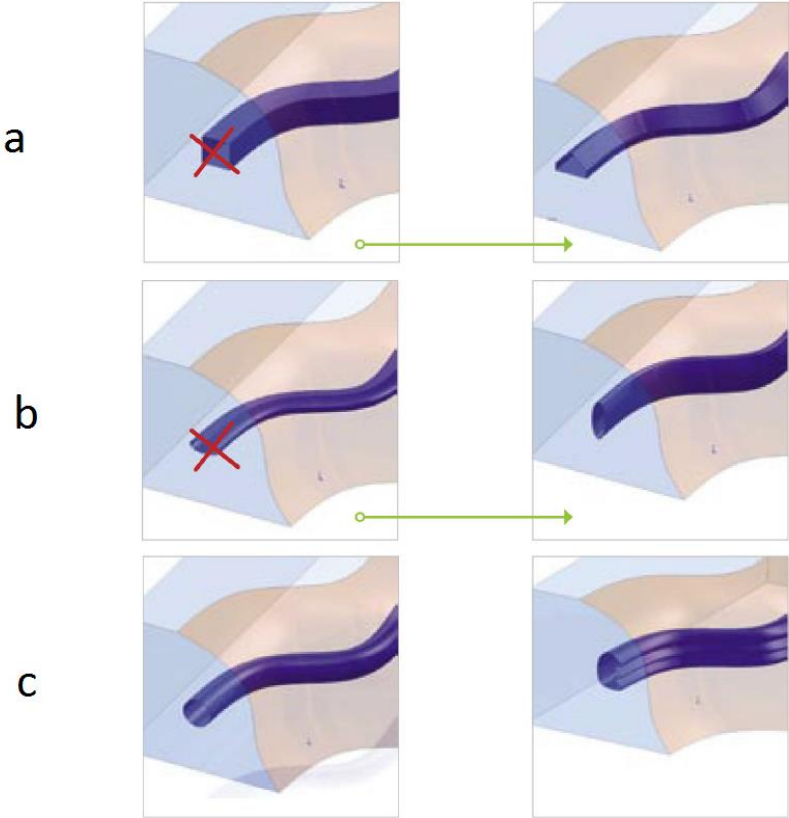


Figure 9 : Different shapes of cooling channels possible with conformal cooling channels

After the initial design of the conformal cooling channels, injection mould simulations with a program such as Autodesk Simulation Moldflow Insights (ASMI or Moldflow) can use the model of the product and the tracks of the channels to simulate the injection of the plastic and the cooling using conformal cooling channels. These results can be used to iteratively change the model and simulate it to obtain the optimal channels design. Moldflow can also simulate the stresses and the deformation in the mould during injection. If stress or deformations are beyond the materials capacity or the set limit, the material or the design of the cooling channels or product have to be altered. The preparation of the mould for production with the SLM machine. This software is normally included in the purchase of an SLM-machine for example, Renishaw delivers a specialized version of AutoFab with their machines. The software allows the generation of the different layers and scan tracks from the input model, the creation of support structures and the placement and orientation of the product on the build plate before exporting the instruction to the machine. Milling of the cavity surface is preferable to get a good surface finish. Surfaces that are to be milled need an excess of material that can be milled of the right dimensions.

2.4 Selective laser melting

SLM is a relatively new 3D-printing technique, currently it is primarily used in the production of prototypes, called Rapid Prototyping. With this technique a moveable base plate is placed within a metal powder bath, a scraper spreads a thin layer of powder, typically only 20 micrometres thick, over the base plate. Then a powerful laser fully melts the first layer of the desired product in a similar fashion to a regular printer. Now the base plate moves another 20 micrometre downwards so that the scraper can spread another layer on top of the previous one. The laser fully melts the second layer of product causing this second layer to be welded on top of the first layer. Using this cycle over and over again a whole product can be created and the remaining loose powder is removed manually. In Figure 10 a visualisation of the principle of an SLM-machine is shown. The full melting of the powder causes the finished product to have a near full density and thereby all the properties of the base material, though this also causes a bad surface quality and heightens the chance of warpage, causing the need for finishing with milling or grinding in most applications. Despite all this, there is still a large advantage over selective laser sintering (SLS), this is a similar technique but here the powder is sintered together instead of fully melted. To obtain a full density an extra infiltration step is needed in which the holes between the sintered powder are filled with bronze. This results in a low surface hardness which is undesirable when making injection moulds.

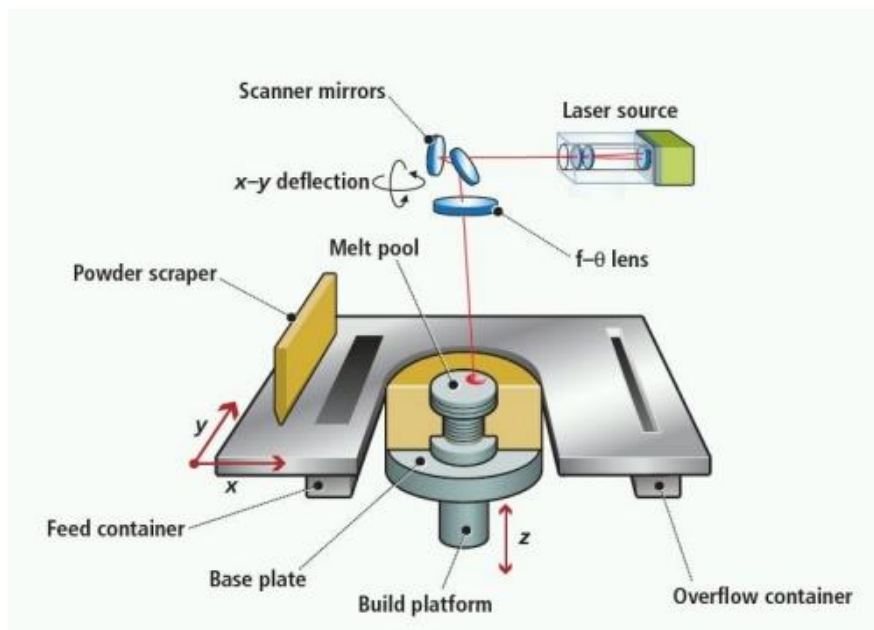


Figure 10: Visualization of the principle of an SLM-machine [11]

V. Petrovic [12] summed up the advantages of the SLM process as following:

- A nearly unlimited design freedom giving the opportunity to optimize a product to fit a specific purpose.
- Near full density prototypes out of metal with the properties of the eventual product can be created within a day.
- A large weight reduction can be achieved using lattice structures and internal cavities for the optimal strength to weight ratio.
- No tools are needed for parts that do not require a smooth surface or micrometre accuracy, the surfaces that do need this accuracy or quality only need a small amount of material milled off. Support structures used to support overhanging structures have to be machined off.
- Maximum material usage is possible, any material that is not molten in the process can be recycled with addition of 30% new fresh powder.
- Custom surgical implants can be created in a short time and lattice structures within this implant enhance the muscle attachment.

The process also has some disadvantage such as:

- The base material is very expensive because powders with a typical particle size of 15-45 μm are required for the SLM process. The production of these powders is complex and expensive for example, 316L stainless steel can cost up to 80 euros (60 Pound) per kilogram. Alloys containing rarer elements are even more expensive.
- Large products with a large volume of bulk material have long production times.
- Overhanging structures need supports which need to be removed afterwards. Overhangs without supports are subjected to geometrical limitations for a good quality, this is elaborated later in this thesis.
- Current maximum build size around 280x280x350 mm.
- Printed materials have anisotropic properties.
- Bad roughness creates the need for an excess of material outside of the 3D-model that is to be milled off for a perfect surface accuracy and finish.

Other limitation and properties are given further on.

2.4.1 *Process properties*

The products made with SLM can be described as products made entirely out of weld lines. Figure 11 shows a schematic representation of how the melt pool is formed by the laser.

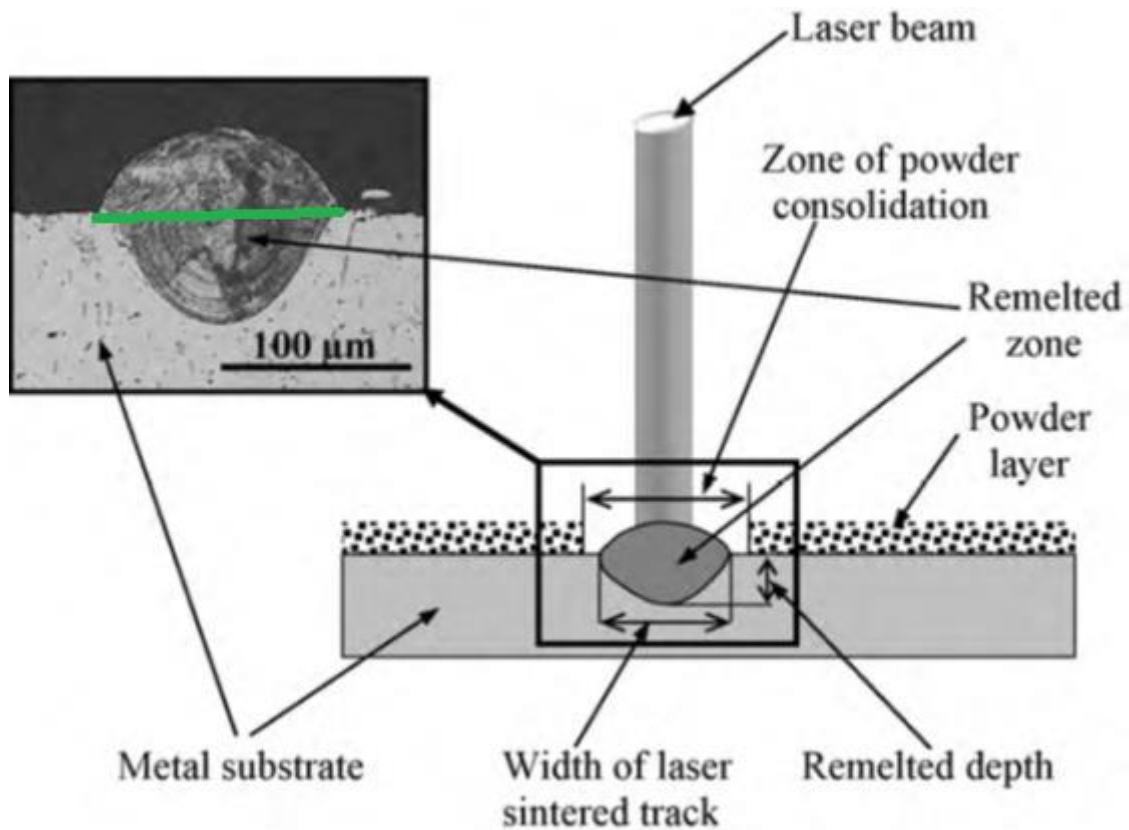


Figure 11 : Schematic representation of a single track being produced by the SLM process, in the top left corner a section of a good single track is seen [13].

The spreader that spreads the next layer of powder could have a soft coater or a hard coater. A hard coater is a solid blade which can make more accurate layers with higher density but is less suited to make small features. The hard coater has a zero tolerance for high roughness of the layers, any defects protruding from the powder layer will block the spreader demanding an abortion of the print job. A soft coater is a silicon cylinder which is less accurate and will pack the powder less dense. These negative properties are counteracted by the fact that the print job does not need to be aborted by protruding defects in the layer, but it will cut a mark in the coater which will affect the spreading of the powder at that spot. This could have an effect on the quality of the part [14].

2.4.1.1 Yield and Tensile strength

I. Tolosa [15] discovered that the yield strength is significantly better for 316L steel printed with SLM than for wrought 316L products with ~540 MPa (lowest strength) to 170-310 MPa (CES [16]), the tensile strength is in the upper reaches of the possible strength of wrought products being around 600 MPa, yet maintaining high values of elongation. He did however see an anisotropy in the printed pieces with horizontal pieces having a strength of more than 100 MPa higher than the vertical pieces.

2.4.1.2 Surface roughness

As mentioned before, bad surface roughness is seen in all cases with surface roughness with a Ra from 9 to 17 μm and a Rt of 150 μm [17], [18]. This means that for injection mould made with SLM the cavity has to be milled and possibly grinded to create good surface quality especially when using variotherm temperature control because any imperfections in the mould surface will certainly be copied in the final product.

2.4.1.3 Density

Near full density pieces can be created with SLM as seen in [15], [17], [19]. This is very important for an injection mould because any pores uncovered by milling and grinding will leave an effect on the mould product, same here with variotherm temperature control.

In [17] a direct proportional relation between density and hardness was observed.

Porosity in SLM produced parts can be caused by unmolten areas between the melt pools of scan tracks as seen in Figure 12 showing a front view of a section of multiple scan tracks, the overlap between the melt pools and the gaps in between are clearly visible. Porosity is also produced by gas bubbles that cannot leave the melt pool before it has solidified (Figure 13, P. 32).

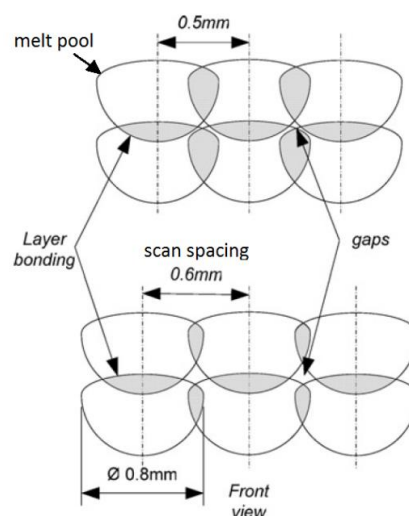


Figure 12 : front view of a sectioned laser track, figure by V. E. Beal [19] (P. 5)

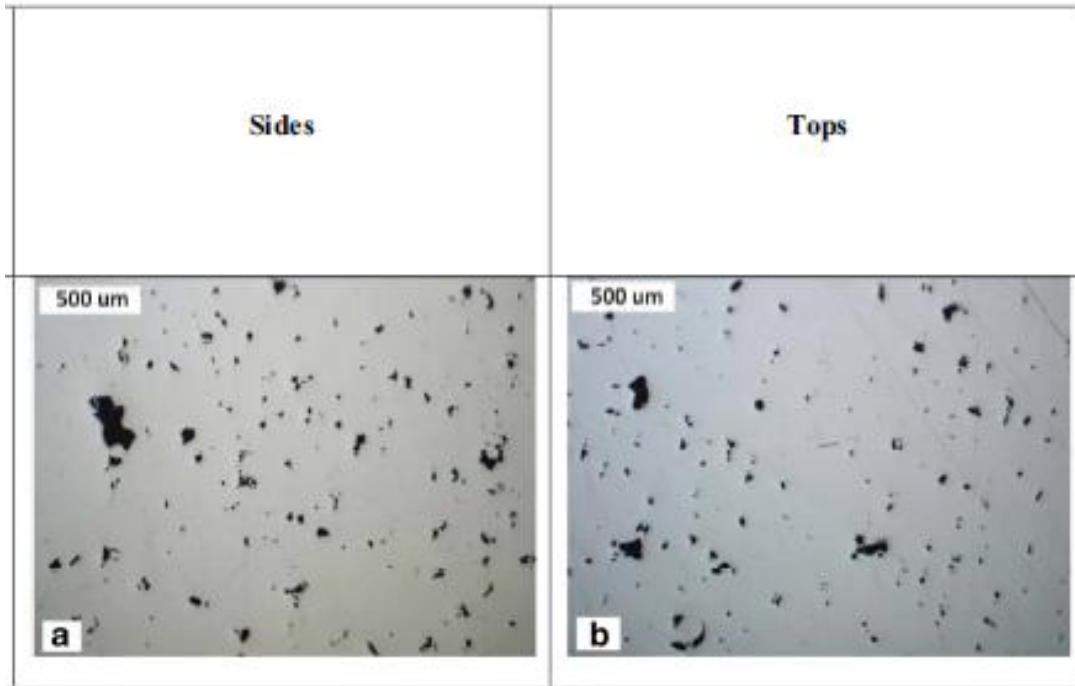


Figure 13 : An example of bad porosity due to low energy density. Left is shown the porosity seen from the side and right is the porosity seen from the top. [16]

2.4.1.4 Materials

Laser based additive manufacturing techniques are almost the only 3D-printing techniques that can reliably print metals. LWP technology offers alloyed material powder with the following materials:

- Copper alloys
- Stainless Steel
- Tool Steel
- Cobalt-Chromium
- Super Alloys
- Aluminum
- Titanium

Table 2 shows some characteristics of stainless steel and tool steel currently offered by Layerwise.

Table 2 : Characteristics of tool steels and stainless steel currently offered by Layerwise

Stainless steels				
		17-4	316L	hardenable stainless
Hardness	As built	230 HV (18 HRC)	230 HV (18 HRC)	300 - 345 HV (30 -35 HRC)
	Ground/polished	400 HV (40 HRC)	/	/
	Hardened	/	/	400-450 HV (40-45 HRC)
Yield strength	Horizontal	540 Mpa	500-540 Mpa	1300 MPa(hardened)
	Vertical	500 Mpa		1300 MPa(hardened)
Tool steels				
		Inconel 718	Maraging Steel	
Hardness	As built	(30 HRC)	33-37 HRC	
	Ground/polished	/	/	
	Hardened	(47 HRC)	50-54 HRC	
Yield strength	Horizontal	1150 MPa (hardened)	1950 MPa (hardened)	
	Vertical	/	1900 MPa (hardened)	

As mentioned before, material for the production of high quantity injection moulds have to possess a minimum hardness of 40 HRC (400 HV). Most conventional tool steels are unavailable to the SLM process due to the residual stresses (see chapter below) and most materials now available to the SLM process do not possess the required hardness, Only Maraging steels and Inconel 718. Inconel 718 is difficult to machine after printing. Only maraging steel, able to reach a hardness of 58 HRC (660 HV) [20], can compete with the hardness of conventional steels whilst maintaining a good machinability for finishing of the mould cavity.

2.4.2 Limitation

2.4.2.1 Residual stresses

Because the basic principle of this process consists of rapid melting and cooling, it can be compared to a local quenching at each new track. This causes non-uniform shrinkage within the material so that each newly solidifying material will tug on the already solid material leading to residual stresses within the material.

Consequences can be deformation of features, also called curl by D. Thomas [21] (Figure 14, left), when material is partially printed on loose powder. When the stresses are against the direction of the applied loads the material can surpass its original strength but when the stresses are in the direction of the applied load early failure could occur.

The most important consequence is that this effect limits the range of materials that can be processed with this process because a large amount of the conventional tool steels used in injection moulds are hardened through quenching. Quenching is the process of cooling a material rapidly from a high temperature. Because this happens locally each time, instead of uniformly like with normal hardening processes, newly solidified material is hard and brittle because of the quenching, causing it to crack under the residual stresses (Figure 14, right). For this reason only materials that don't increase in hardness when quenched can be used.

The amount of residual stress is dependent on the cooling speed which, in turn, is dependent on the temperature gradient. Through preheating of the base plate the temperature gradient can be reduced. Using this method, a conventional M2 Tool steel has been successfully processed by K. Kempen [22], this process parameter is discussed further on.

To obtain the required hardness for mould production, materials who get their hardness from aging must be used, this is a process in which an alloyed material is kept under a relatively low temperature for a long time causing microscopic and hard alloy balls to form, giving the necessary hardness to the material. Examples of such materials are alloyed aluminium, High-alloyed steel and maraging steel.

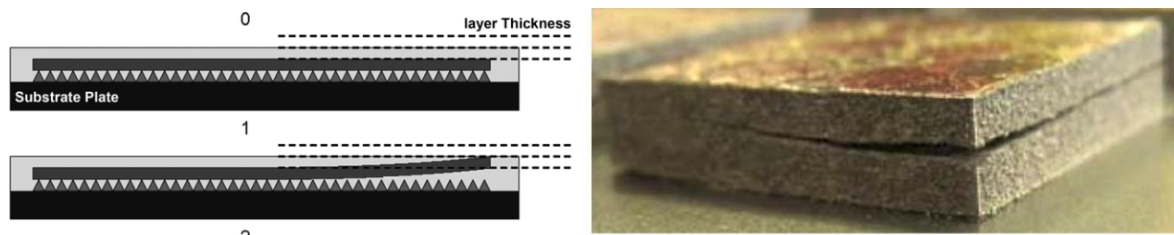


Figure 14: Left: Representation of curling [21], Right: Cracking due to residual stress in M2 Tool steel [22]

2.4.2.2 Delamination

Delamination is when a layer is not bonded to the layer below causing it to detach from the product as the layer cools and shrinks. This is caused by under penetration due to wrong parameter settings such as laser power too low or scan speed too high. [21]

2.4.2.3 Balling

A common problem in the SLM process is balling, a phenomenon that occurs when too much energy is radiated without enough penetration in the previous layer, causing a bad attachment to the underlying substrate. The melt pool forms a free cylindrical tube upon the substrate, dependent on the parameters this cylinder will have a certain contact surface with the previous layer. The amount of contact surface is indicated by a contact angle (Φ). As the contact angle becomes bigger the chance of a capillary instability occurring increases. This effect will cause the cylinder to gather in a ball due to the inherent nature to go to a state with less energy. The same phenomenon is seen in the forming of droplets from a waterjet [14]. In Figure 15 a schematic representation of a melt pool with a high contact angle is seen at point (a), the dimension L represents the length of the molten cylinder and D the diameter of the melt pool, point (b) gives an example of a capillary instability occurring. In [19] the critical point for capillary instability is reached at the equation given in Figure 15 (c). Melt pools with a contact angle smaller than 90° are stable at any length (value is adjusted to the representation as shown in Figure 15). Figure 16 shows an extreme case of balling in a single scan track. These balls often protrude from the next powder layer causing damage to a soft coater or even blocking a hard coater.

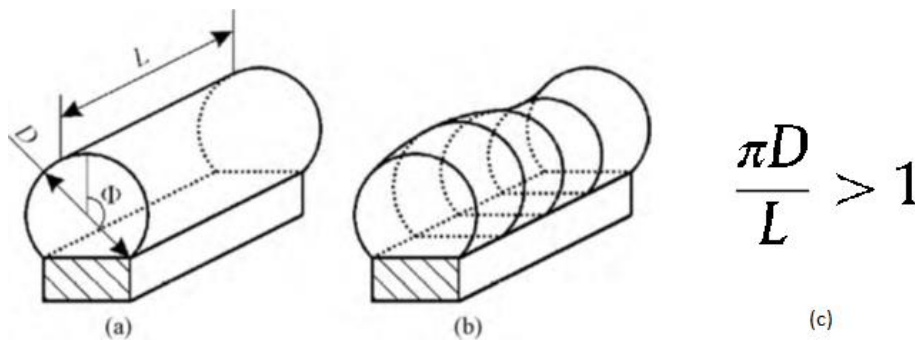


Figure 15 : Cause of balling in the SLM process image from [13].

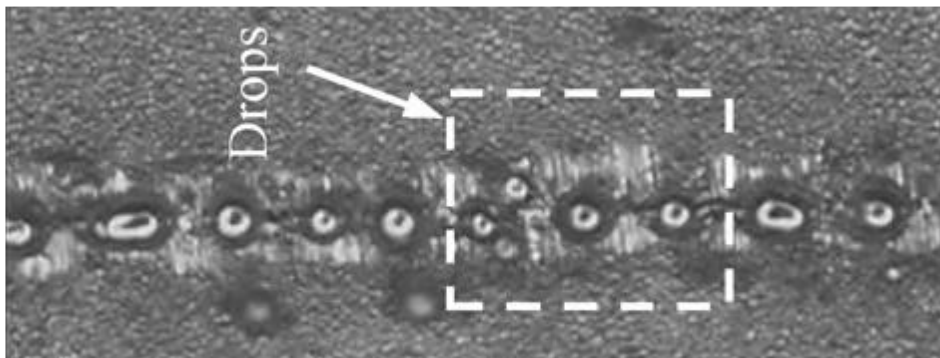


Figure 16 : An extreme case of balling seen in [13].

2.4.2.4 Stair effect

The stair effect is seen in most of the additive manufacturing techniques, this stair effect is illustrated in Figure 17. This causes high roughness on sloped surfaces which need more milling to be smoothed out. Lower slopes (α) and higher layer thickness make this effect more profound.

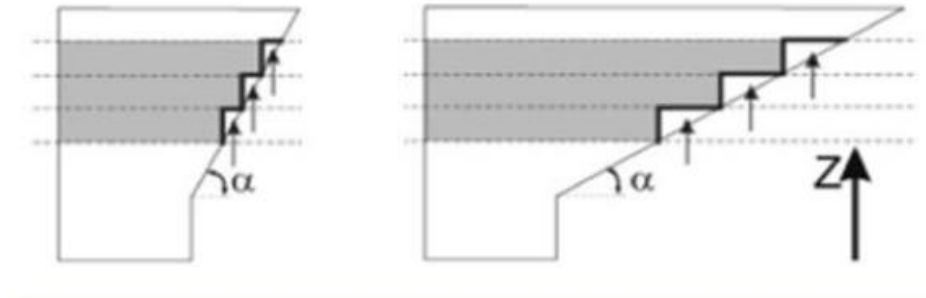


Figure 17: Stair effect in sloped surfaces. Taken from a presentation by Layerwise

2.4.2.5 Overhangs

As mentioned before overhangs are very hard to produce with SLM. An overhang is defined by a layer printed on top of loose powder. M. Van Elsen [14] describes the following defects commonly occurring in the production of overhangs. Whenever possible overhangs should be supported with support structures to negate errors in the build dimensions, these will have to be removed afterwards.

The bobble effect is the occurrence of a small bobble at the beginning of a scan track, this is explained by a theory that at the start of the track more adjacent powder is available to be pulled into the melt pool, creating a bobble. A possible solution would be to start each new layer at a different point to prevent any build-up of this effect. Stalactites are formed when the penetration of the laser into the previous layer is too deep, the melt pool attracts powder from below, thereby sinking into the powder. Satellites are particles of powder attracted by the melt pool during its solidification, the particles are not able to penetrate the solid melt pool and are visible on the surface of it. An example of a 5 mm long overhang is shown in Figure 18 by J-P Kruth [18].

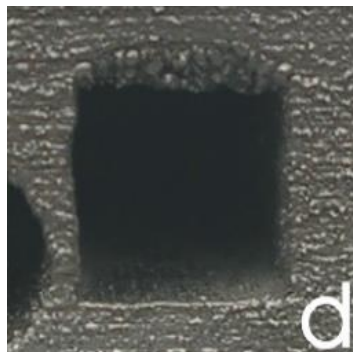


Figure 18: A 5 mm long horizontal overhang made in 316L with SLM [18]

2.4.2.6 Horizontal circular holes

Horizontal circular unsupported holes have similar problems as overhangs. At the top of the hole there is sagging material due to over penetration but there is also an inward deformation due to curling creating the undersize material and oversize material in the left picture of Figure 19. there is more sagging of the ceiling and curling as the diameter of the holes gets bigger as seen by D. Thomas [21] (Figure 19, right). Because of the sagging and the roughness of the surface, cooling channels will be smaller than they are modeled in the CAD software. An excess diameter must be used for the hole, for example a hole of 2 mm diameter has to be modeled as a diameter of 2,1 mm.

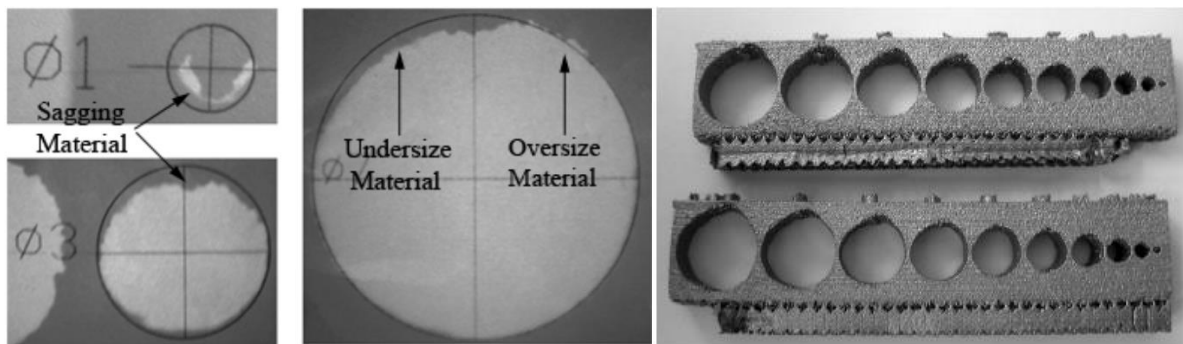


Figure 19 : Left: Sagging of the ceiling of holes with a diameter of 1 mm, 3 mm and 7 mm, Right; Horizontal circular holes with diameters from 1 mm to 10 mm [21].

In larger holes a sink mark on the side wall caused by the curling at the top of the hole has been seen by D. Thomas (Figure 20), his experiments conclude that a self-supporting geometry reduces this sink mark but does not eliminate it. He also found that no sink mark can be seen when a hole of 10 mm has a wall thickness higher than 8 mm from the side surface.

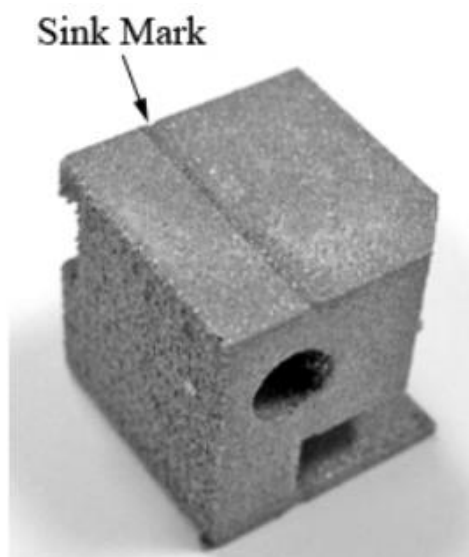


Figure 20 : Sink mark caused by curling in a horizontal hole on the side of a part of 20x20x20 mm (part is placed on its side)

2.4.3 Influence of process parameters on material properties

The SLM process has a large number of process parameters that directly affect the physical and geometric properties of the printed product. In this chapter the overall effect of each process parameter on the material properties is discussed based on literature. The literature study is focused on 316L stainless steel because this is the material used in my project.

Throughout the literature study I have noticed that it is exceedingly hard to find a consistent theory to link a specific parameter to a specific consequence. The effect of the parameters seems to be different for every material, every machine and every laser and so forth. Mrs. Mertens, a PhD student on a subject about SLM from the University of Leuven, confirmed this. The fact that most articles about selective laser melting research the shape of melt pools for different parameters and less the mechanical properties attributed to these parameters makes it harder to make a good correlation.

M. Van Elsen [14] gives a very complete overview of the parameters influencing the SLM process. I am only going to address the parameters that have the most effect on the process and can be changed within one machine.

2.4.3.1 Environment within process container

The first parameter is the effect of the environment within the process container. Due to the high temperature and large surface area of the powdered metals any oxygen would oxidize the powder instantly, so it is necessary to use inert gas to shield the melt pool from oxygen. Some machines even use a vacuum to minimize the contact with oxygen.

B. Zhang [19] found that for 316L stainless steel powder a maximum of 0,5 % oxygen can be present in the process chamber without causing oxidation. Figure 21 shows that inert gasses such as argon, argon-hydrogen mix, nitrogen and nitrogen-hydrogen mix give near full density for a specific machine with specific process parameters.

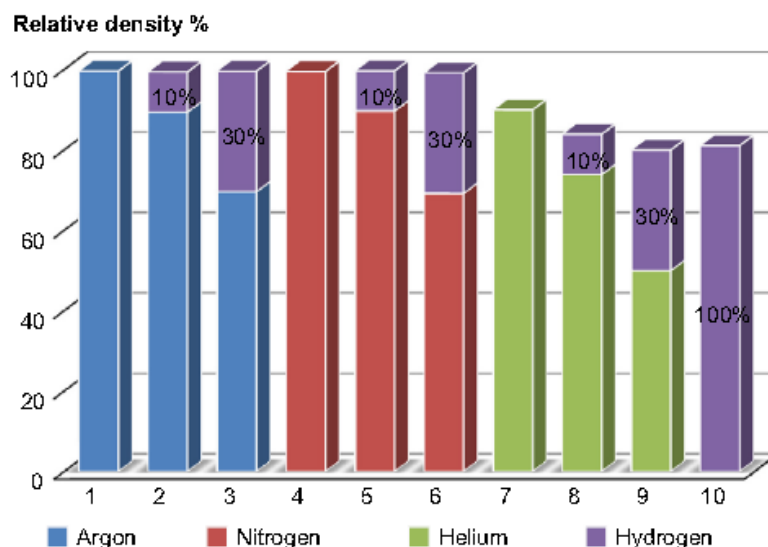


Figure 21: Relative density for 361L using different inert gasses by B. Zhang [19]

Helium, Helium-hydrogen mixes and pure hydrogen give a great reduction of the density. The cause for this is the high ionization energy needed to ionize helium gas to plasma, this causes the plasma to disconnect from the melt pool limiting the energy transfer to the melt pool. Hydrogen gas acts as a deoxidizer in the process chamber, though the results indicate that this is not needed, pure argon or nitrogen will also give near full density.

2.4.3.2 Preheat temperature

The preheat temperature is the temperature within the process chamber before the process starts. This involves preheating the chamber to a certain level, the energy from the laser will keep the temperature at around this level.

Preheating is the main method of reducing residual stress in an SLM printed product. This is seen by P. Mercelis [23] and B. Zhang [19] for 316L and K. Kempen [22] for M2 Tool steel. It is the only way materials like titanium, tool steel and other materials that harden after heat treatments can be used in the SLM process. A higher base powder temperature reduces the temperature gradient between the melt pool and the solidified material reducing the thermal stresses.

Experiments with 316L by B. Zhang [19] attribute the best density (99,7 %), tensile strength (594 MPa), Young modulus (150 GPa) and deformation (7%) to a higher preheat temperature of 200°C, whilst the prints with no preheat have far lower density (98.6%), tensile strength (450 MPa), young modulus (195 GPa) and deformation (15%). I. Tolosa [15] found values with even more strength, though in this article no preheat temperature was mentioned. The differences found by B. Zhang [19] have to be dependent on other parameters because standard parameters for the processing of 316L stainless steel on a Renishaw AM250 do not include preheating of the baseplate.

2.4.3.3 Layer thickness

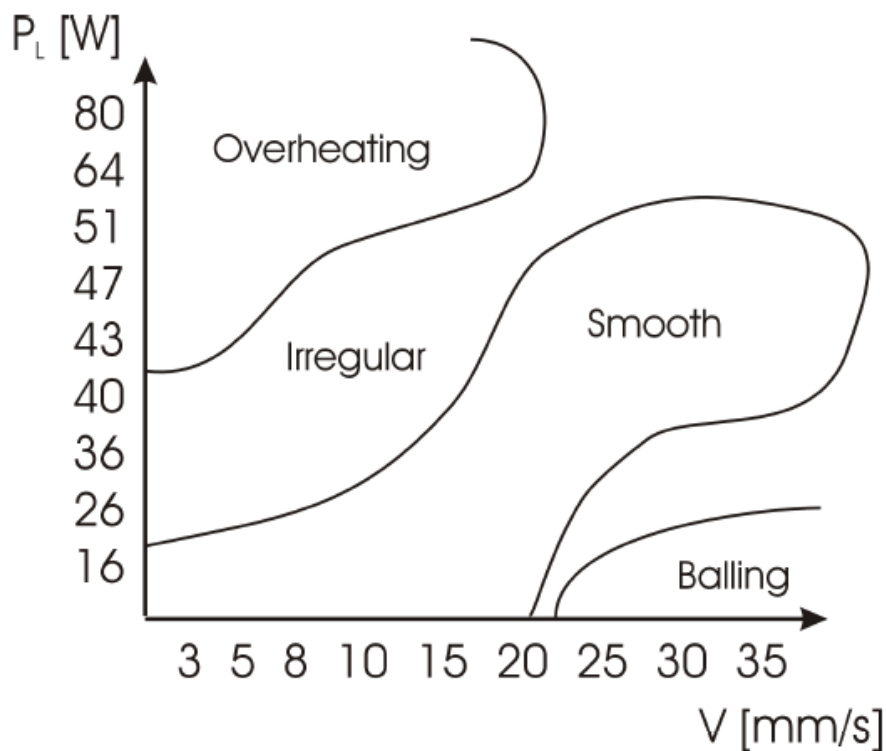
The layer thickness says how thick every new layer of powder is. It determines the effect of the stair effect as seen in chapter 2.4.2.4, higher layer thickness will give a more profound stair effect.

In B. Zhang's research [19] the contact angle of tracks increases when the layer thickness goes up because the energy of the laser cannot penetrate deep enough into the previous layer to bond them together, possibly leading to balling which could damage the spreader and lower the density [14]. R. D. Li [24] had the same results for a 90W-7Ni-3Fe material explaining that besides not penetrating deep enough, the heat was also concentrated at the top of the melt pool causing it to overheat, resulting in bad wetting characteristics and lower density. Gasses escaping from the melting powder are trapped in the large solidifying melt pool, decreasing the density. A lower layer thickness will give a higher production time if the laser travel speed or scan spacing are not increased.

2.4.3.4 Laser power

The laser power describes the amount of energy output of the laser per second. Together with the layer thickness, the laser power affects the penetration in the previous layer. A higher laser power will penetrate deeper and thereby make a better bonding between the layers and giving a lower contact angle of the melt pool, this in turn will reduce the chance of balling, this was concluded by B. Zhang [19](P. 3). The same was seen by I. Yadroitsev [13] who also added that the track width goes up with higher power, he also saw that higher laser powers can sustain a larger range of scan speeds with good quality.

Though the previous researches indicate that a higher laser power will give better quality, making overhangs with high laser penetration is not desired, this would cause stalactites to form beneath the printed surface. Graph 1 made by M. Elsen [14] shows that lower laser power (P_L) and higher scan speeds (V) give smoother surfaces when printing on loose powder. J-P Kruth [18] saw also that deep penetration is the cause for bad overhang quality.



Graph 1: The quality of a surface printed on loose powder at different laser powers (P) and different scan speeds (V) [14].

2.4.3.5 Scan speed

Scan speed is the speed at which the laser spot travels over the surface of the powder. Besides traveling at a continuous speed through the use of a continuous laser, some machine use a step by step movement called a pulsed laser.

A continuous laser radiates a set amount of energy continuously whilst moving at a continuous speed over the scan tracks. In this case there is only the scan speed as a parameter. A pulsed laser divides the track into points on a set distance from each other called the point distance. A parameter called exposure time is added, this parameter represents the time each point is radiated by the laser before jumping to the next point. There are different types of pulsed laser modes, the Renishaw AM 250 uses such a modulated laser. In his own literature study M. Elsen [14] found that the pulsed laser can more easily melt powder due to the higher peaks that are possible, but faster solidification causes higher temperature gradients, making the structure more brittle than structures made with a continuous laser.

Most studies use a continuous laser to do their experiments A. Cherry [17] however has studied the effect of the exposure time and point distance on the quality of the pieces. She found that exposure time had little effect on the roughness, whilst variation in the point distance caused a large variation in roughness explained by the reduced overlap of the laser spot as illustrated in Figure 22. Both parameters separately did not seem to affect the hardness or density.



Figure 22 : Schematic representation of the effect of higher point distance on the roughness

I. Yadroitsev [13] found that an optimal range of scan speed for a laser power of 50 W and layer thickness of 50 μm is between 0,08 and 0,2 m/s, this range increased in size as the laser power increased. If the speed was too low irregular tracks and distortions were found and when the speed was too high the track suffered from severe balling. He also saw that the track width was linearly dependent on the scan speed. K. Kempen [22] saw that for M2 Tool steel the scan speed had little effect on the surface roughness for 105 W and scan speeds between 150 and 500 m/s.

For the creation of overhangs in 316L, M. Van Elsen [14] found that higher scan speeds give a smoother surface when printing single tracks upon loose powder. When creating plates on loose powder a slightly higher than standard scan speed gave the best results.

2.4.3.6 *Spot size*

The spot size is the diameter of the circle of energy created by the laser on the powder surface. Most manufacturers use this to indicate the area in which 86 % of the laser power is contained, but at the KU Leuven they prefer to use 96 %. Most lasers have a circular laser spot but there are also lasers with an elliptical spot, these will have 2 values for the axis of the ellipse.

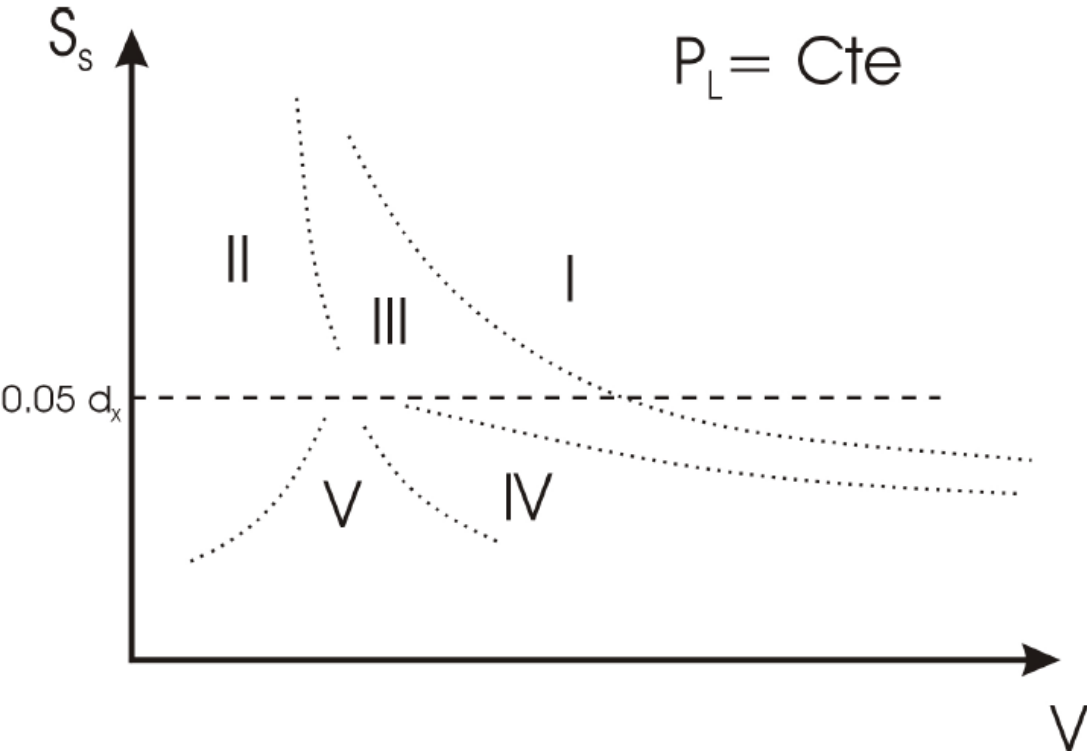
M. Van Elsen [14] (P. 146) calls it one of the key factors in the SLM process because a smaller spot size gives more energy on less surfaces influencing the penetration of the melt pool significantly. But he was unable to prove the effect of a change in spot size. Generally a smaller spot size will need smaller scan spacing and higher scan speeds to maintain an equal overlap of the tracks and the same energy density.

2.4.3.7 *Scan spacing*

The scan spacing is the distance between parallel scan tracks of the laser. In the literature this is also called hatch spacing.

V. E. Beal [25](P. 5) saw that there was little difference in density with different scan spacing using M2 tool steel though he made a sound reasoning about a method in which scan spacing would affect the density. This is made clear by the front view of a section of laser tracks as shown in Figure 12 in chapter 2.4.1.3. This figure clearly shows that when only the scan spacing is enlarged the overlap between the scan spacing is smaller causing gaps between the tracks. Higher scan spacing will also reduce build times drastically.

For the creation of overhangs M. Van Elsen's research [14] indicates that lower scan spacing gives better overhang quality, he found the best results when going to such extremes as a scan spacing of only 5% of the spot size, resulting in very large overlaps of the track's melt pools. His theory is that if scan track lengths are not too big, one big melt pool would over span a gap between solid materials. Relatively good results were found with printing 10x10 single layer plates on loose powder and a bridge over spanning a gap of 10 mm. Based on these results M. Van Elsen made Graph 2 showing the scan spacing (S_s) versus the scan speed (V) with zones of different quality.



Graph 2 : Different quality zones for the 10x10 plates on loose powder dependent on the scan spacing (S) and the scan speed (V).

The zone with the best quality was zone V, this zone is positioned below the $0,05 d_x$ line meaning that the scan spacing is 5% of the spot size of the laser. Zone II is that of the standard parameters for his machine.

2.4.3.8 Scan strategy

The scan strategy is the way in which the scan tracks are placed. There are a number of different scan strategies used in modern machines but I am only going to mention those that are available in the Renishaw software. Figure 23 shows an example of the scan strategies that are described below.

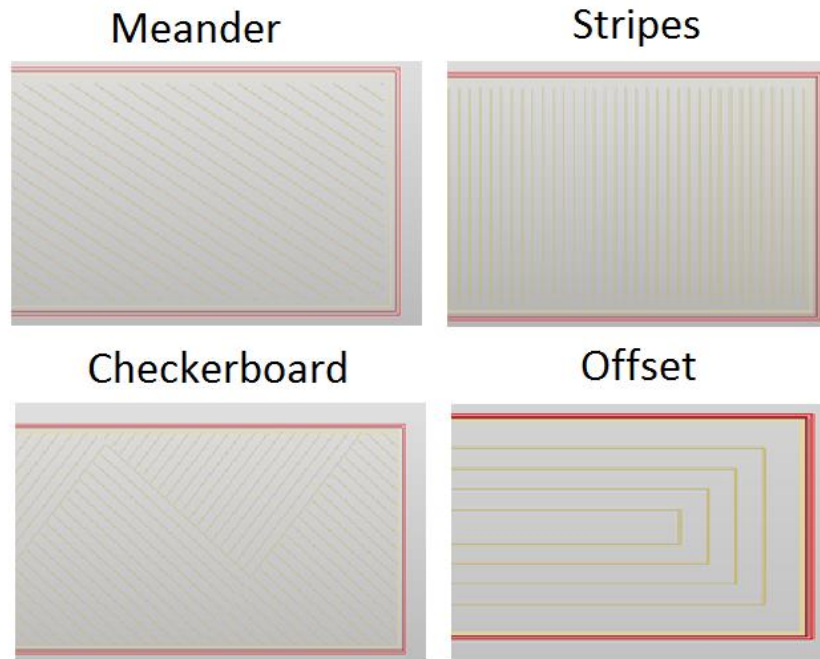


Figure 23 : Scan strategies available in the Renishaw software

The most straightforward is the meander pattern as it is named in the Renishaw software, in the literature it is also called a filling pattern. With this strategy the paths are placed parallel to each other with the laser going in the opposite direction with each following track, each track is one continuous line from one edge to the other of the printed product. Every new layer the pattern is rotated with a specific angle. V. E. Beal [25] saw that using a high layer thickness and high energy caused a lot of splatter of molten material, leaving less material to be molten for the next track.

Checkerboard, also called island scanning strategy, is a pattern that splits the surface in squares with a particular size under a set angle. Within each square a meander pattern is used parallel to the edge of the square, every adjacent square had a meander pattern perpendicular to the first square. J-P. Kruth [26] proved this strategy to lower the residual stresses within a product, a size of 10x10 mm for each checkerboard square will reduce the residual stresses, smaller squares will give no further reduction of the residual stress.

Stripes are tracks under a chosen angle to the edge of the product, they are basically the same as meander track, the only difference is that they are not rotated for the next layer, instead they are shifted a very small distance perpendicular to the scan track direction so that the next layer's laser tracks are between those of the previous layer. This strategy is normally not used to print bulk material. No literature about this strategy was found.

The offset strategy allows the creation of tracks parallel to the edge geometry. Renishaw does not use this strategy in its standard parameters and no literature was found about it.

2.4.3.9 Energy density

The energy density is not a parameter on a SLM machine. Energy density combines previous parameters into one, for an easy correlation with material properties. It is defined differently by different authors, M. Van Elsen [14] defines it as the energy per surface unit and A. Cherry [17] defines it as the energy per volume of printed material. Because the experiment in this thesis is largely based on an article by A. Cherry, her definition for the energy density is used here, the formula is:

$$\text{Energy density} \left[\frac{\text{J}}{\text{mm}^3} \right] = \frac{\text{laser powder} \left(\frac{\text{exposure time}}{\text{scanspacing} * \text{point distance}} \right)}{\text{layer thickness}}$$

A. Cherry [17] correlates the energy density to the material properties. Seeing, for 316L, at an energy density of around 72,6 J/mm³ a maximum density of 99,62 % and a minimum roughness of Ra = 9 µm. A maximum hardness of 225 HV (16 HRC) was found around 87,9 J/mm³. The hardness seemed to be directly proportional to the density.

2.4.3.10 Re-melting

Re-melting is a process in which the layer that has just been lasered is lasered again, in most cases with different parameters. This can be done for every single layer to increase density or only for the top surface of the model to increase the surface quality.

J-P Kruth [26] saw that for 316L stainless steel re-melting every layer can maximize the density from 99,23 % to 99,968 %, only one re-melting scan per layer is needed. Re-melting of the top surface can reduce the surface roughness from Ra = 12 µm to 1,5 µm. With the right parameters any resulting deformations, usually caused by the re-melting, can be eliminated.

Re-melting increases the density also increasing the residual stress, in M2 Tool steel this caused cracks [22]. Pores in the material interrupt the building of the residual stress but lasering solid material causes higher temperature gradients because the solid material conducts heat far better than powder. Re-melting also increases the build time.

2.4.3.11 Heat treatment

Heat treatment is not a parameter of the SLM process. Heat treatment of 316L stainless steel can alter its properties (not for hardening due to the low carbon content). For normal 316L stainless steel there are 2 kinds of heat treatments used, a solution annealing (a) and a stress relieving (b) treatment (Figure 24).

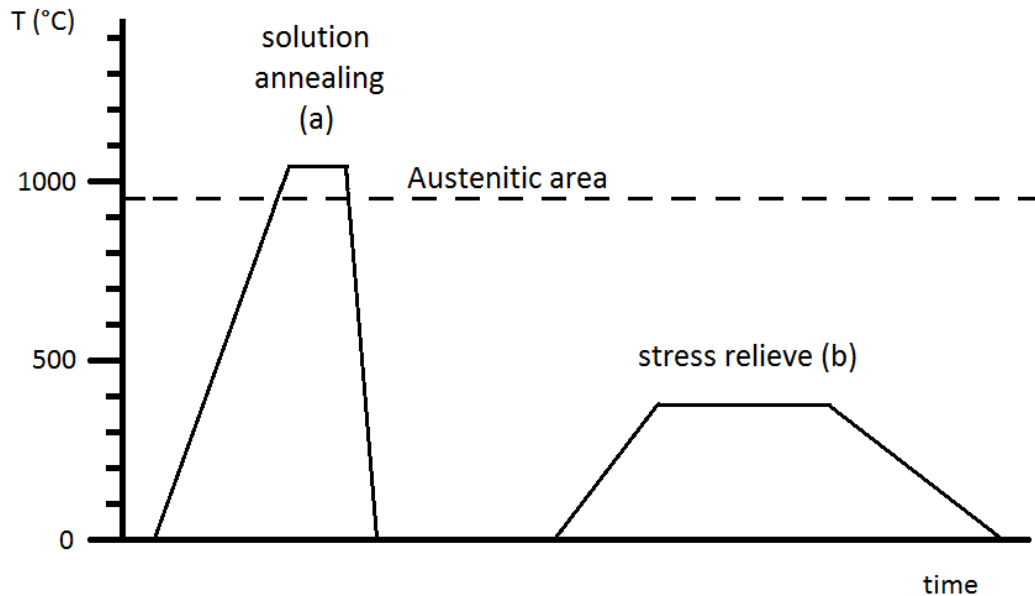


Figure 24 : Solution annealing (a) and stress relieve (b)

Solution annealing is conducted by holding the material at a temperature of 1040 to 1080 °C [27]. This is done in an inert gas environment to negate any corrosion during the process. The material will be brought into austenitic area where all microstructures are reformed to an austenitic state. This will relieve any residual stress in the material, give better corrosion resistance, but will give a lower yield and ultimate tensile strength. It will also have a homogenizing effect on the material [28]. This could possibly undo the anisotropy seen by I. Tolosa [15]. When using a solution annealing a rapid cooling is advised to reduce the chances of sensitisation, but this will induce new residual stresses within the product, cooling slowly will cause sensitisation in the material. This sensitisation is a phenomenon that occurs in stainless steel when staying at elevated temperatures for a long time. It involved the precipitation of chrome carbides drawing away the chrome molecules from the edges of the microcrystals, creating areas between the crystals that are depleted of chrome molecules. Since chrome is the element causing the protective corrosion layer these areas will be sensitive to corrosion, degrading the stainless character of the steel. [29]

K. Saeidi [30] has performed some research into the heat treatment of SLM printed stainless steel 316L. He said the following “The laser melted 316L stainless steel samples consisted of austenite with small amount of ferrite and a microstructure consisting of submicron (<0.5 μm) cells with dislocation and Mo-enriched boundaries within large (10–100 μm) size grains.” High temperatures eventually lead to a structure of austenite crystals with some ferrite structure. He also saw a large effect on the hardness of the material and a minor effect on the strength as shown by Table 3.

Table 3 : Effects of heat treatment at different temperatures on the hardness and yield strength and ultimate tensile strength seen by K. Saedi [30].

	as build	800°c 1h	900°c 1h	1100°c 1h	1400°c 1h
Hardness (HV)	325	250	230	190	200
Yield strength (MPa)	456				419
Tensile strength (MPa)	703				674

Stress relieve treatment without loss of corrosion resistance can be obtained by a longer treatment at a maximum of 400°C as advised for 316L [27] with a slow cooling. The low temperatures will ensure that no sensitization of the material occurs during the slow cooling and residual stresses are relieved without inducing new stresses.

3 SLM Experiment setup

3.1 Goal

The goal of this experiment is to expand the knowledge of selective laser melting of 316L stainless steel using a Renishaw AM250. As mentioned before, it is not easy to get a full view on the effect of parameters on the material properties from the available literature. To expand this knowledge I will build upon the research conducted by A. Cherry [17] who used the same machine and material. It also serves as a starting point for the production of cooling channels in a mould made out of Maraging steel, so the parameters are steered towards better overhangs. To this end properties like the geometrical freedom and dimensional accuracy are attempted to be optimised. It is important that material properties such as density, surface quality, strength are sufficiently retained.

The general idea to reach these goals is by varying parameters around the standard parameters now used by Renishaw. Which parameters are to be used is based on the literature.

3.2 Product design

The test product used in this experiment is built upon the benchmark designed by J-P. Kruth [18]. Tubes in different shapes were added to simulate the production of cooling channels. The original design by J-P. Kruth [18] is a block of 50x50x10 mm and entails a set of geometrical features that have proven to be difficult for laser and powder based additive manufacturing techniques to produce. Table 4 (P. 51) shows the shapes and the sizes of their important features by J-p Kruth [18] and those added in this experiment, Figure 25 (P. 51) shows where each feature is situated.

There are circular holes with different dimensions. A channel of 2 mm is the smallest conformal cooling channel that permits a useful flow of coolant, 3 mm is the most likely size to be used for conformal cooling. A tube with a diameter of 5 mm is already included in the original design. Diameter 8 mm is the largest horizontal channel deemed possible by Layerwise [31], to see whether this machine outperforms or underperforms to this standard tubes with 9 mm and 7 mm are also present.

Next are triangular holes with different angles, these represent the possibility to make channels that follow the surface of a sloped product. M. Van Elsen [14] wrote that the minimum possible slope is 45°, this angle is used here and to check whether this is the limit triangles with 40° and 50° were added. Layerwise [31] says that the lowest angle possible is 60° and again variation of the angle in the form of 55° and 65° were added.

Square channels with straight edges in different sizes were added to see what overhangs were possible. The smallest overhang is one of 0,75 mm which should have a good quality because the largest overhang deemed possible by Layerwise [31] is 1 mm. From this point on the overhangs grew larger with 1 mm until the size of 5 mm, as in the original design by J-P. Kruth [18].

Circular tubes with turns were also added. Each turn had a radius equal to the diameter of the hole. These had similar diameters to the circular tubes with the 2 mm diameter being the smallest considered useful and 3 mm the most likely to be used. The one with 5 mm is to compare with the tube in the original design and a diameter of 6 mm is the largest that could fit into the 10 mm high part.

All horizontal tubes were 15 mm long. Though in chapter 2.4.2.6 was said that the diameter should be slightly bigger than the intended hole diameter, the holes were modelled with the diameters as seen in Table 4.

The biggest tubes, which are most likely to fail, are positioned above the smaller tubes. In that way the smaller tubes, less prone to fail, are printed before the coater can be damaged. The idea was to have the spreader move in the direction of the axis of the overhangs so if the coater gets damaged the other overhangs would not be hindered. During the execution however the spreader direction was perpendicular to the overhang axis.

Nr.	Shape	Direction	Important feature	Sizes			Unit			
J-P Kruth										
1	sharp corners	vertical	top angle	14	30	45	°			
2	thin walls	vertical	wall thickness	0,5	1	0,25	0,25	mm		
3	circular holes	vertical	diameter	0,5	1	2	5	mm		
4	cilinders	vertical	diameter	0,5	1	2	5	mm		
5	sloped corner	side wall	from side wall	80			°			
6	thin plane	horizontal	thickness	2			mm			
7	circular tube	horizontal	diameter	5			mm			
8	sqaure tube	horizontal	horizontal length	5			mm			
9	round corner	horizontal	radius	3			mm			
Added features for this experiment										
10	circular tube	horizontal	diameter	2	3	7	8	9	mm	
11	triangular tubes	horizontal	lower angle	40	45	50	55	60	65	°
12	sqaure tubes	horizontal	horizontal length	0,75	1	2	3	4	mm	
13	upward circular turn	transition	turn radius = diameter	2	3	5	6	mm		

Table 4 : The shapes and the sizes of the important features in the experimental design

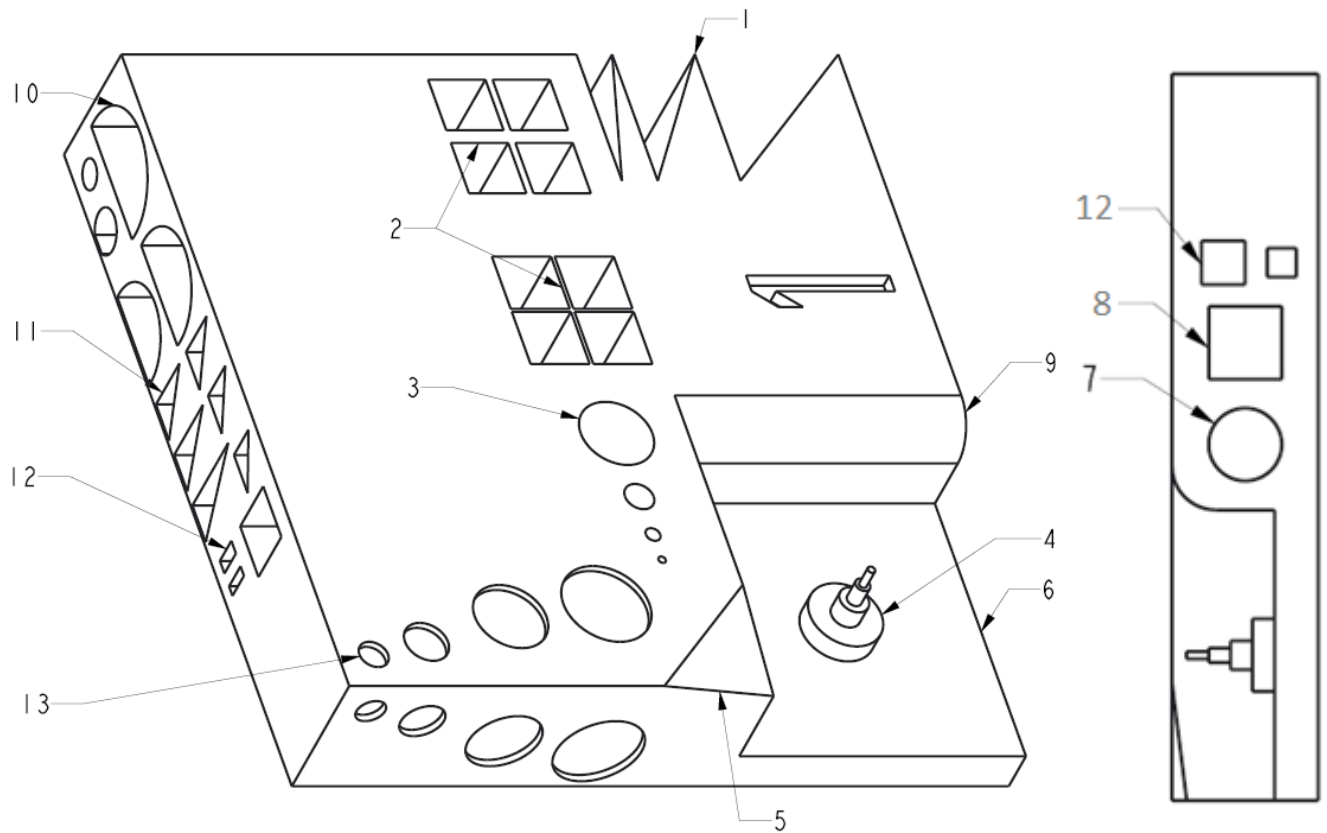


Figure 25 : The experimental design with indication of the position of the different shapes

To assess the strength, elongation and density, tensile pieces were added as shown by Figure 26. Based on the possible strength seen in an article by I. Tolosa [15] the diameter had to be reduced to be able to use them on the 10 kN tensile test bench in Derby. The reduced diameter is featured in Figure 26.

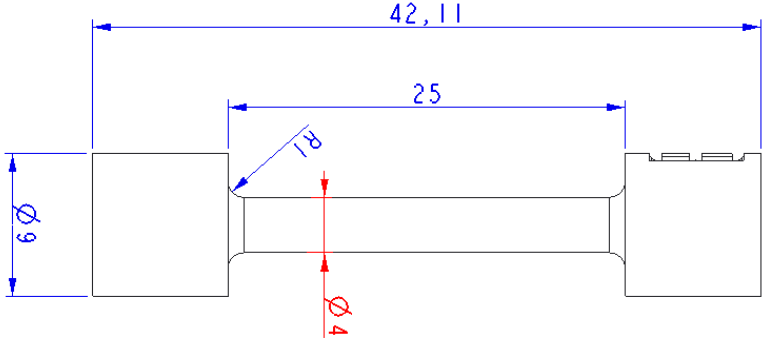


Figure 26 : The design of the tensile test pieces used in this experiment.

3.3 Setup

The machine used for this experiment is a Renishaw AM250 (Table 5, Figure 27) situated at the Institute for Innovation in Sustainable Engineering (IISE) at the University of Derby. This machine possesses a modulated ytterbium fiber laser from SPI Lasers with a wavelength of 1.070 μm and a spot size of 0.07 mm. It has a baseplate with a surface of 250x250 mm, is capable of printing pieces up to 300 mm high and creates a vacuum in the build chamber before inert gas is injected. The machine uses a soft coater to distribute a new powder layer.

Table 5 : Technical specification Renishaw AM250

AM250	
Max. part building area	245 mm x 245 mm x 300 mm (X, Y, Z) (360 mm Z axis by request)
Build rate*	5 cm ³ - 20 cm ³ per hour
Layer thickness	20 μm - 100 μm
Laser beam diameter	70 μm diameter at powder surface
Laser options	200 W
Power supply	230 V 1 PH, 16 A
* Build rate is dependent upon material, density and geometry. Not all materials process at the highest build rate.	



Figure 27: The Renishaw AM250 at the IISE in Derby

The software used by the Renishaw machine is a custom version of AutoFab, called Renishaw AutoFab. This software can be used to slice the model into layers, select and customize the parameters, create support structures and arrange the to-be-printed product on the build plate before sending it to the SLM machine.

The baseplate (Figure 10), upon which the product is printed, is a ground stock 15 mm thick plate made out of mild steel BS 4659 B01 equal to oil-hardened and cold worked AISI O1 steel. Using mild steel instead of 316L stainless for the baseplates reduces the cost without loss of quality. 15 mm is the minimum thickness to prevent thermal deformation in the baseplate.

The powder used is a 316L stainless steel powder (1.4404) (Table 6) with a spherical particle size of 15 to 45 μm produced by LWP technologies [32] but supplied via Renishaw. The chemical composition of the powder is shown in Table 7.

Table 6 : Properties of 316L stainless steel produced with SLM from Layerwise

Stainless Steel AISI 316L		UNS S31603	DIN: X2CrNiMo17-12-2	EU: 1.4404
Dimensional	Typical part accuracy*	small parts	$\pm 50 \mu\text{m}$	
		large parts	$\pm 0.2 \%$	
	Typical surface roughness*	Ra	4 - 6.5 μm	
		Ry	20 - 50 μm	
Density	Relative density	approx. 100 %		
	Absolute density	7.9 g/cm ³		
Mechanical	Ultimate tensile strength	645- 670 MPa		
	Yield strength (Rp 0.2 %)	500-540 MPa		
	Elongation at break	30-38 %		
	Young's modulus	165-177 GPa		
	Hardness	220 HV 20 HRC		
	Impact toughness (notched)	30 J/cm ² DMV _{probe}		
Thermal	Coefficient of thermal expansion	0 - 100 °C	16.4 $\mu\text{m}/\text{m}\cdot^\circ\text{C}$	
		0 - 300 °C	18.6 $\mu\text{m}/\text{m}\cdot^\circ\text{C}$	
	Thermal conductivity	at 20 °C	15 W/m.K	
		at 100 °C ¹	16.3 W/m.K	
		at 500 °C ¹	21.5 W/m.K	
	Specific heat capacity ¹	500 J/kg.K		
Melting point ¹	1375 - 1400 °C			
Electrical ¹	Electric Resistivity	740 n Ω .m		
	Magnetic Permeability	1.008		

Table 7 : Composition of 316L stainless steel powder by LWP technologies [32].

Elements	C	Cr	Cu	Fe	Mn	Mo	Ni	P	S	Si
percentage	0.03 max	17.5-18.0	0.50	Bal	2.0 max	2.25-2.50	12.5-13	0.025 max	0.01 max	0.75 max

3.4 SLM Parameters

3.4.1 *Constant parameters*

Table 8 shows an overview of the constant SLM parameters. The variable parameters used for the experiment are described below.

Table 8 : Overview constant SLM parameters

Layer thickness	For 316L stainless steel standard parameters for two layer thicknesses are supplied by Renishaw being 30 μm and 50 μm . A layer thickness of 50 μm was chosen because this is the value used in the IISE and almost all the literature about 316L used 50 μm layer thickness, it also decreases build time.
Shielding gas	As shielding gas was used Argon. This gas is standard for any AM250 and is proven to give the best density by B. Zhang [16] as seen in chapter 2.4.
Preheat temperature	Though preheating of the build plate showed significant improvements in B. Zhang's [16] experiment, no preheat temperature is employed in the standard Renishaw parameters. Setting a preheat temperatures would change the effect of the standard parameters because the temperature difference between powder and melt pool would be far less, possibly causing unwanted properties such as less dimensional accuracy. This is why no preheat temperature is used here. Another reason is that A. Cherry [14] does not use preheat temperatures either.
Scan strategy	The standard Renishaw parameter set has 2 different types of scan strategies. As seen in chapter 2.4 these are the checkerboard and meander type, both scan strategies have different laser parameters. Checkerboard was chosen because J-P. Kruht [21] had proven this to reduce the residual stresses within a product. The contours of every layer are traced with different parameters as is standard in the Renishaw software.
Volume area	The volume area consists of the laser parameters for the bulk material of the product.
Overhang area	The overhang area consists of the laser parameters for the production of overhangs. The use of the overhang area parameter seemed very interesting because overhangs are needed to make internal conformal cooling channels. But the parameters for the overhang areas being not active in the standard parameters and the energy density being far below that of the volume area led to the decision not to use these parameters.

Volume offset area	The volume offset hatch gives the parameters for the creation of added volume outside the original model, this can be used to create smooth surfaces by milling of the offset volume to the original model size. Offset volume is not necessary in this experiment.
Volume border	Volume border gives the laser parameters used to trace the contours of the volume area. This is standard activated in Renishaw parameter.
Overhang border	Overhang border are the laser parameters for the contours of the overhang areas.
Skin area	The skin area parameters are used when the top surface is re-melted to get a better surface finish..

Within this checkerboard parameter set different laser parameters can be used for different areas. Figure 28 shows the areas that are distinguished by the Renishaw software. The main parameters are used in the yellow checkerboard patterned area. This is the volume area. The contours of this area are lined in red, called the volume border. The grey area using the stripes pattern is called the overhang area used to create overhangs, in this case horizontal tubes with turns.

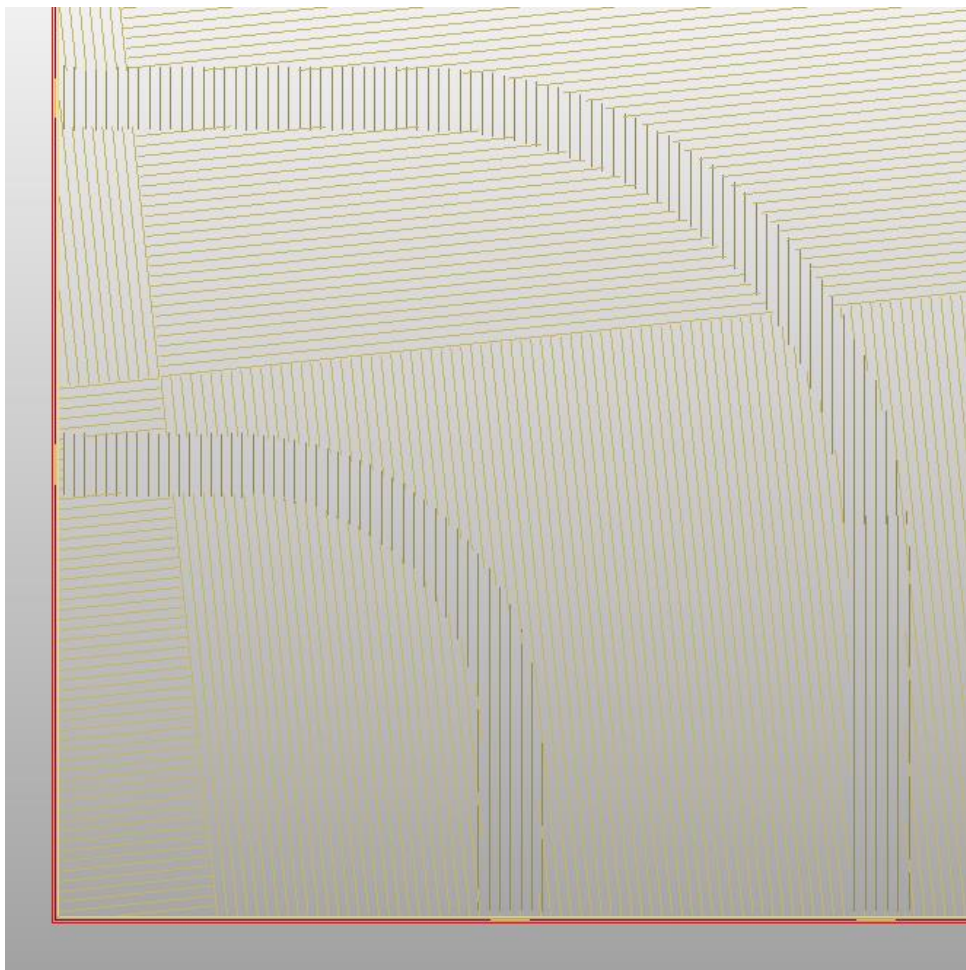


Figure 28 : An image from the Renishaw AutoFab software showing the different areas.

In the standard parameters, as delivered by Renishaw, most of the options are not active, meaning only the volume area parameters are used and their volume border parameters. The values for the different parameters are given in Table 9, the first column shows whether the sub area of column two is used in the standard parameters.

In Standard parameters	sub area	scan spacing (mm)	Power (W)	Scan speed		scan speed (m/s)	Spot size (mm)	Energy density (J/mm ³)	hatch type
				Exposure time (μs)	Point distance (μm)				
	volume area	0,11	200	120	50	0,417	0,07	87,27	checkerboard
inactive	overhang area	0,12	100	50	40	0,8	0,07	20,83	stripes
inactive	volume offset hatch	0,11	200	100	65	0,650	0,07	55,94	checkerboard
	volume border	/	50	150	80	0,533	0,07	26,79	
inactive	overhang border	/	100	50	40	0,800	0,07	35,71	
inactive	skin area	0,12	100	100	60	0,600	0,07	27,78	meander

Table 9 : Standard Renishaw parameters for checkerboard and 50 μm layer thickness

The standard parameters were used, leaving all inactive sub areas in the standard parameters inactive and changing only the volume area parameters.

3.4.2 Variable parameters

The parameters that are varied are power and scan spacing. The main reason for this choice is the fact that A. Cherry [17] has already investigated the parameters making up the scan speed as was seen in chapter 2.4.3.5, using the same machine and the same material. The next parameters that are most important to the SLM process are the laser power and the scan spacing. Where ever possible the parameters are kept the same as those used by A. Cherry [17] to consolidate the correlation between my project and her study.

The secondary focus of this experiment was the creation of overhangs. As mentioned in chapter 2.4.3.4 lower laser power is needed to make good overhangs, the penetration within the previous layers is less with lower laser power causing less stalactites on the underside of the overhang.

M. Van Elsen [14] found that lower scan spacing give better overhangs. In this experiment it would be a too big leap from the standard Renishaw parameters to go to a scan spacing lower than 5% of the spot size, such as used by M. Van Elsen [14]. The idea is that as the overlap of the melt pools is higher, the newly melted pool melts better into the adjacent track, preventing the melt pool from spreading into the powder below, creating stalactites. A visual representation is shown in Figure 29.

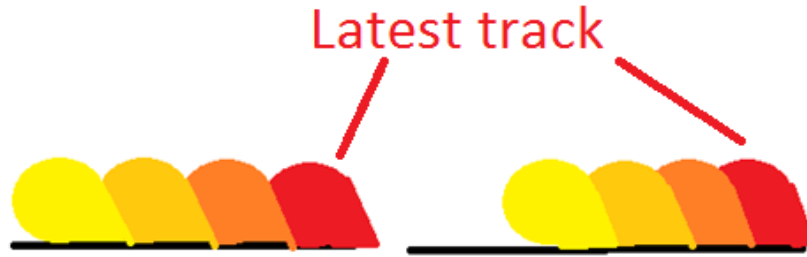


Figure 29 : Representation of the theory behind lower scan spacing

The values of the scan spacing and laser power used in this experiment are shown in the top left table of Table 10, in the top right table the parameters that were used by A. Cherry [17] are shown for comparison, each table contains the energy densities used. It has to be noted that the laser density values are different than those in the article, doing the same calculation as explained by the article, I calculated different energy density values for the parameters, these are the ones used here. These parameters are only varied for the volume area, the rest of the parameters stay as they were given in Table 3, the constant parameters here and from A. Cherry [17] are also given in Table 10, the parameters between brackets are those that are variated. In both experiments no preheating, no re-melting and Argon shielding gas was used.

Table 10 : Top Left: the parameters for laser power and scan spacing used in this experiment. Top Right: the parameters used by A. Cherry in her experiment, each table contains the energy density belonging to each parameter set. Down middle: the setting of the other parameters for this experiment and for the experiment by A. Cherry

Parameters used in this experiment

	Energy density (J/mm ³)	Power (W)		
		150	175	200
Scan spacing (mm)	0,13	55,38	64,62	73,85
	0,11	65,45	76,36	87,27
	0,09	80,00	93,33	106,67

Parameters used by A. Cherry

	Energy density (J/mm ³)	Point distance (μm)		
		25	50	75
exposure time (μs)	75	87,10	43,55	29,03
	100	116,13	58,06	38,71
	125	145,16	72,58	48,39

	Scan spacing (mm)	Power (W)	Exposure time (μs)	Point distance (μm)	Layer thickness (μm)	Spot size (mm)	Energy density (J/mm ³)	hatch type
Renishaw (Now)	(0,11)	(200)	120	50	50	0,07	87,27	checkerboard
A. Cherry	0,124	180	(75)	(25)	50	0,07	87,10	meander

There can be seen in Table 10 that the scan spacing goes to 0,13 mm because A. Cherry [17] at 72.6 J/mm³ saw that the track width is 0,07 to 0,08 mm thereby advising not to go over double this value for the scan spacing, going down to a laser power of 150 W will make the track width even smaller, making 0,13 mm around the border of that limit. To make it a balanced experiment the same increment downwards was used resulting in a scan spacing of 0,09 mm. The laser power was only decreased because the maximum power output of the Renishaw machine is 200W and lower laser power should give better overhangs. The amount of variation of power is based on the fact that A. Cherry [17] saw the best properties for energy densities from 72,58 to 87,10 J/mm³. In this experiment the energy density was kept around those values.

This brings the total to 9 different parameter sets. With each parameter set 1 test piece and 3 tensile pieces in different directions are printed. The parameter set with the standard Renishaw parameters has an extra set of 3 tensile pieces in different directions for possible heat treatment.

3.5 Test design

Due to a limited budget I was only able to perform one print job for this experiment. This meant I had to use the baseplate surface as efficiently as possible leading up to the experimental setup as seen in Figure 30.

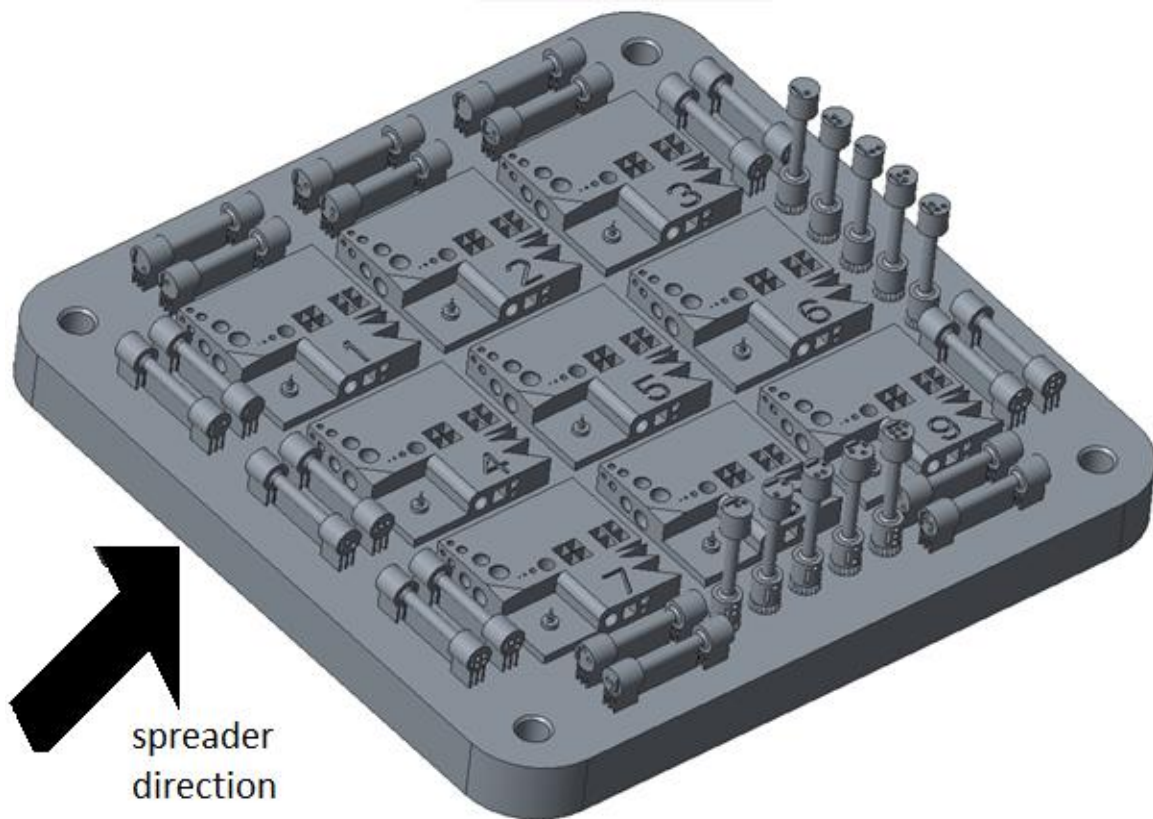


Figure 30 : Experimental setup of print job

The test pieces themselves are placed flat upon the baseplate and are numbered from 1 to 9 corresponding to the number of the used parameter set. Due to the anisotropy seen by I. Tolosa [15] for each parameter set 3 tensile test pieces were printed in different directions, one vertical (T0.3), one horizontal with its axis perpendicular to the direction of the movement of the spreader (T0.1) and one also horizontal parallel to this movement (T0.2). In total there were 30 tensile pieces marked with simple and easily distinguishable markings that are compatible with the capabilities of the process. The spreader direction was perpendicular to the overhang axis, as shown by the black arrow in Figure 30.

The way the pieces were printed is shown in Figure 31, in Table 11 the code of the pieces corresponding to their parameters are given.

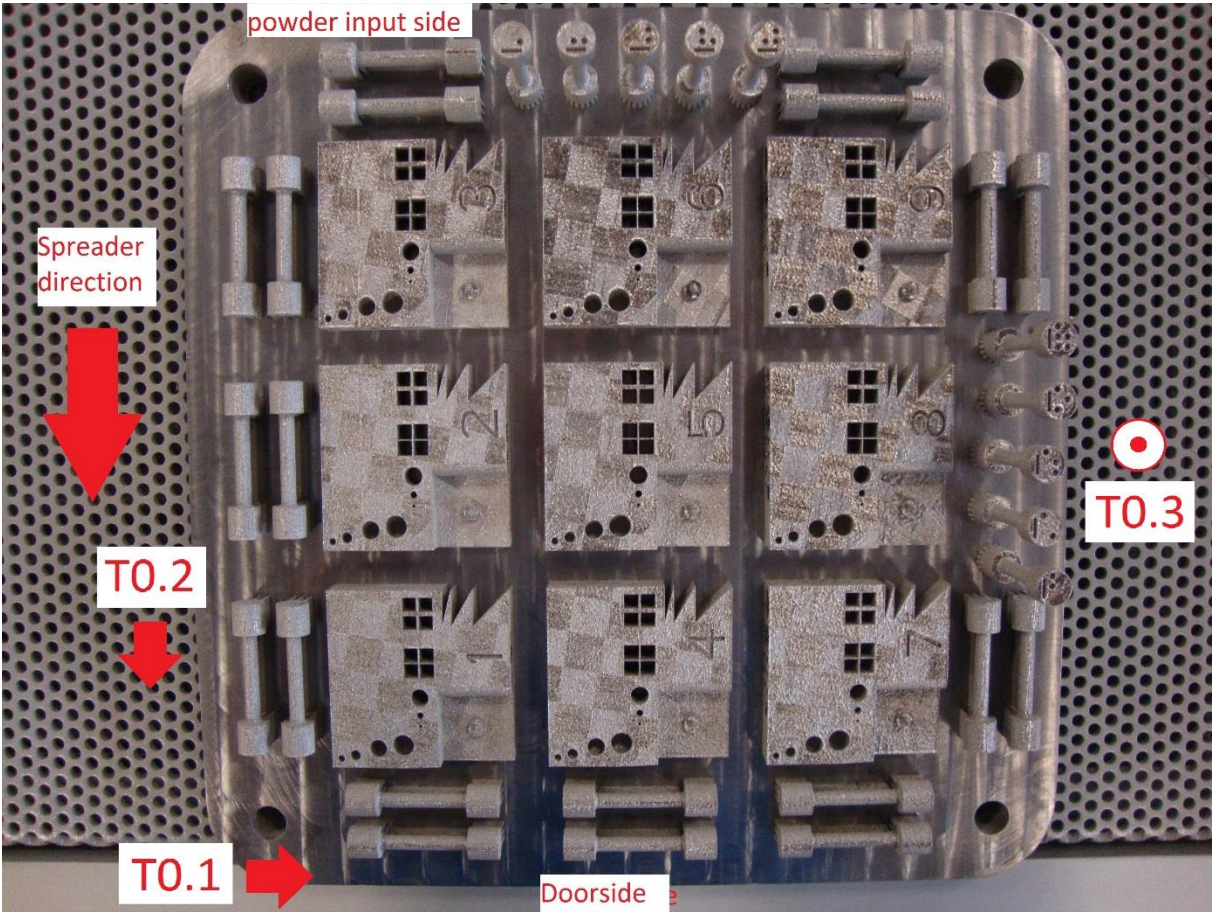


Figure 31 : The base plate after printing in the position it was printed

Table 11 : The coding corresponding to each parameter set

		Scan spacing (mm)		
		0,13	0,11	0,09
Power (W)	200	3	6	9
	175	2	5	8
	150	1	4	7

Figure 32 visualizes the coding of the tensile pieces with the first number representing the used parameter set and the second number representing the direction in which it is printed. This code is represented in the print with stripes and dots (Appendix B).

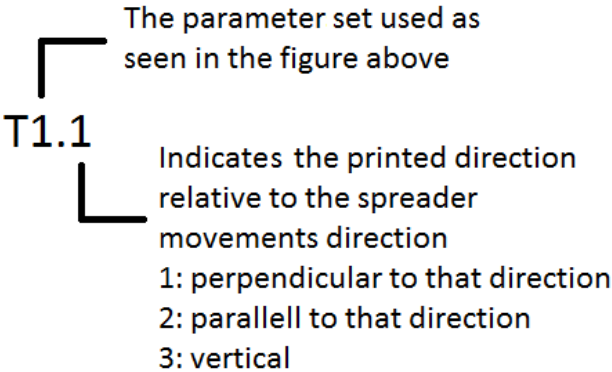


Figure 32 : Explanation of the tensile pieces coding

4 Experiment execution

4.1 Execution

In the first attempt the baseplate moved far below the normal height and printing proceeded incorrectly. A second and a third attempt showed a bad spread of powder.

After adding an extra few empty layers to the model to negate any defects caused by flawed first layers, another attempt was made. There were no problems with the plate moving downwards or with the spread of the powder and the printing process was started. A close eye was kept on the first few layers to spot any difficulties. Some of the parameters viewable on the panel of the SLM machine were kept track of for the first layers, these are displayed in Table 12. The "baseplate T" is the temperature of the baseplate, with no preheating, the temperature starts at room temperature. The dosing is the percentage of powder used for every layer relative to an unknown amount of powder per layer. The chamber pressure is self-explanatory and the oxygen level (Bottom) is the oxygen level at the bottom of the chamber where the melt pool is made.

Table 12 : Important parameters over different layers

Layer	baseplate T (°C)	Dosing (%)	chamber pressure (mbar)	Oxygen level (bottom) (ppm)
0	22	100	17	470
2	27	100	17	59
4	31	100	17	4,8
5	33	100	17	1,4
6	34	100	17	0,128
8	36	40	18	0,003
10	38	60	17	0,001
13	40	60	16	0
14	40	60	17	0
18	42	60	17	0
170	53	50	10	0
171	52	50	10	0

The fact that even without preheating, the baseplate temperatures rises to an equilibrium at 53 °C is due to the balance between energy input from the laser and the cooling of the baseplate. Mrs. Mertens, a PhD. student at the KU Leuven suspects that the temperature probe of the Renishaw AM250 is placed farther from the baseplate because normal temperatures measured during a print with 316L at the KU Leuven are around 100°C. The chamber pressure was always at vacuum and the amount of oxygen at the bottom of the chamber is zero after a few layers and remains so.

The first few layers use a maximum amount of powder per layer to get enough powder into the chamber. After the first layers the dosing is set to a standard of 40 % to conserve powder. However at this switch a notable area depleted of powder was seen at the door side, farthest from the powder input. Figure 33 shows this area covering a large part of piece 7 (right) and a part of piece 4 (left) and all the tensile piece after these. Increasing the powder dosing to 60 % solved this problem promptly, later the dosing was decreased to 50% again.

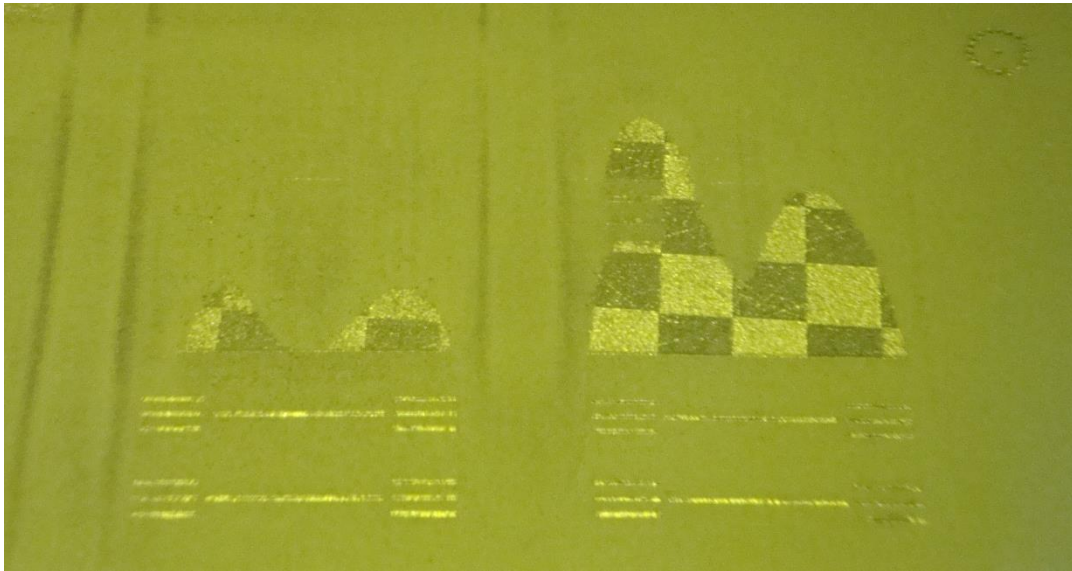


Figure 33 : Picture of the powder depleted zones at layer 9, the left piece is part number 4 and the right piece is part number 7

The print was started 12/05/2015 at 16:20 and finished 14/05/2015 at 03:00. The estimate build time was 26 h with a build rate of 7,44 cm³/h, the actual build time was 34,5 (5,30 cm³/h). The settings for the calculation of the build time were incorrect.

The time to print one surface of 50x50 mm was timed in 1 layer for the 3 separate pieces. These results (Table 13) clearly indicate that the print time is directly proportional to scan spacing. The time between each layer has to be calculated in when calculating the build time, this time can be chosen in the settings. Generally spreading powder faster gives more chances of flawed layers.

Table 13 : Scan spacing compared to print time of 1 layer of 1 test piece

Scan spacing (mm)	difference (%)	pieces	time (s)	average (s)	speed (mm ² /s)	timed percentage (%)
0,13	118	1	48,18	48,42	52	117
		2	48,45			
		3	48,62			
0,11	100	4	56,42	56,58	44	100
		5	58,23			
		6	55,1			
0,09	82	7	68,36	68,41	37	83
		8	67,92			
		9	68,96			

4.2 Visual inspection

4.2.1 Analysis

Inspection of the soft coater after printing shows no major cuts in the silicon, this indicates that there were no major failures for any of the pieces. A lot of small scratches are seen in the silicon, presumably because of the large surface printed.

The only flaw of which the consequence is clearly seen in the pieces is a protruding piece that has brushed away the powder of a set of layers, dependent on when the cut was made. The consequence is a line across pieces 1, 2 and 3. The cut (black circle) and its consequences (red arrows) are shown in Figure 34. Notable also was that more and deeper marks were seen from left to right, this could be caused by a slight misalignment of the spreader or could be linked to the apparent rising roughness from left to right, from higher scan spacing to lower scan spacing.

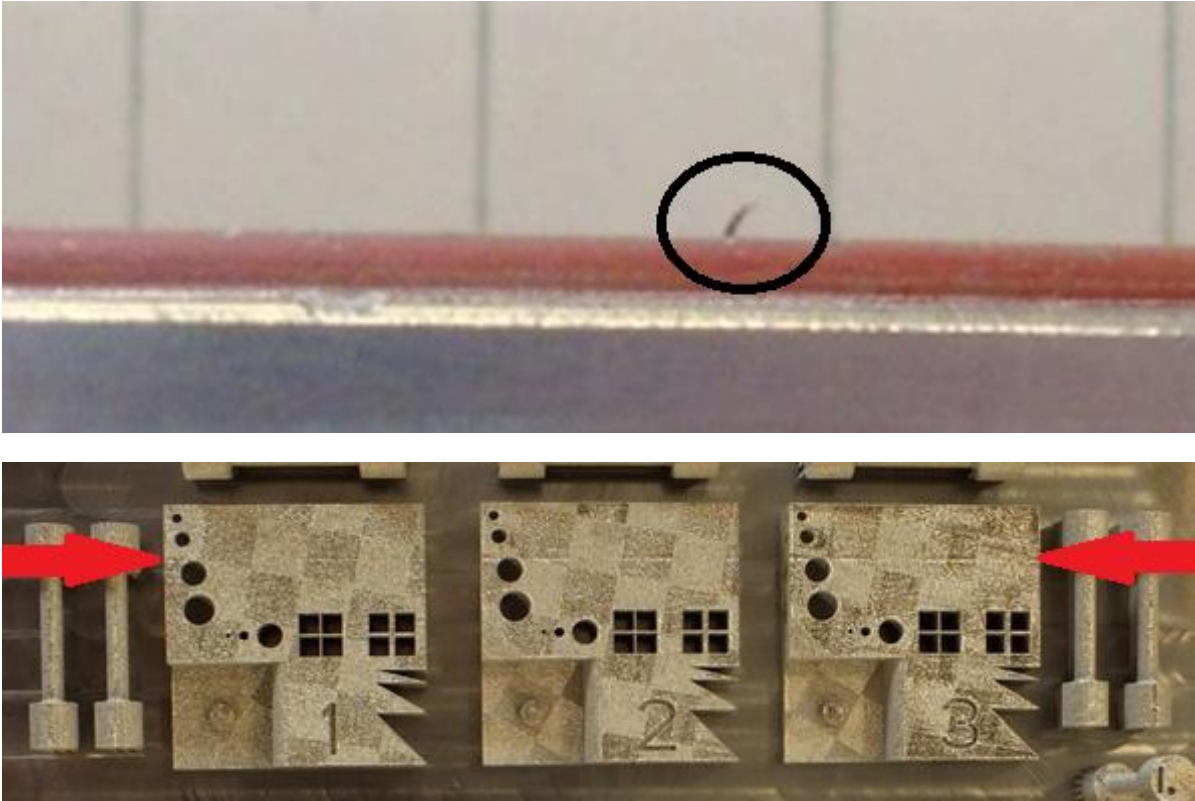


Figure 34 : Top: A protruding piece caused by a cut in the soft coater. Bottom: The consequence of the protruding piece a clear line across pieces 1, 2 and 3.

Figure 35 shows an overview of the finished print job, the number on the test pieces corresponds to the number of the parameters sets shown in Table 11 (P. 61).

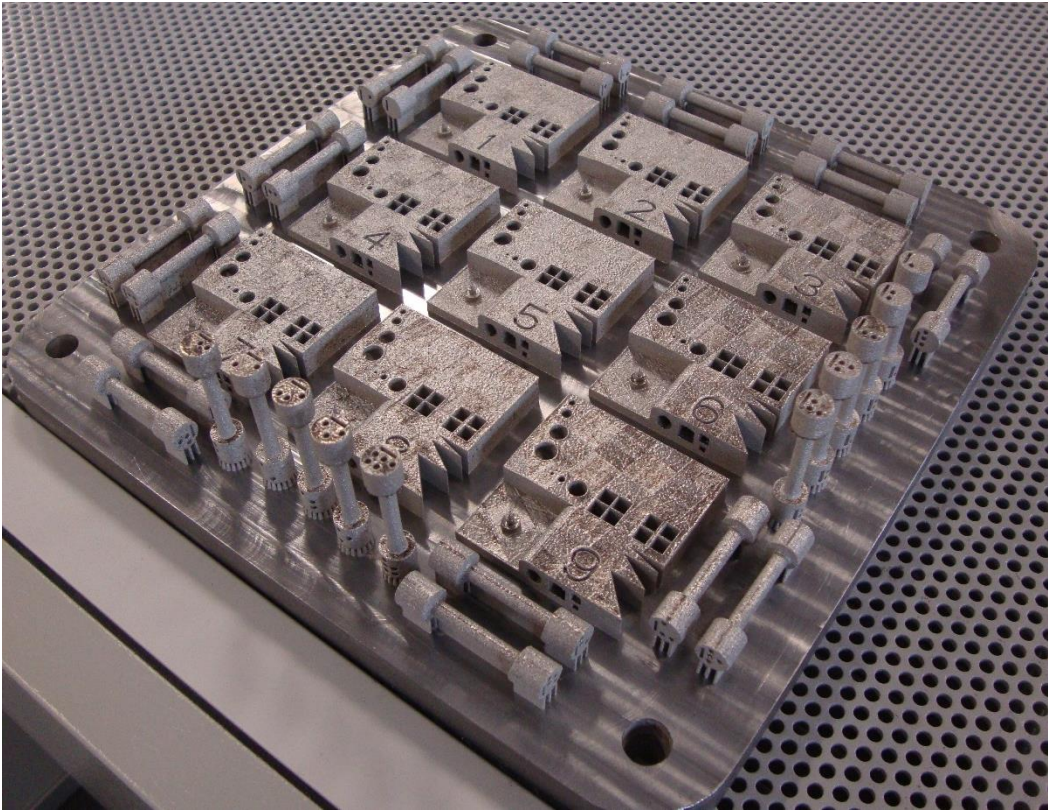


Figure 35: The baseplate after the finished print job

Because EDM is very expensive and this project has a lot of surface, a cheaper alternative is removing the tensile pieces with an angle grinder and cutting the plate in pieces for easier access for the visual assessment.

In general all vertical features had an excellent quality for all of the pieces. Figure 6 shows a top view of piece number 6 as an example. Though all the pieces show some balling and protruding edges on the sides.

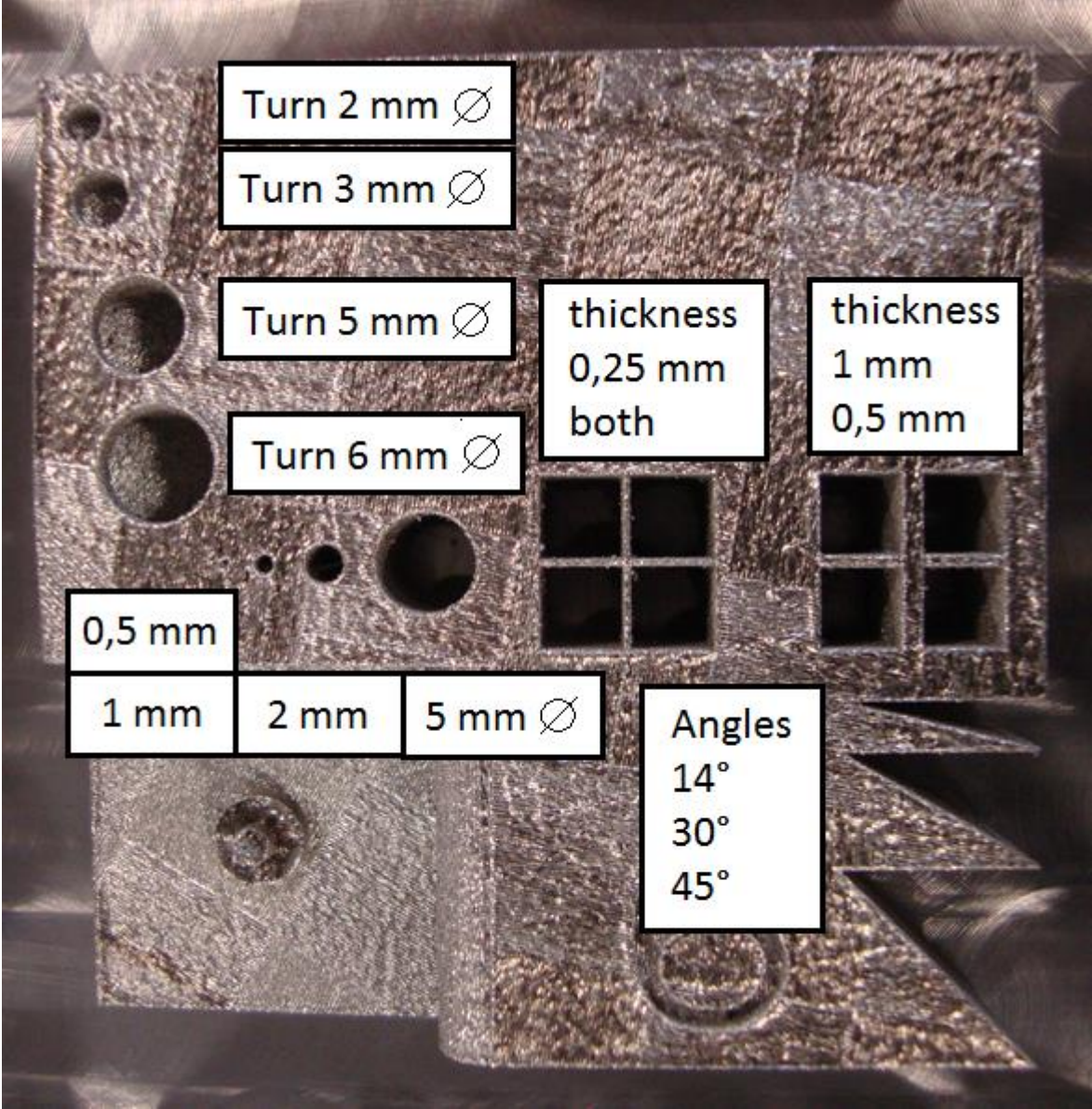


Figure 36 : Top view of a piece number 6

The cylinder of 5 mm, 2 mm, 1 mm were all made very well in all the pieces. The 0,5 mm cylinder was very fragile, some were sloped and balling on the side easily distorted the cylinder. This was not related to the difference in parameters, none of the laser parameters were able to create this feature.

Only the 0.5 mm vertical hole seemed to be affected by the difference in laser power and scan spacing. A too low energy density seen in piece 1 creates a severely misshapen hole, while a medium energy density in 2, 3, 4, 5 and 7 has an open hole with little obstruction. A too high energy density seen in piece 6, 8, 9 has the whole nearly closed.

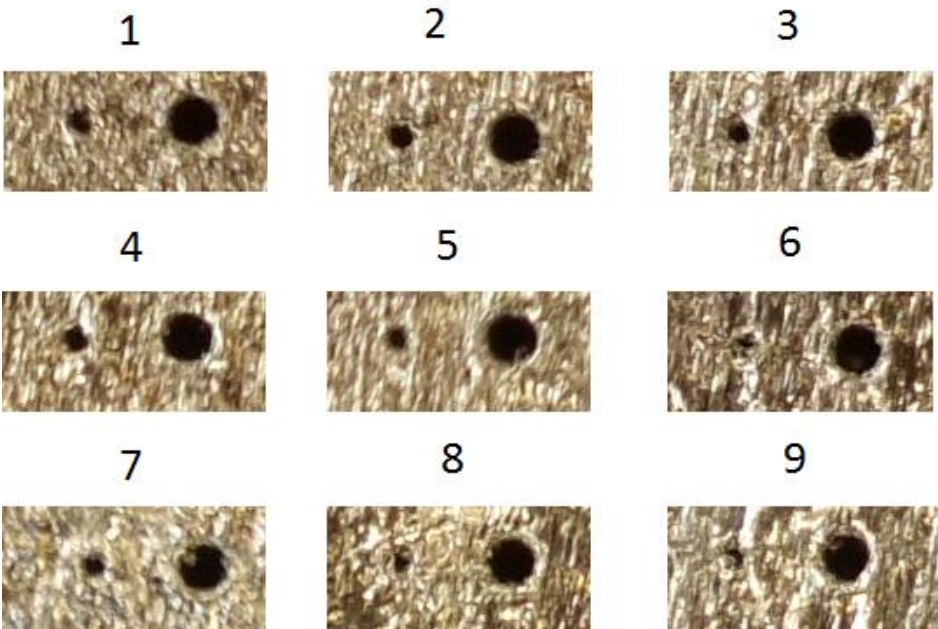


Figure 37: Comparison of the 0,5 mm and 1 mm diameter vertical holes

The top surface of all the pieces contained balls and was very rough. Pieces with higher scan spacing and higher energy contained more balling, Figure 38 shows an example of such balling (black and red circles) on piece number 6 (200W; 0,11 mm; Renishaw standard parameters).

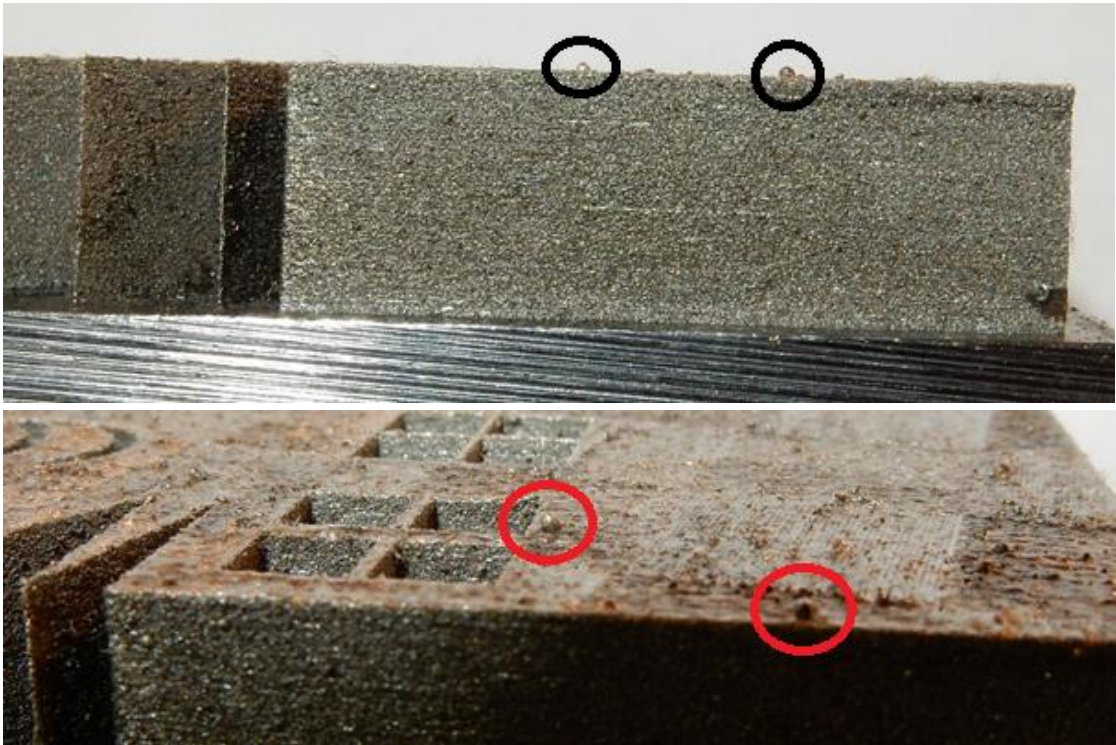


Figure 38: Example of the balling seen on the top surface, piece number 6 in this example

A sink mark, such as described in chapter 2.4.2.6 by D. Thomas [21], was seen at the horizontal circular tubes of 9 mm as shown in Figure 39. This thermal deformation was the same for all of the pieces, it is apparent that a wall of 1 mm at the thinnest point is too little to have a good shape. The deformation starts 10 mm from the edge as shown in Figure 39 (bottom picture). Tubes of 15 mm length with a diameter of 9 mm and a smallest wall thickness of 1 mm can only be 5 mm long. In all the pieces this side showed an increase in balling on the side surface.

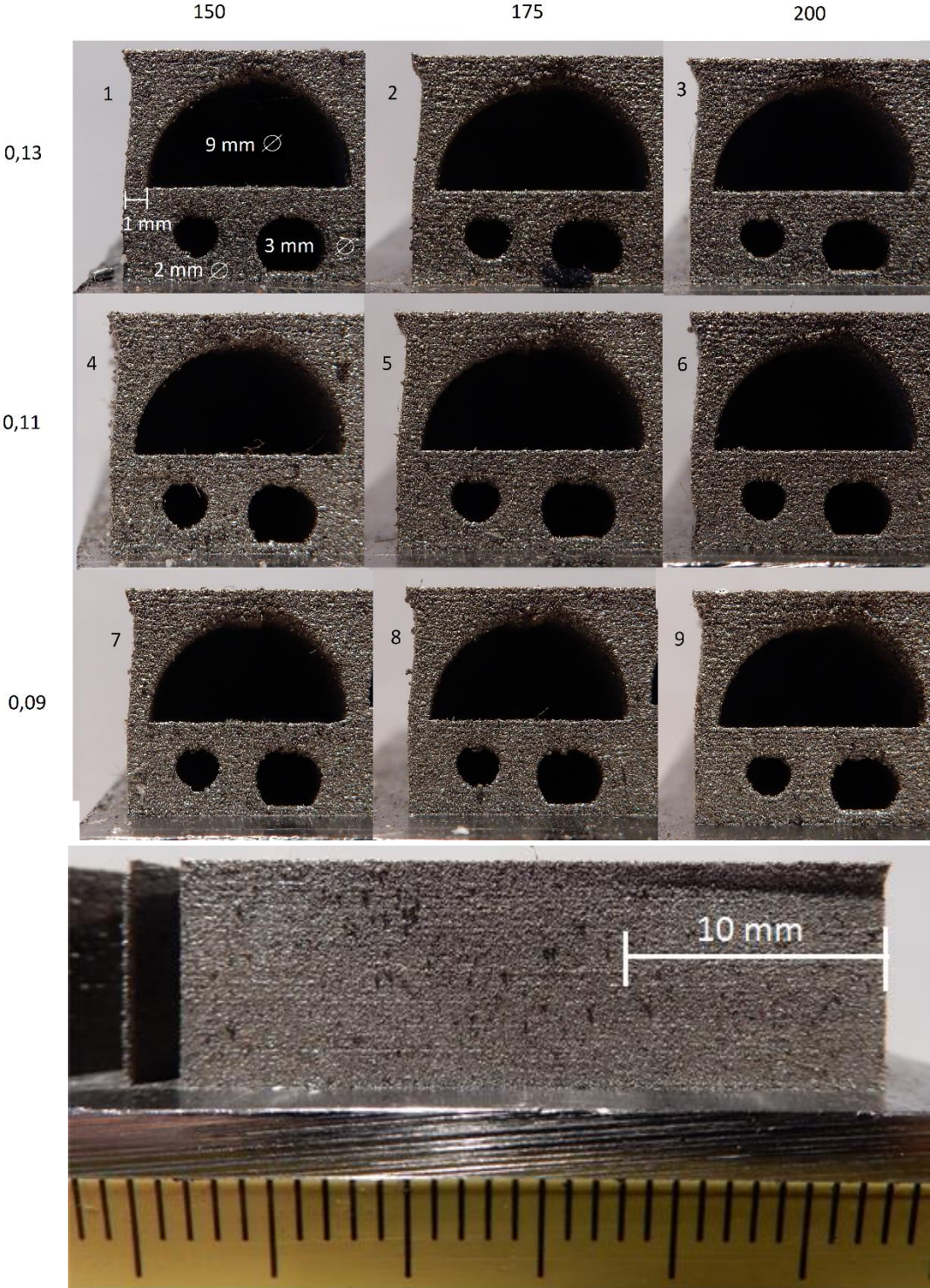


Figure 39: Top comparison of the deformation around the horizontal circular tube of 9 mm diameters, below: side view of the deformation of piece number 5

Figure 39 also shows a few of the horizontal circular holes, the holes all look very similar, but when going into the details piece 1 has the best overhang quality of all the pieces. The quality gets worse as the scan spacing decreased and power rose, this can be seen as the overhang gets lower and lower. This is consistent with the theory of the higher penetration due to the higher laser power but not with the theory that the lower scan spacing would give better overhangs. In this case the increased energy density caused by the lower scan spacing has a larger effect on the overhang quality. Despite the sagging of the 9 mm diameter hole, as was seen also by D. Thomas [21] in chapter 2.4.2.6, the quality is acceptable for industrial use for all the pieces. As mentioned in the experiment design Layerwise [31] claimed that 8 mm was the maximum possible diameter of the hole. The overhangs with diameter 8 and 7 mm were also of acceptable quality for all the pieces.

The triangular tubes (Figure 40) with angles 45° to 65° had a good quality for all the pieces. Those with 40° have a small imperfection at the top of the triangle (marked with a red arrow). For the larger angles, blobs of molten material can be seen in the bottom horizontal area, these are not seen in any of the other overhangs and grows as the laser power increases. These results confirm M. Van Elsen’s [14] statement of 45° being the maximum angle possible.

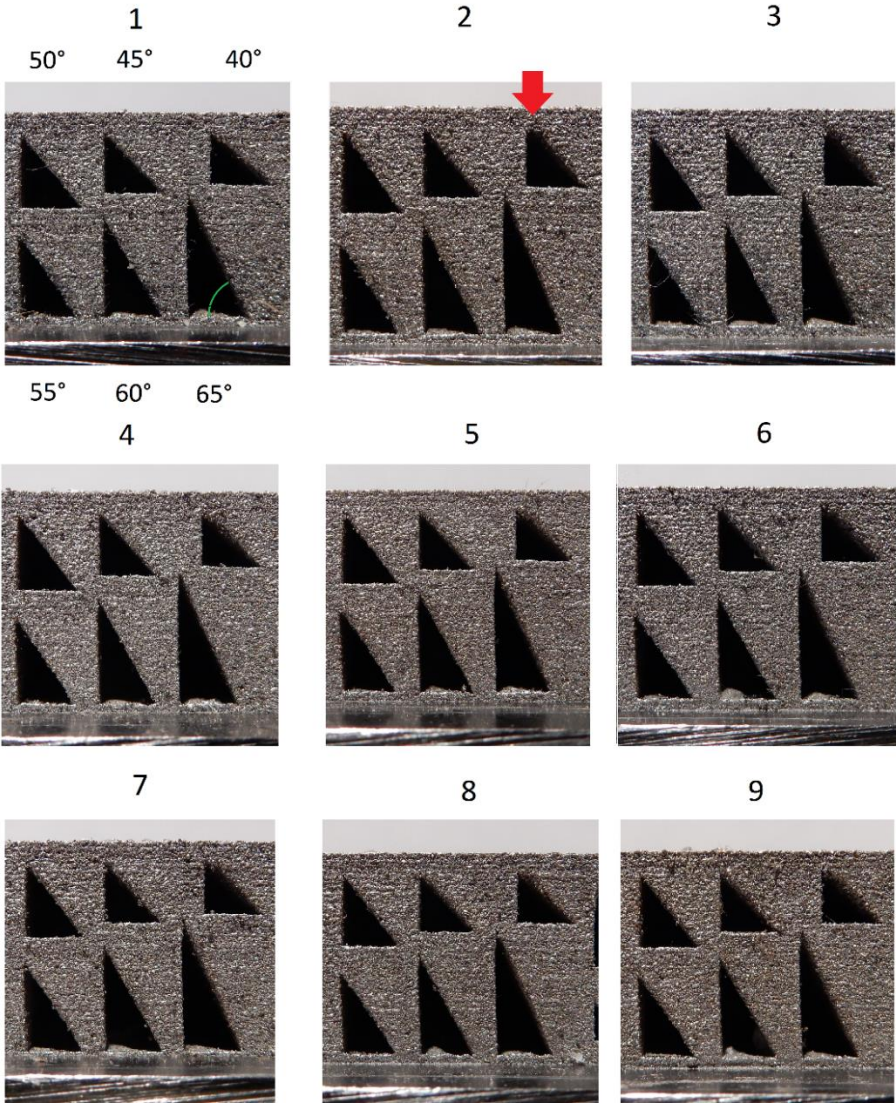


Figure 40 : Comparison of the triangular tubes, the angle values at piece 1 show the value for the green marked corner

From the outside the square tubes (Figure 41) have a similar quality for all the pieces. The smaller overhangs, starting from 2 mm, have a lower quality than the large overhangs.

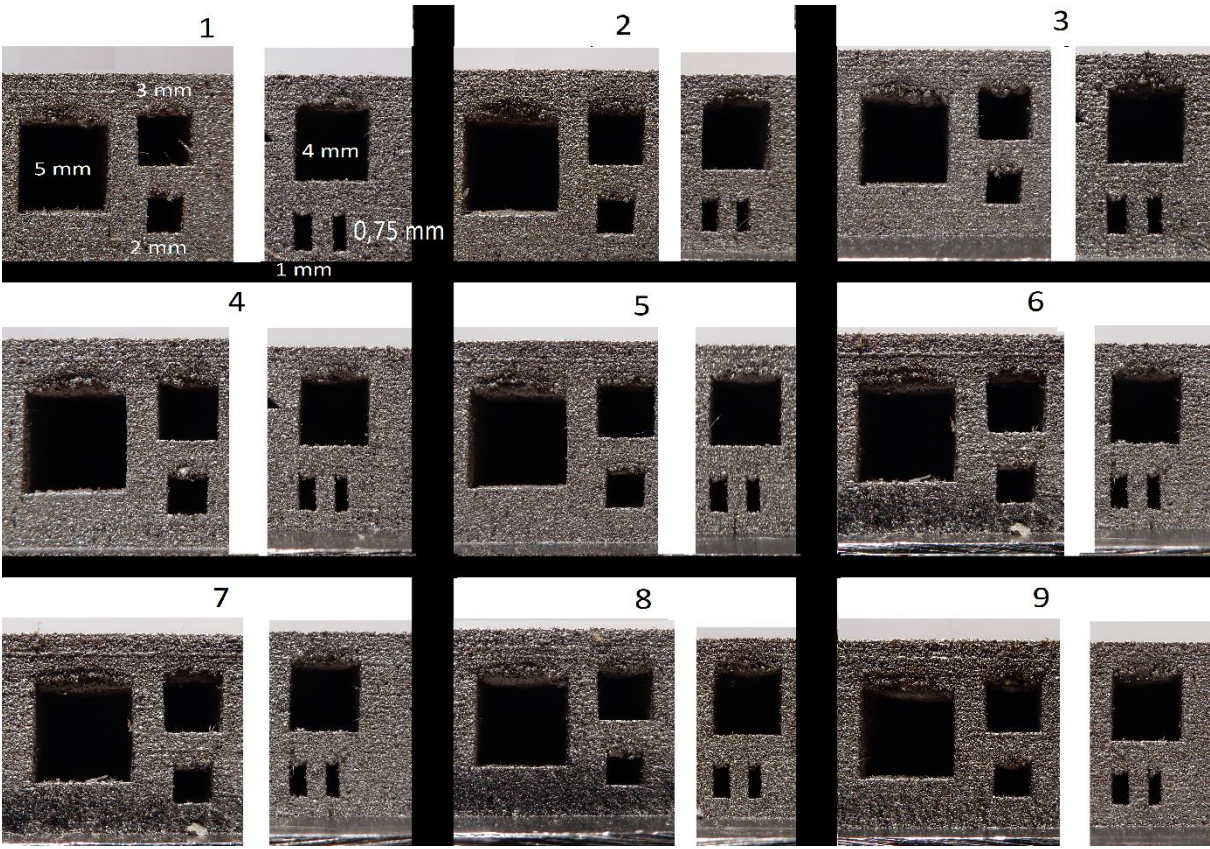


Figure 41 : Comparison of the square tubes

All of the upwards turns were of pristine quality with only occasional small balls on the top of the circle. Piece 6 as an example is shown in Figure 42.

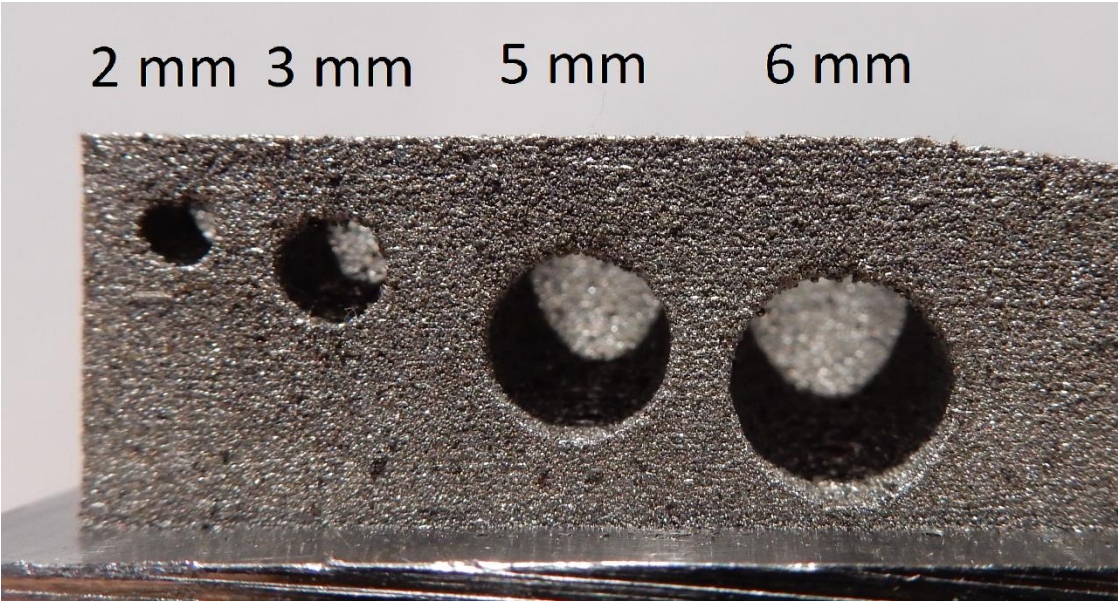


Figure 42 : Side holes of the upwards turn

The reason for the upwards turns to be of such a good quality is that the actual part of the horizontal tube is so short, making a very small melt pool and creating less chance of stalactites because there is not a lot of energy gathered there.

The vertical tensile pieces had a horizontal overhang of 1,5 mm long ending in a 90° corner upwards. Stalactites covered the whole of this surface for all of the pieces and some even had large balls hanging from the corner. This did not have an effect on the tensile tests themselves because the stalactites stopped as soon as the rounded corner of the smaller part starts. The balling of some of the pieces is shown in Figure 43.



Figure 43 : Example of the stalactites on the overhang of the tensile pieces

4.2.2 Summary

Overall the effect of the laser power and the scan spacing on the geometries is small. Most of the top surfaces contained large balls, but as A. Cherry had concluded that lower energy density yields smaller balling while higher energy density have larger balling, the same conclusion can be made here. All horizontal circular holes were of acceptable quality with only slight improvements with decreased energy density. All of the features in the vertical position were of pristine condition for all pieces. Curling and sagging was seen at the 1 mm thick wall of a 9 mm hole. These horizontal triangular tubes confirm M. Van Elsen's [14] statement of 45° being the maximum angle possible. Same results for square holes as J-P Kruth [18] were seen with smaller holes having a lesser quality. The turns were all of pristine condition and large balling was seen on the edges of the overhangs of the tensile pieces.

4.3 Density

4.3.1 Method

The density was measured using the Archimedes density test. This involves weighing a sample of the material first dry and then weighing the same sample suspended under water. The dry mass minus the apparent mass underwater equals the upwards force exerted by the water on the sample. This force is equal to the weight of the displaced volume of water. Knowing the exact density of the water at that temperature allows the calculation of the volume of the sample (including closed porosity, excluding open porosity). From the dry mass and the volume, the density can be extracted. The tensile pieces (unbroken) were used as samples weighing dry around 10 g.

The reference density used for bulk 316L stainless steel is 8 g/cm^3 , the standard reference value used at the KU Leuven.

The norm followed for this test is BS EN ISO 3369:2010 (ISO 3369:2006). Following deviations from this norm were applied. The wire breaking the surface of the water is more than 0.25 mm in diameter, it is 0.70 mm. Deionized water is used and this is taken as being the same as distilled water when it comes to the relation of the density to the temperature.

The analytic scale, including the Archimedes test setup, used for these tests is produced by Mettler Toledo measuring up to 0,1 mg in resolution, it is shown in Figure 44. The scale is linked to the computer and can export the measured value directly to an excel sheet.



Figure 44 : Close up of the setup

After successfully removing the remaining supports and any unnecessary geometry, which could trap bubbles of air. The pieces were cleaned, first with compressed air and then placed in an ultrasonic bath as shown by Figure 45. This ultrasonic bath however seemed to induce some kind of cavitation in the pores just under skin of the samples breaking away tiny particles from the surface of the samples. The medium used in the sonar bath and on the scale was deionized water with one drop of wetting agent in the form of dishwasher rinse aid Una. After the bath the pieces were dried with acetone.



Figure 45 : Tensile pieces in the ultrasonic bath,

A phenomenon seen after a few minutes in deionized water was the forming of surface corrosion on the pieces. Though a study by B. A. Johnson [33] states that 304 stainless steel does not rust in deionized water, this might suggest that the 3D printing process does not provide the material with its usual anti-corrosive properties straight from the machine. Forums such as one called Eng Tips [34] suggest that the purer the water is the more corrosive it is to any metal. The deionized water is, as the name says, devoid of ions, causing it to attract ions and thus ionizes any metal it comes in contact with. A treatment to increase the corrosion resistance such as solution annealing or passivation is most likely required before this material should be used in an injection mould with deionized water as coolant. Examples of the corrosion can be seen in Figure 46.

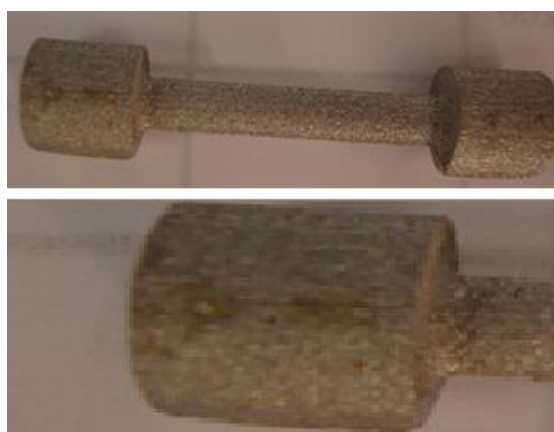


Figure 46 : Corrosion of the tensile piece after minutes in deionized water

Measures were taken to ensure an equal temperature for the measurement of the same sample. A piece was measured at least ten times in dry state and directly afterwards the piece was held in the sonar bath for 10 seconds to clear small bubbles in the surface roughness, larger bubbles in the deep markings (The stripes and dots indicating the parameter set) were removed manually. After this, the piece was measured at least ten times suspended in water. The temperature was monitored throughout the test and measurements with a large deviation from the overall average of that sample were measured again, afterwards these measurements were excluded if they deviated more than 3 times the standard deviation. The same procedure was used for all thirty pieces.

The distribution of the measurement is assumed as being Gaussian. This means a standard deviation can be calculated, as mentioned above all measurements that lay farther than 3 times the standard deviation from the average value were excluded. The dry measurements and the measurements in water are averaged separately, giving one values for m_1 and one value for m_2 for each piece, these values are the average of their respective 10 measurements.

The calculation method for the density is the following equation:

$$\frac{m_1 \cdot \rho_w}{m_2} = \rho_{sample}$$

m_1 = The average mass of the sample measured dry.

ρ_w = The density of the deionised water at the measured temperature.

m_2 = The difference between the average mass of the sample measured dry and the average mass hanging in water.

The error on these values is seen as two times the standard deviation because the BS EN ISO 3369 norm demands that 95% of the measurements from the same laboratory lay within a repeatability interval of 0,025 g/cm³. All of the measurements comply with this demand.

4.3.2 Results and discussion

The results of the test are shown in Table 14.

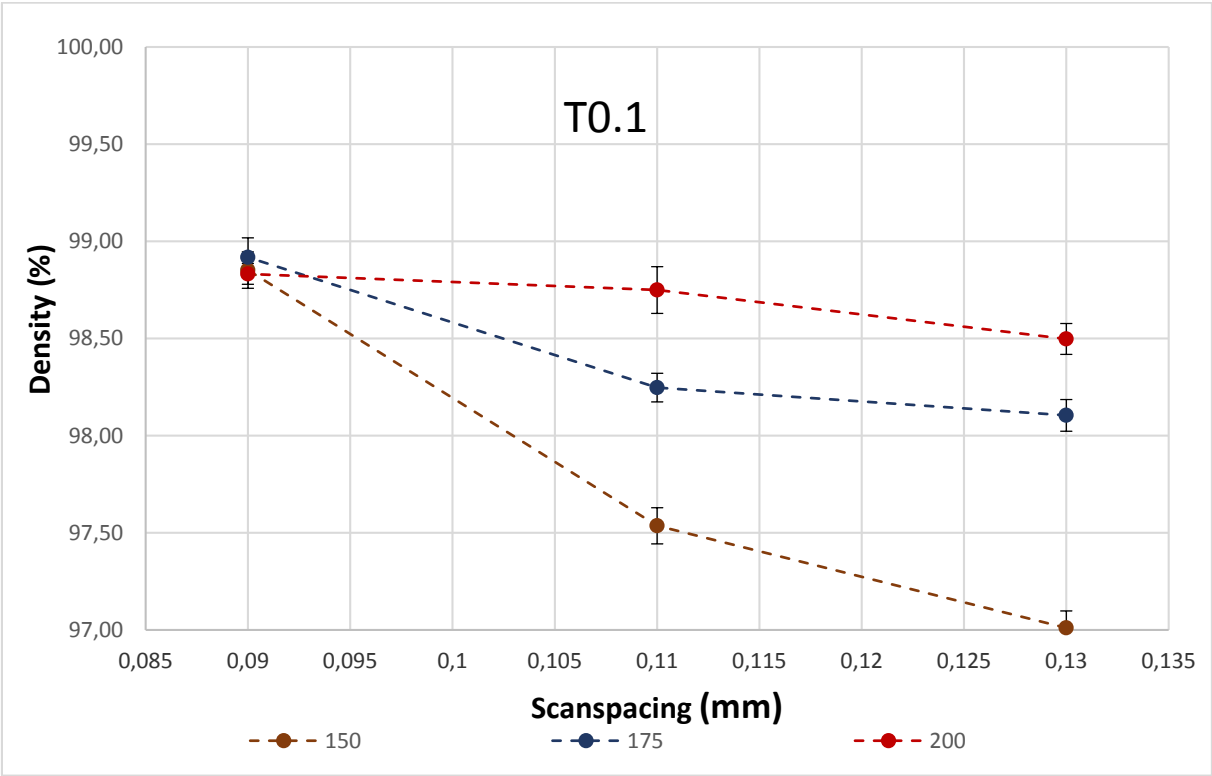
Table 14 : Table with results from the Archimedes test

Scan spacing (mm)	Laser power (W)	Energy density (J/mm ³)	Code	Orientation	Relative Sample density(%) Relative to a bulk density of 8 g/cm ³
0,13	150	55,38	T1.1	Hor. Perpendicular	97,01 ± 0,09
			T1.2	Hor. Parallel	97,54 ± 0,12
			T1.3	Vertical	98,85 ± 0,09
0,13	175	64,62	T2.1	Hor. Perpendicular	98,10 ± 0,08
			T2.2	Hor. Parallel	98,31 ± 0,12
			T2.3	Vertical	98,82 ± 0,05
0,13	200	73,85	T3.1	Hor. Perpendicular	98,50 ± 0,08
			T3.2	Hor. Parallel	98,71 ± 0,09
			T3.3	Vertical	99,11 ± 0,10
0,11	150	65,45	T4.1	Hor. Perpendicular	97,54 ± 0,09
			T4.2	Hor. Parallel	98,17 ± 0,04
			T4.3	Vertical	97,98 ± 0,04
0,11	175	76,36	T5.1	Hor. Perpendicular	98,25 ± 0,07
			T5.2	Hor. Parallel	99,02 ± 0,13
			T5.3	Vertical	99,12 ± 0,09
0,11	200	87,27	T6.1	Hor. Perpendicular	98,71 ± 0,05
			T6.2	Hor. Parallel	98,82 ± 0,06
			T6.3	Vertical	98,78 ± 0,09
0,09	150	80,00	T7.1	Hor. Perpendicular	98,89 ± 0,09
			T7.2	Hor. Parallel	97,41 ± 0,04
			T7.3	Vertical	98,29 ± 0,09
0,09	175	93,33	T8.1	Hor. Perpendicular	98,92 ± 0,10
			T8.2	Hor. Parallel	97,50 ± 0,07
			T8.3	Vertical	98,89 ± 0,09
0,09	200	106,67	T9.1	Hor. Perpendicular	98,83 ± 0,05
			T9.2	Hor. Parallel	98,52 ± 0,06
			T9.3	Vertical	98,70 ± 0,04
0,11	200	65,45	T10.1	Hor. Perpendicular	98,79 ± 0,07
			T10.2	Hor. Parallel	98,49 ± 0,06
			T10.3	Vertical	98,65 ± 0,08

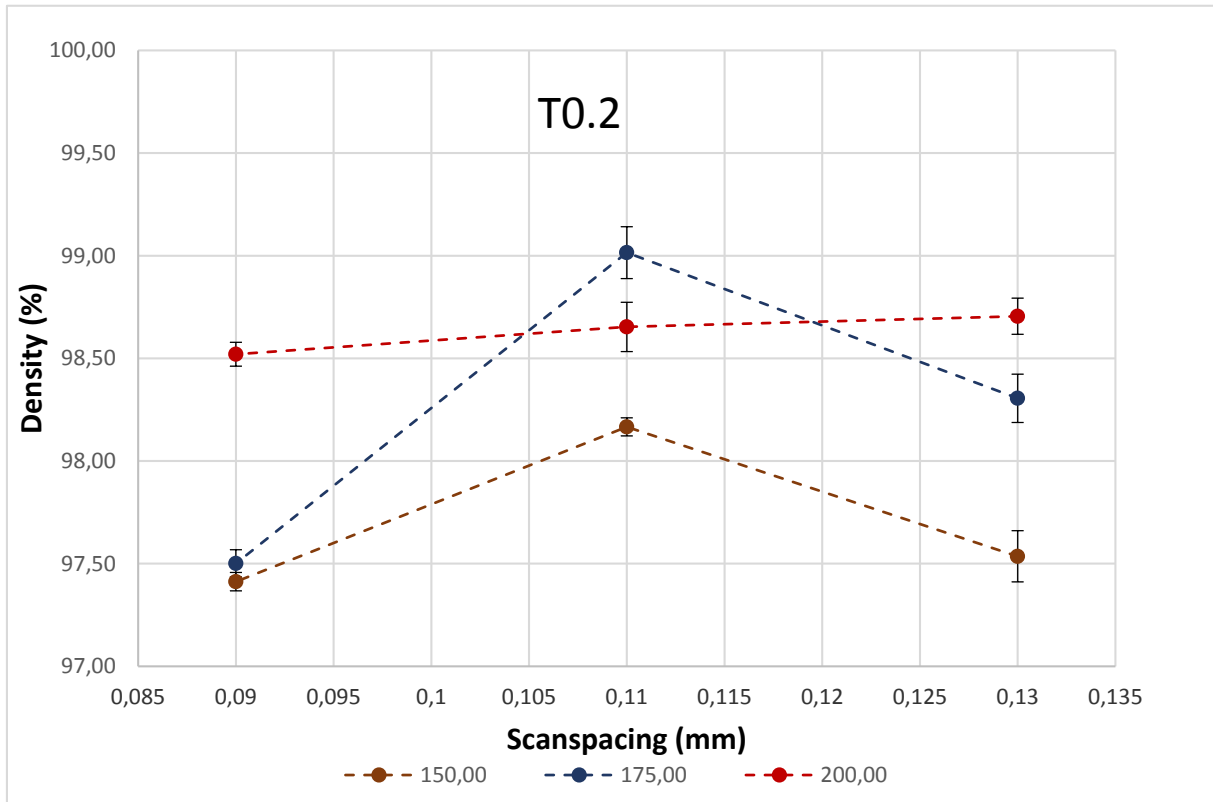
In the graphs below there is a distinction between the directions in which the tensile pieces are printed. This was explained before in chapter 3.5 but it is reiterated here to improve the clarity of the following graph. The indication of the direction is done in the following manner:

- T0.1 = in horizontal plane, perpendicular to the spreader direction
- T0.2 = in horizontal plane, parallel to the spreader direction
- T0.3 = vertical position

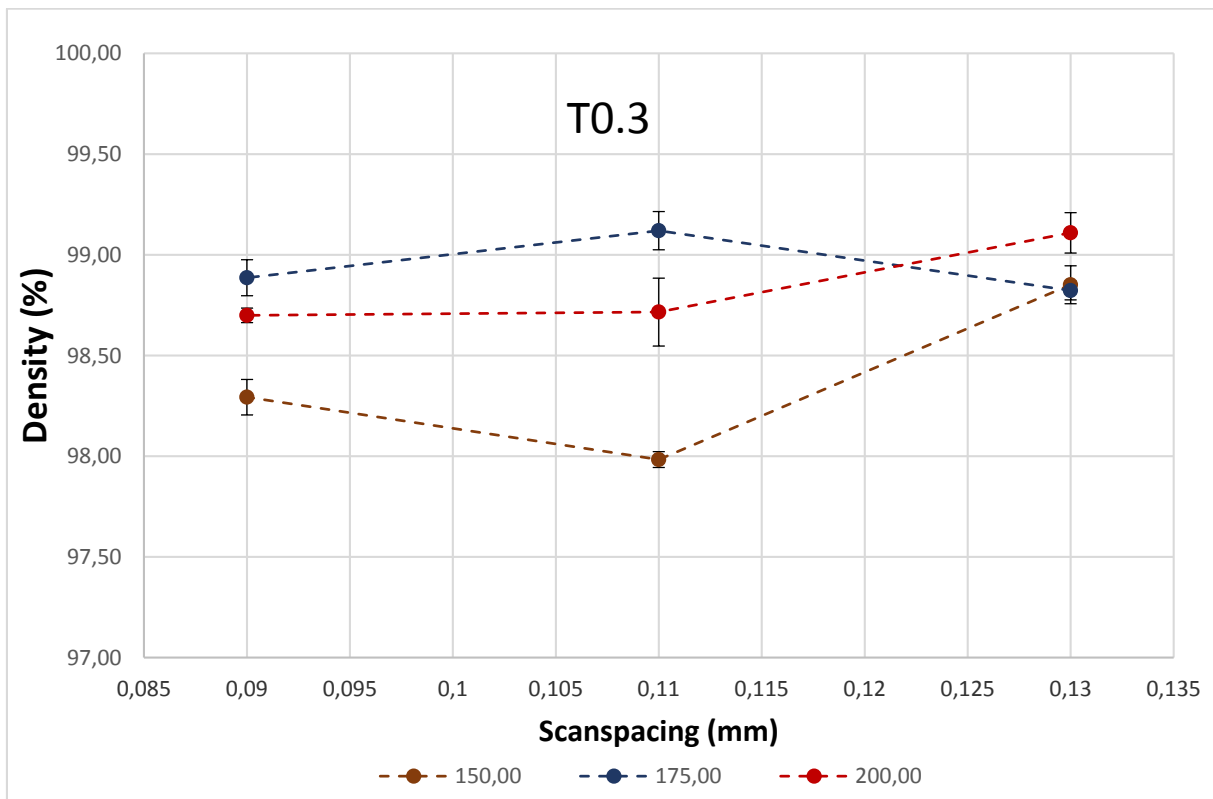
Graph 3, Graph 4 and Graph 5 showing the density versus the scan spacing, indicate that for a laser power of 200W, represented by the red line, the density stays within 98,5 to 99,0 % for all scan spacing. This in contrast to the density for the other laser powers which changes when the scan spacing changes. These changes are inconsistent for the different printing directions. There is no direct proportional relationships between density and scan spacing.



Graph 3 : Pieces in the horizontal direction and perpendicular to the spreader (T0.1): density vs scan spacing

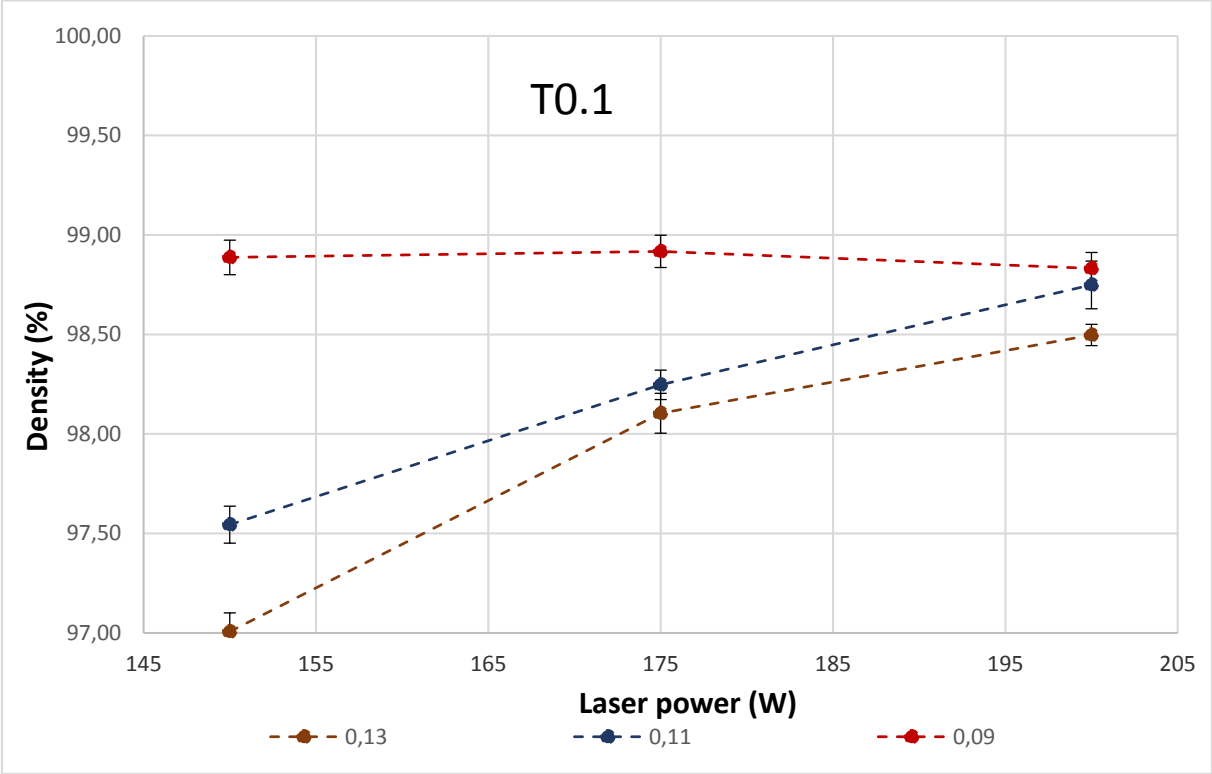


Graph 4 : Pieces in a horizontal plane parallel to the spreader (T0.2): density vs scan spacing

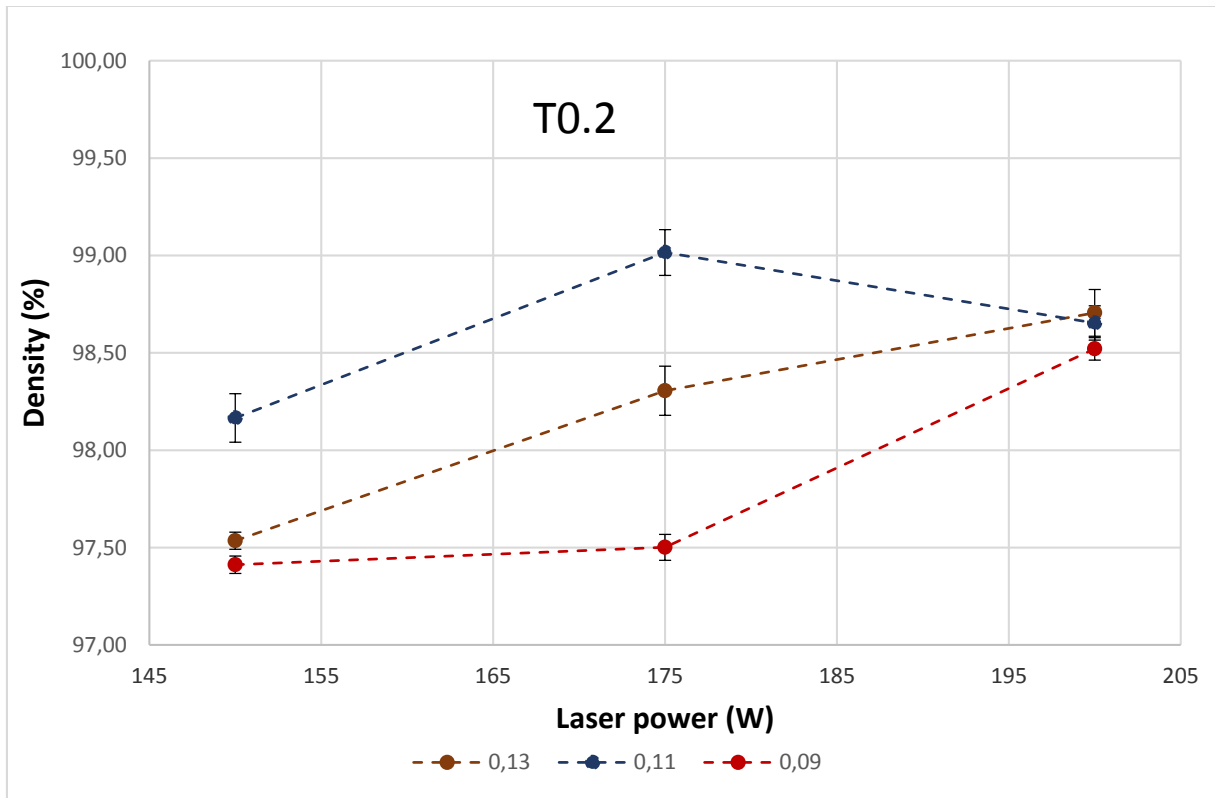


Graph 5 : Pieces in vertical direction (T0.3): density vs scan spacing

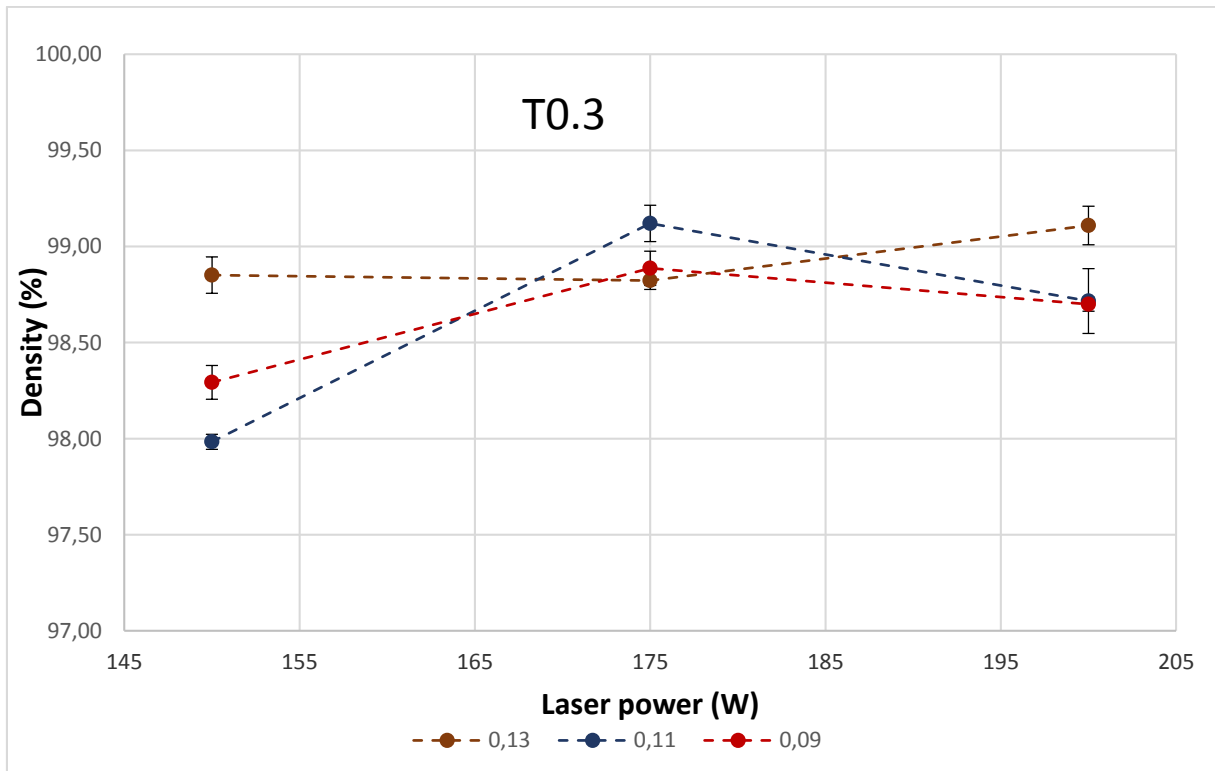
Graph 6, Graph 7 and Graph 8 showing the density versus laser power for all direction separately. The general trend over different scan spacing and different print direction is that the density rises as the power rises. This is an expected result, more laser power means more energy, bigger melt pool and so less chance on porosity.



Graph 6 : Pieces in the horizontal direction and perpendicular to the spreader (T0.1): density vs laser power

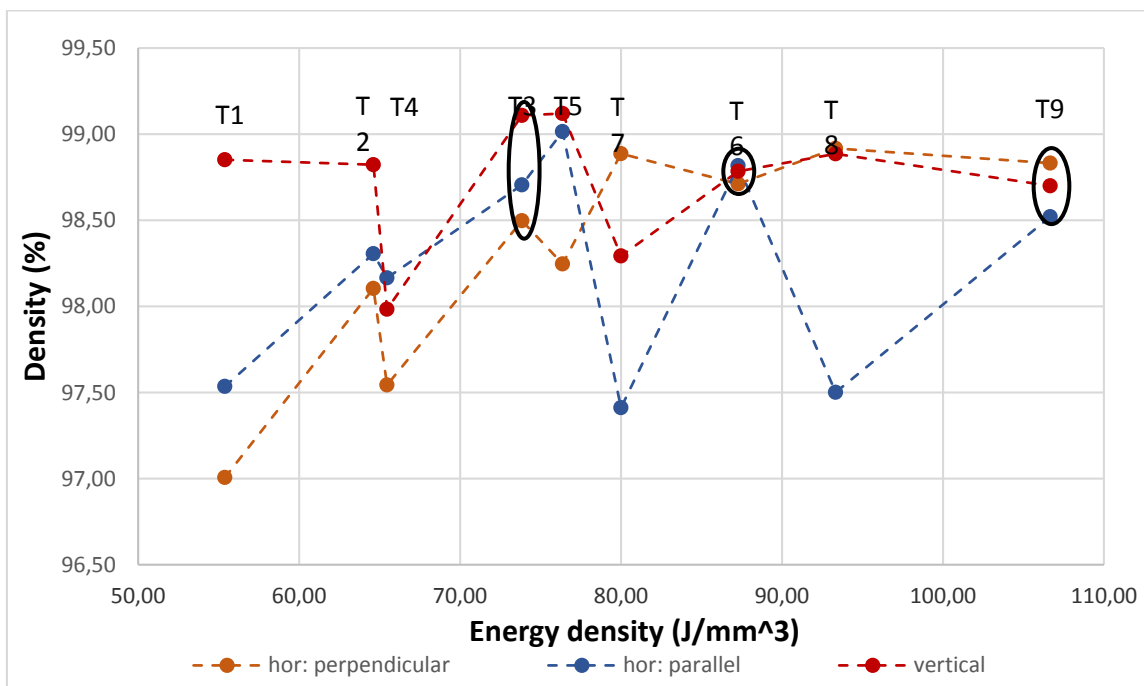


Graph 7 : Pieces in a horizontal plane parallel to the spreader (T0.2): density vs laser power

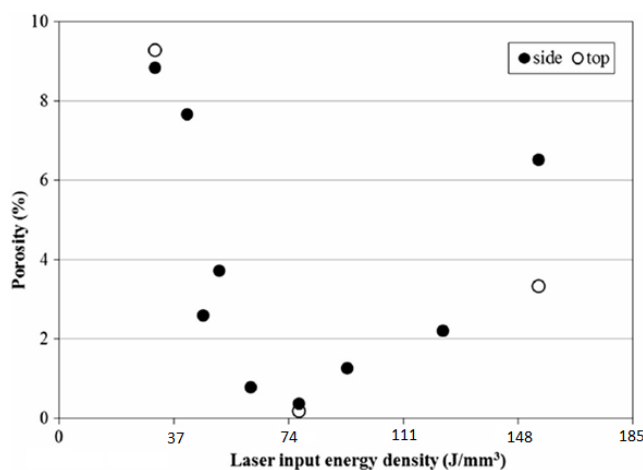


Graph 8 : Pieces in vertical direction (T0.3): density vs laser power

In Graph 9, showing the density versus the energy density, large differences between the different directions in which the pieces are printed can be seen. The parameter sets for 200 W (T3, T6, T9 encircled with black) are the only ones who consistently have a very close grouping of the density in all directions. For lower laser powers and lower energy densities this spread is higher and the density is generally lower, indicating that a laser power and energy density in the higher area of the machine's maximum capacity of 200W are needed. Though all three curves follow the same zigzag trend until 75 J/mm³ there is not enough evidence to suggest a real relation between the energy density and the density since the curves do not hold very much similarity after passing the 75 J/mm³ mark. In these curves no top is seen like the one seen by Mrs. Cherry [17] as shown in Graph 10 (The X-axis of the graph was adjusted, A. Cherry works with porosity which is just 100% minus the density).



Graph 9 : Density vs Energy density per direction



Graph 10 : Graph of porosity (density) and energy density made by A. Cherry [17].

Because the tensile pieces were placed at the borders of the build plate with some positions at a significant distance from each other, the effect of the position of the pieces is checked with the following graphs and figures. Figure 47 (p. 84) shows the top view of the print job in the position it was built. Table 16 (p. 85) shows the code, parameters set and the energy density (in the colored boxes, J/mm^3) for each piece in their respective position on the print job. This can be correlated to Table 17 (p. 86) showing the density of every piece in their respective positions, the middle values for the test pieces are the average values for their respective tensile pieces.

The density shows signs of being influenced by the position of the piece by showing higher density at the top. The pieces in the lower area are generally made with a lower laser densities as seen in Table 16. The previously seen Graph 9 shows that lower energy density corresponds to a lower density, especially for the horizontal pieces. It is clear that the vertical piece generally have a higher density.

A good indicator is given by the density difference between T6 and T10 (Table 15). These have the same building parameters, due to the density difference between each direction, only the pieces printed in the same direction can be compared. T6.1 is in the lowest position (close to the machine door) and T10.1 is situated in the highest position, there is no significant difference. Though both values lay just outside the error margins. T6.2 is in the top left corner and T10.2 the bottom right corner, T10.2 has a significantly lower density. T6.3 is closer to the top and T10.3 closer to the bottom both on the right side. There is a difference of 0,13 % whilst the error is 0,09 % for both.

T4.3 is seen having a suspiciously sudden high deviation, this is attributed to an error during the test, a hidden air bubble that persisted over the 10 measurement is a reasonable cause. A second Archimedes test was not possible since the pieces were already broken during the tensile tests, influencing the original density of these pieces.

Table 15 : Table with the results for T6 and T10

code	Scan spacing (mm)	Laser power (W)	Sample density(%)	Difference (%)	Position
T6.1	0,11	200	98,71 ± 0,05		Right below
T6.2	0,11	200	98,82 ± 0,06		Left top
T6.3	0,11	200	98,78 ± 0,09		Right top
T10.1	0,11	200	98,79 ± 0,07	0,08	Right top
T10.2	0,11	200	98,49 ± 0,06	0,33	Right below
T10.3	0,11	200	98,65 ± 0,08	0,14	right below

Overall the density is lower in the area closer to the door. This could indicate that the spreader is pushing more powder closer to the powder input, compressing the powder tightly, as the heap of powder decreases the layer is less compressed. Further research to confirm this theory is necessary. The effect of the position on the density was not the focus of this experiment.

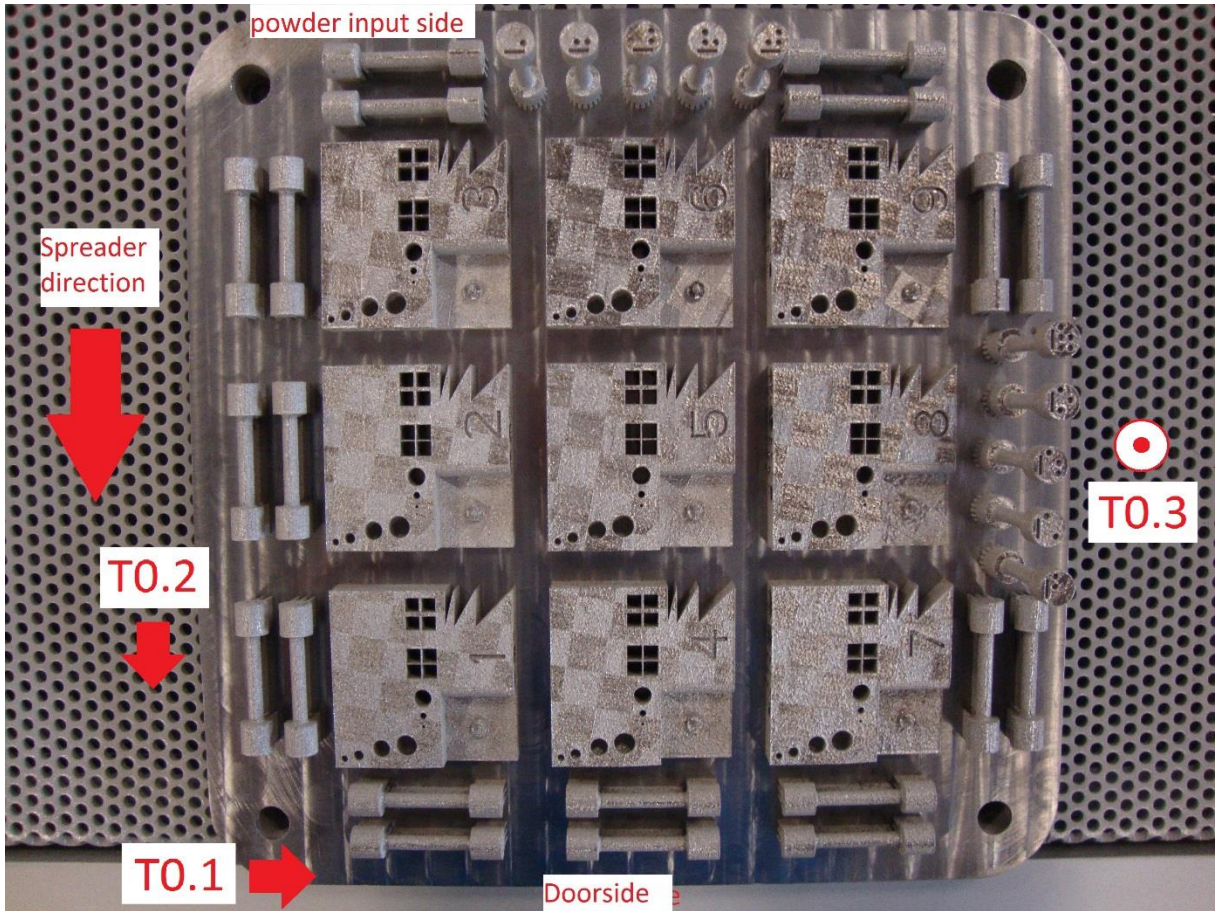


Figure 47: Top view of the finished print job

Table 16 : 2D Graph of the code, parameters (power, scan spacing and energy density in J/mm³) for each piece in their respective position

		T8.1; 175 W; 0,09 mm 93,333333	T1.3; 150 W; 0,13 mm	T2.3; 175 W; 0,13 mm	T3.3; 200 W; 0,13 mm	T4.3; 150 W; 0,11 mm	T5.3; 175 W; 0,11 mm	T10.1; 200 W; 0,11 mm 87,27272727	
		T7.1; 150 W; 0,09 mm 80	55,3846154	64,6153846	73,8461538	65,4545454	76,3636363	T9.1; 200 W; 0,09 mm 106,6666667	
T6.2; 200 W; 0,11 mm	T5.2; 175 W; 0,11 mm	3; 200 W; 0,13 mm		6; 200 W; 0,11 mm		9; 200 W; 0,09 mm		T7.2; 150 W; 0,09 mm 80	T8.2; 175 W; 0,09 mm 93,33333
87,2727	76,3636	73,84615385		87,27272727		106,6666667		T6.3; 200 W; 0,11 mm 87,27272727	
T4.2; 150 W; 0,11 mm	T3.2; 200 W; 0,13 mm	2; 175 W; 0,13 mm		5; 175 W; 0,11 mm		8; 175 W; 0,09 mm		T7.3; 150 W; 0,09 mm 80	
65,4545	73,8462	64,61538462		76,36363636		93,33333333		T8.3; 175 W; 0,09 mm 93,33333333	
		64,61538462		76,36363636		93,33333333		T9.3; 200 W; 0,09 mm 106,6666667	
T2.2; 175 W; 0,13 mm	T1.2; 150 W; 0,13 mm	1; 150 W; 0,13 mm		4; 150 W; 0,11 mm		7; 150 W; 0,09 mm		T10.3; 200 W; 0,11 mm 87,27272727	
64,62	55,3846	55,38461538		65,45454545		80		T9.2; 200 W; 0,09 mm 106,667	T10.2; 200 W; 0,11 mm 87,2727
		T1.1; 150 W; 0,13 mm 55,38461538		T3.1; 200 W; 0,13 mm 73,84615385		T5.1; 175 W; 0,11 mm 76,36363636			
		T2.1; 175 W; 0,13 mm 64,61538462		T4.1; 150 W; 0,11 mm 65,45454545		T6.1; 200 W; 0,11 mm 87,27272727			

Table 17: 2D graph with the density of every piece in their respective position

		98,92	98,85	98,82	99,11	97,98	99,12	98,79		
		98,89						98,83		
98,82	99,02	98,20		98,77		98,68		97,41	97,50	
								98,78		
98,17	98,71	98,41		98,79		98,44		98,29		
								98,89		
								98,70		
98,31	97,54	97,80		97,90		98,20		98,65		
								98,52	98,49	
		97,01		98,50		98,25				
		98,10		97,54		98,71				

4.3.3 **Conclusion**

The standard Renishaw parameter combination of 200 W laser power and 0,11 mm scan spacing seems to be the best method to print parts with equal density in all directions, maintaining a relative density of around 98.87 %. The rest of the parameters have large deviations in density between pieces built in different directions. The density for 200 Watt laser power is also independent from scan spacing whilst this is not true for the laser power of 150 W and 175 W. A general trend among all scan spacing is that the density increases as the laser power or the energy density rises. The density is higher where the powder is compressed more tightly, close to the powder input at the back of the machine.

The large differences in density between the different directions could have moved particles so that some areas contain less particles than others, making it harder for lower laser powers to penetrate larger heaps of powder. The higher density of the vertical pieces compared to the horizontal pieces suggests there is more porosity between tracks than between layers. More research is needed to confirm the effect of position on the density.

Stainless 316L steel shows signs of corrosion when submerged into a sonar bath with deionized water. It might need a corrosion resistance enhancement treatment like solution annealing or passivation before usage in a mould cooled with deionized water. Parts produced with SLM seem to lose mass because of cavitation in pores just below the surface of the part when placed into a sonar bath, causing not fully melted powder particle to separate from the surface of the part.

4.4 Strength

4.4.1 Method

These tests are based on the BS EN ISO 6892-1:2009. The settings prescribed by this norm did not yield the expected results, a different original gauge length, strain rates and E-modulus determination method were used.

The machine used to perform the tensile tests is a type Zwick Z050/TH3A at the Cell Kunststoffen shown by Figure 48. This machine can reach a maximum force of 50 kN, since the design of the tensile test pieces permits them to be broken with the tensile test bench of 10 kN present at the university of Derby, this tensile bench did not have any trouble with the test pieces. The machine has two ways of measuring the elongation of the test piece, one is by measuring the movement of the crosshead as indicated in Figure 48. This measurement includes any elongation in the machine itself making the measurements from the crosshead unreliable. Another method is with the multiXtens extensometer measuring the elongation of the piece directly on the part with two claws clamping onto the tensile piece. Due to the small length of the tensile piece the extensometer must clamp unusually close to each other.

The piece in Figure 48 is clamped in such a way that the clamp does not touch the removed support structure. This way the part is evenly clamped on a nearly perfect round geometry.



Figure 48 : Left: Tensile test bench Zwick Z050, Right: Example of how a horizontal piece is clamped in the machine

The support structure along the length of the pieces was manually filed down so that an even section along the length of the thin part was resulted. The balling at the overhangs was also removed with a chamfer to negate any chance of bad clamping in the tensile test bench.

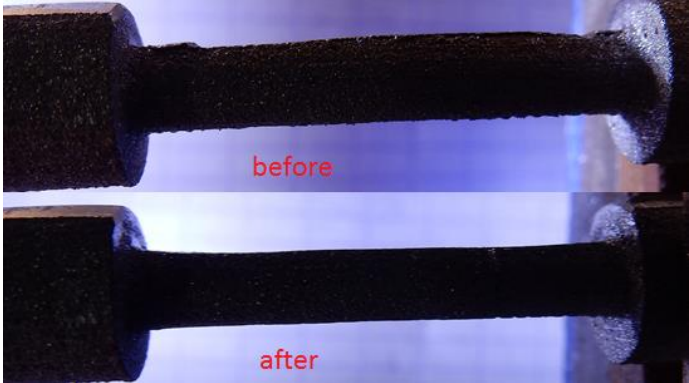


Figure 49 : Removal of the support structure, top: before removal of support structure, bottom: after removal of support structure.

The tensile tests proved to be problematic, settings taken from the norm resulted in low Young-modulus and early failures. For this reason the first 5 tests have unreliable results. These are the piece T1.2, T1.3, T2.1, T2.2 and T2.3. Settings for the following tests were extracted from previous tests. The most important settings are seen in Table 18.

Table 18 : The settings used in the tensile tests and their explanation

Parameter	Value	Explanation
Preload	15 N/mm ²	The stress induced in the tensile piece to settle the piece into the claw before the actual test
Strain rate	5 mm/min	The speed at which the tensile piece is strained during the test
Parallel length	23,7 mm	The length with the same cross section over the middle of the piece
Original gauge length	10 mm	The distance between the claws of the extensometer

To get a more reliable value for the Young modulus each piece was strained within the elastic area a few times and the values for the Young modulus were averaged. This gave good results for some pieces but still a lot of deviation for most pieces. The first strain test was always excluded because the piece was settling (moving) into the clamps, any other test showing an irregular curve were also excluded. Figure 52 shows the stress-strain curves of T3.1 with straight lines showing the Young-modulus. The first test shows the piece settling into the clamps and is therefore excluded, the next tests show a clear direction of the curve.

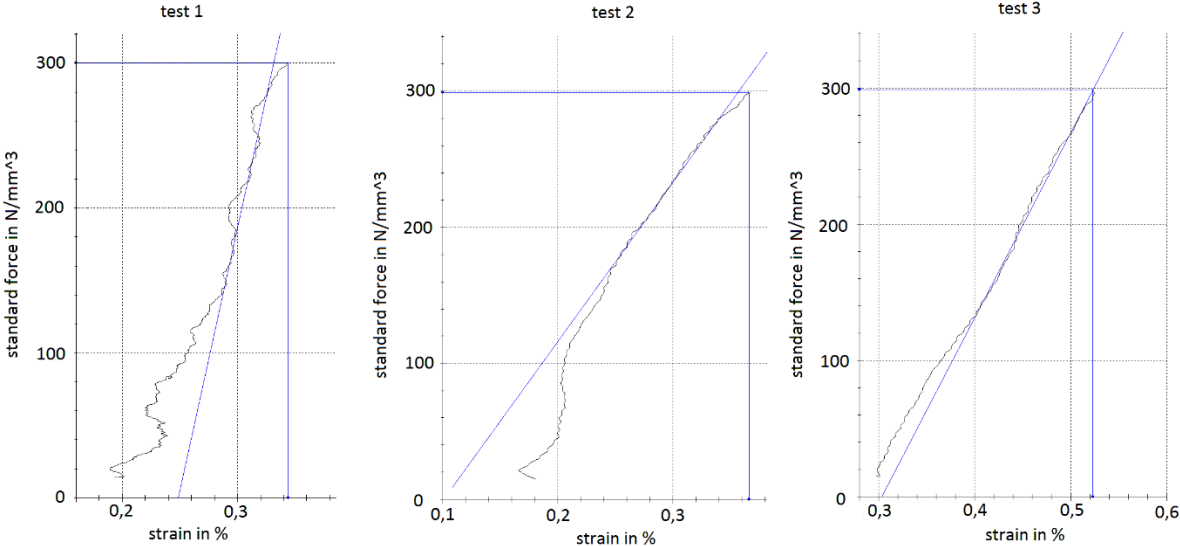


Figure 50 : Stress-strain curves until $300 N/mm^2$ of 3 successive tests on piece T3.1

4.4.2 Results and discussion

Table 19 shows the results. Values noted between brackets are deemed unreliable. The “number of measurements” column represents the number of times the test pieces were stretched and released plus the actual break test.

Table 19: Compiled results of the tensile test

Scan spacing (mm)	Laser power (W)	Energy density (J/mm ³)	code	Orientation	Nr. of measurements	Young modulus (GPa)	Rp x (N/mm ²)	Rm (N/mm ²)	Elongation at Rm (%)	Elongation at break (%)
0,13	150	55,38	T1.1	Hor. Perpendicular	3	±	462,5	590	7,7	9
			T1.2	Hor. Parallel	1	(226) ± /	(592)	(607)	(0,7)	(0,7)
			T1.3	Vertical	1	(131) ± /	(454)	(587)	(19,5)	(22,2)
0,13	175	64,62	T2.1	Hor. Perpendicular	1	(225) ± /	(598)	(624)	(0,7)	(0,7)
			T2.2	Hor. Parallel	1	(82) ± /	(563)	(617)	(1,8)	(1,8)
			T2.3	Vertical	1	(90) ± /	(537)	(619)	(3)	(3)
0,13	200	73,85	T3.1	Hor. Perpendicular	8	165 ± 61	508	646	6,7	10,5
			T3.2	Hor. Parallel	11	168 ± 87	482	630	7,7	11,0
			T3.3	Vertical	10	163 ± 37	461	586	9,5	14,9
0,11	150	65,45	T4.1	Hor. Perpendicular	18	163 ± 70	476	599	8,3	9,4
			T4.2	Hor. Parallel	16	166 ± 82	485	619	9,4	12,3
			T4.3	Vertical	11	167 ± 28	490	594	6,9	7,5
0,11	175	76,36	T5.1	Hor. Perpendicular	13	166 ± 119	505	625	10,3	15,0
			T5.2	Hor. Parallel	11	194 ± 45	498	641	7,5	11,2
			T5.3	Vertical	12	169 ± 81	473	586	11,1	13,3
0,11	200	87,27	T6.1	Hor. Perpendicular	9	173 ± 67	494	616	8,4	9,4
			T6.2	Hor. Parallel	11	169 ± 94	490	620	7,6	10,8
			T6.3	Vertical	9	147 ± 17	454	573	8,3	9,7
0,09	150	80,00	T7.1	Hor. Perpendicular	5	194 ± 222	490	633	6,2	9,3
			T7.2	Hor. Parallel	8	194 ± 262	462	593	4,5	10,2
			T7.3	Vertical	8	147 ± 93	447	511	1,4	1,7
0,09	175	93,33	T8.1	Hor. Perpendicular	12	160 ± 53	497	628	8,8	12,3
			T8.2	Hor. Parallel	4	137 ± 40	436	553	7,1	8,3
			T8.3	Vertical	7	159 ± 72	466	576	9,4	14,0
0,09	200	106,67	T9.1	Hor. Perpendicular	10	144 ± 40	484	623	7,8	10,5
			T9.2	Hor. Parallel	5	124 ± 49	477	614	8,4	10,7
			T9.3	Vertical	8	150 ± 50	446	563	10,4	12,6

The results of the tensile tests (Table 19) clearly show that there is a large deviation on the values for the Young modulus, making it uninteresting to analyze the difference between the different tensile pieces. Though the yield strength is dependent on the Young modulus, the values that are found do look realistic in the stress-strain curves.

Both the comparison of the yield strength (R_p) and ultimate tensile stress (R_m) with the print direction as shown by Graph 11 and Graph 12 (p.93) Respectively show that the pieces printed in the vertical position are weaker than those printed in the horizontal position for most of the parameter sets, the only exceptions are T4 and T8 for the yield strength and T2 and T8 for the ultimate tensile strength. This corresponds with the findings by I. Tolosa [15]. This is explained by the bonding between layers being weaker than the bonding between the tracks within one layer. All of the horizontal pieces have a sloped break line, but in some sets the vertical pieces have a break line perpendicular to the edge, suggesting delamination. Figure 51 shows the break lines for T1, T3 and T7. The delaminated pieces are encircled in red in Graph 11 and Graph 12, these should have less strength than the other vertical piece but this is not the case, indicating other microstructural causes are to blame.

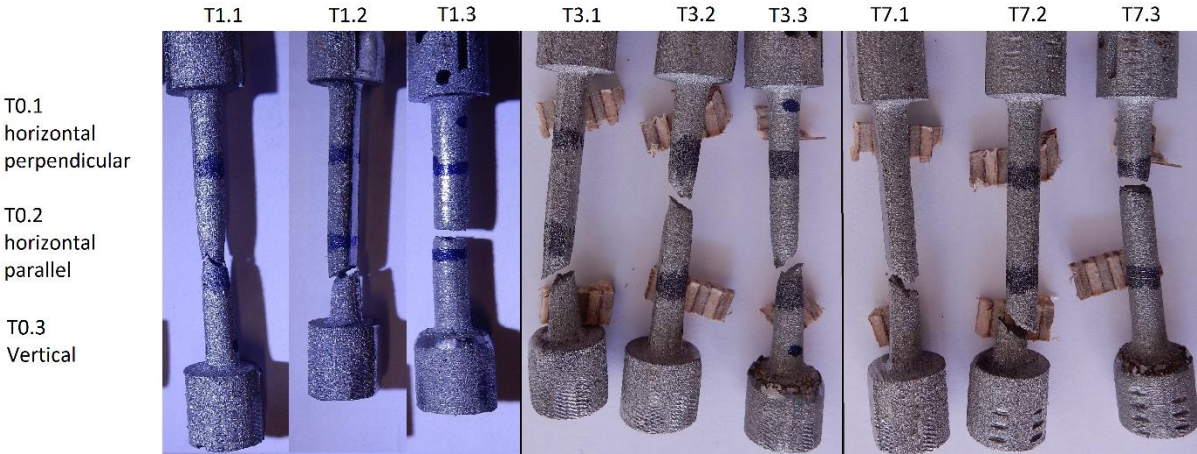
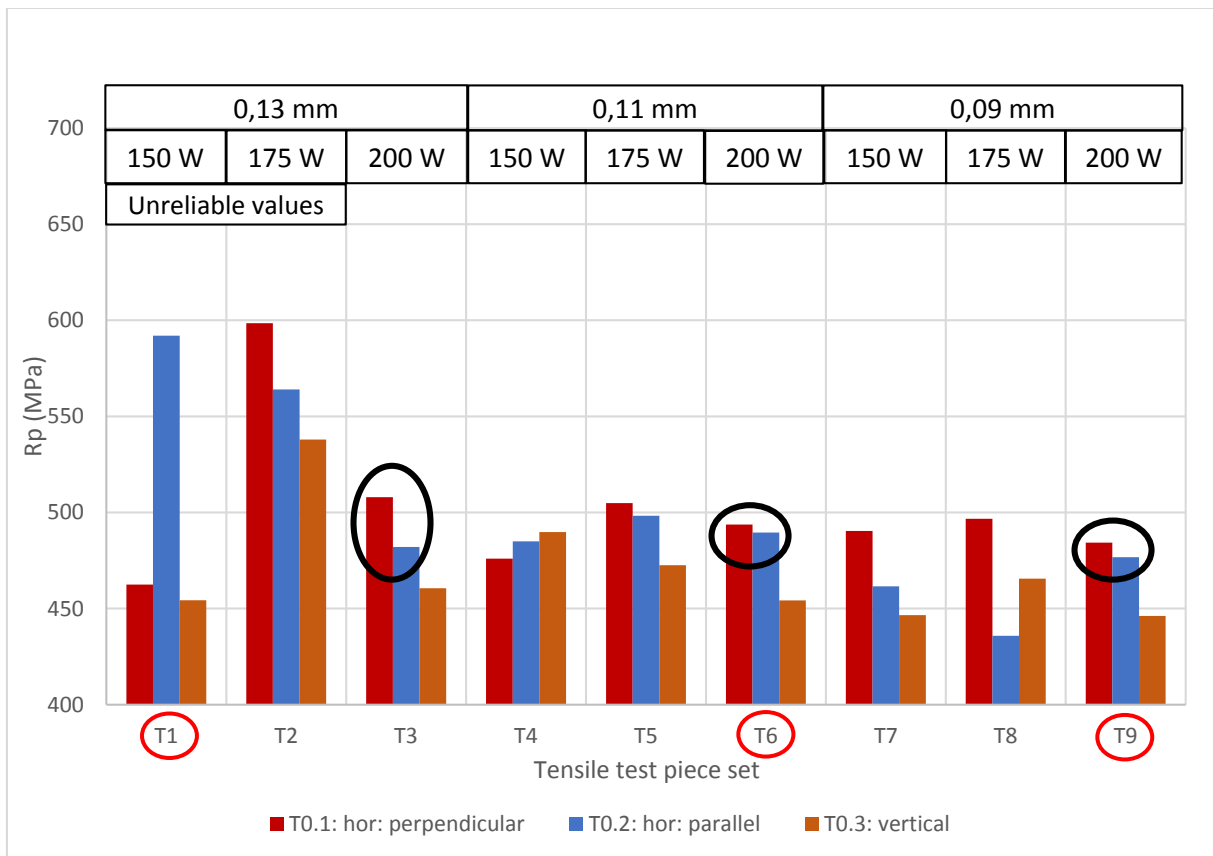
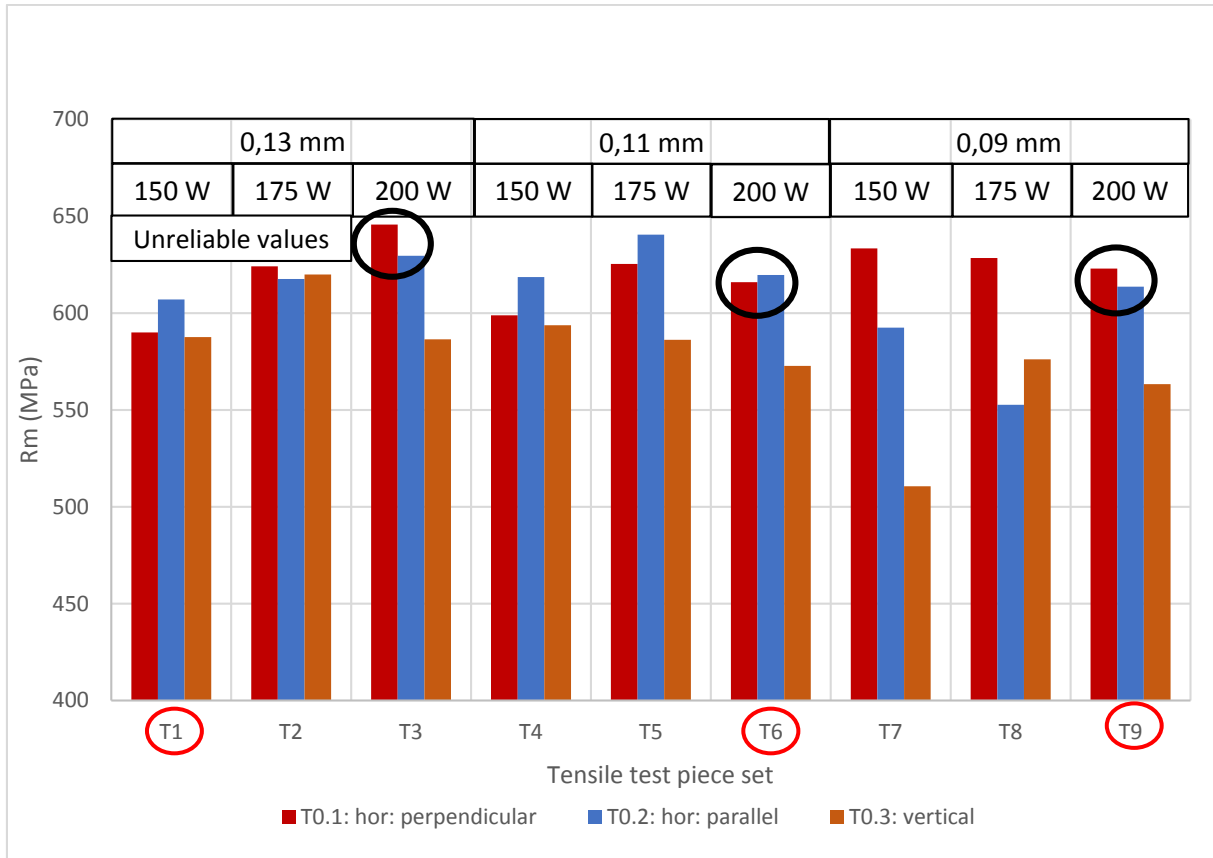


Figure 51 : Break lines of the pieces of parameter set T1, T3 and T7

The parameters using a laser power of 200 W are encircled in black in Graph 11 and Graph 12. They show similar yield strength and ultimate tensile strength for the horizontal pieces. The parameter set with the highest strength is T5 with 175 W laser power and 0,11 mm (error on these values could not be calculated).

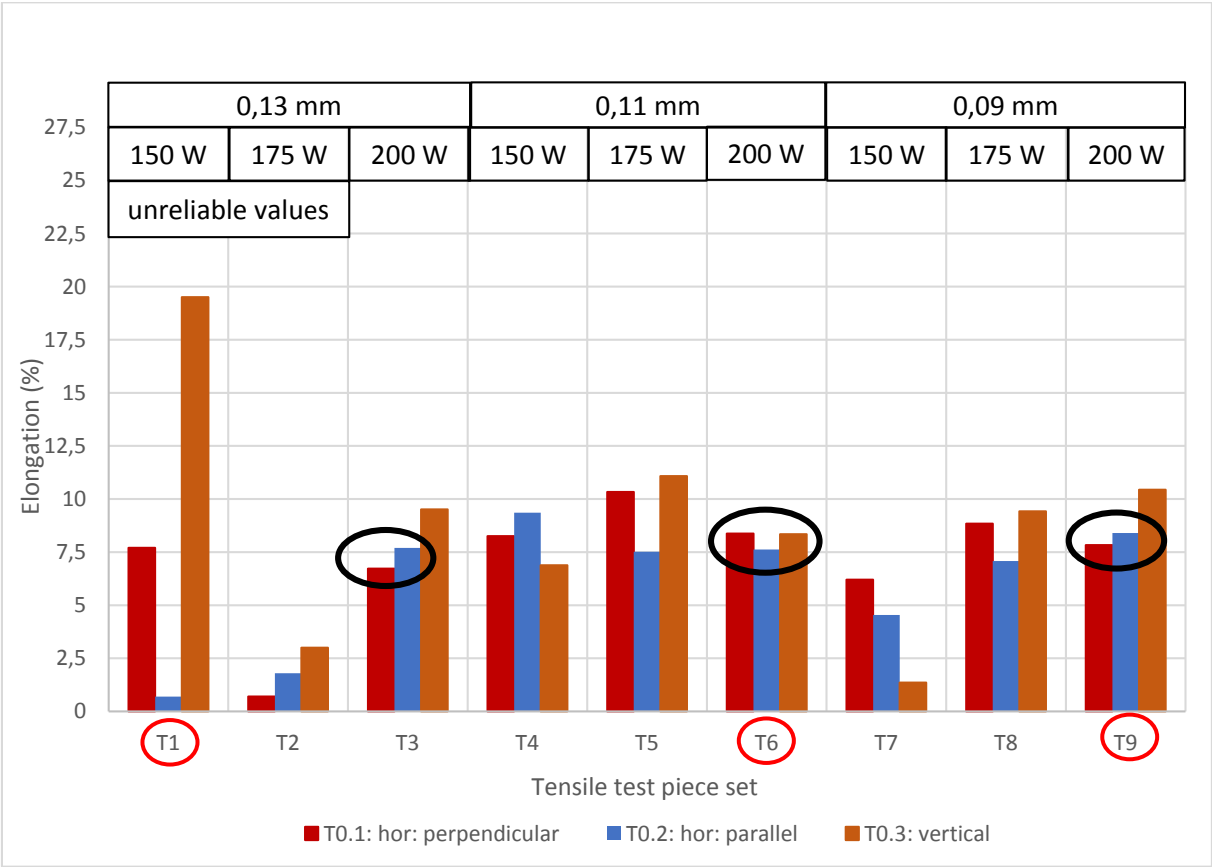


Graph 11 : Yield strength per print direction per tensile piece set

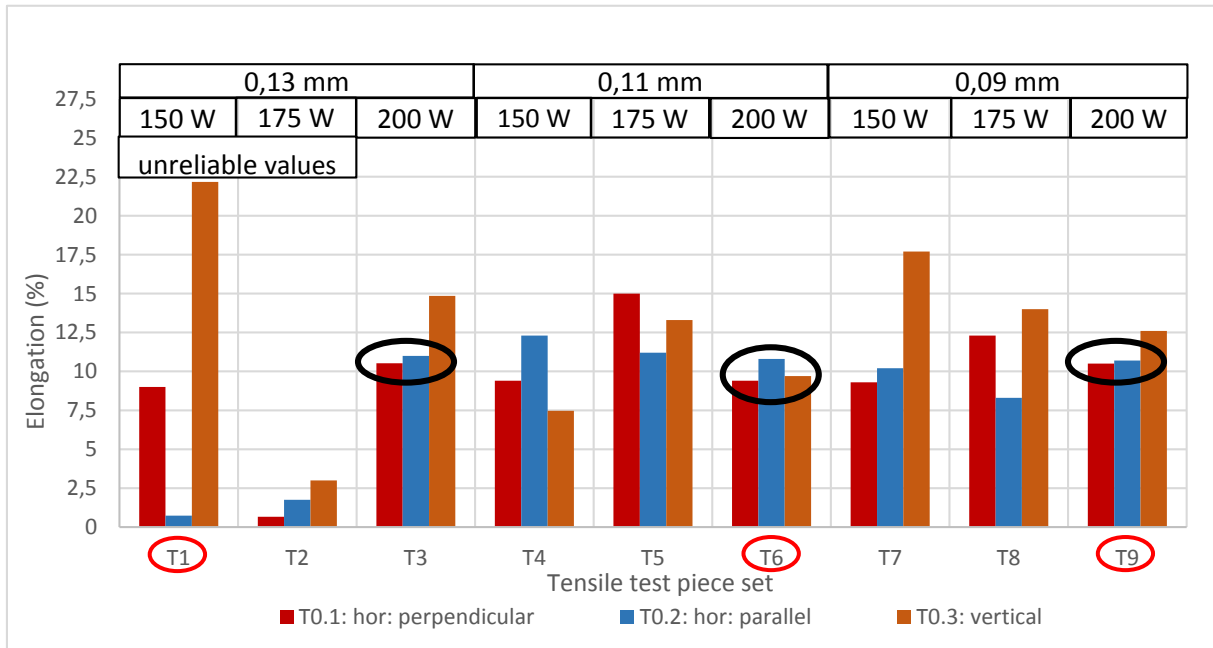


Graph 12 : Ultimate tensile strength per print direction per tensile piece set

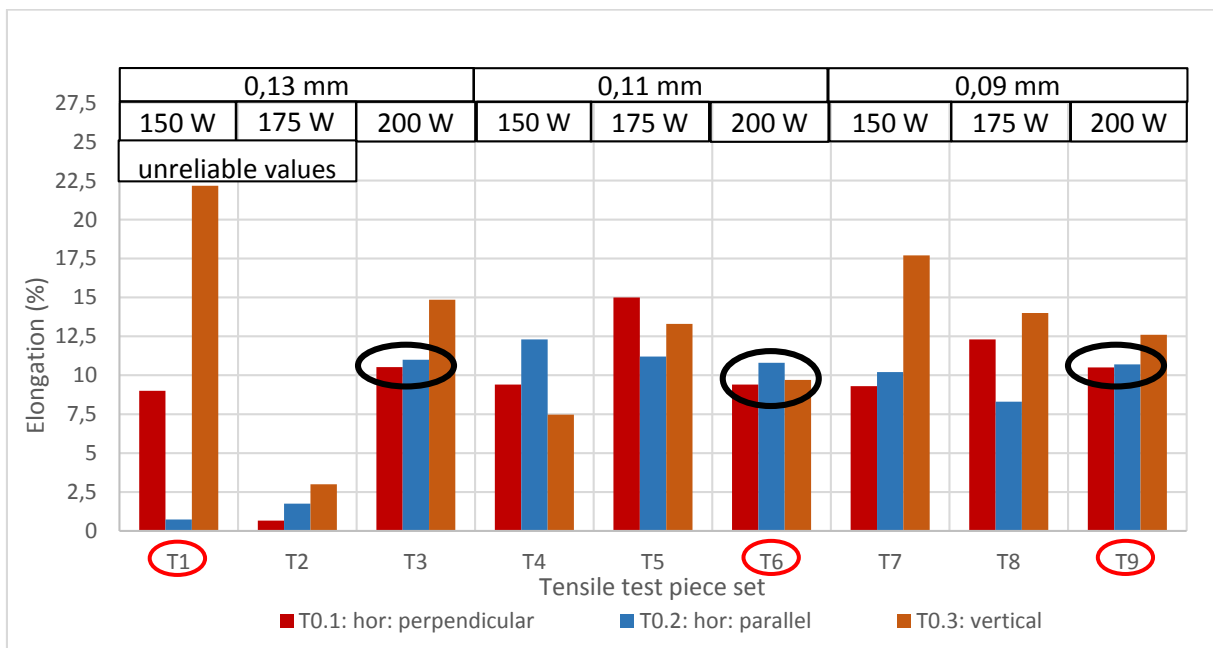
The elongations in both Graph 13 and Graph 14 for the horizontal parts (T0.1 and T0.2) made with 200 W (encircled in black) have similar elongations in both directions, the same as seen in Graph 11 and Graph 12 when compared with the deviations between direction seen in the other pieces. For 200 W and 0.11 mm the vertical piece (T0.3) even has a similar elongation to the horizontal pieces. The post uniform elongation shown in Graph 15 (p. 95) is the difference between elongation at Rm and the break elongation. If there is really delamination the vertical pieces should have less elongation overall yet the opposite seems to be true as, this was also seen by I. Tolosa [15]. Graph 16, Graph 17 and Graph 18 (p. 96) show that the elongation follows the same trend as the strength of the part, this is peculiar because in general materials with a higher strength have less elongation. This phenomenon cannot be attributed to a reduction in the section surface area due to porosity because the elongation is only based on the change in parallel length, less section surface area should still hold the same elongation if nothing else has changed.



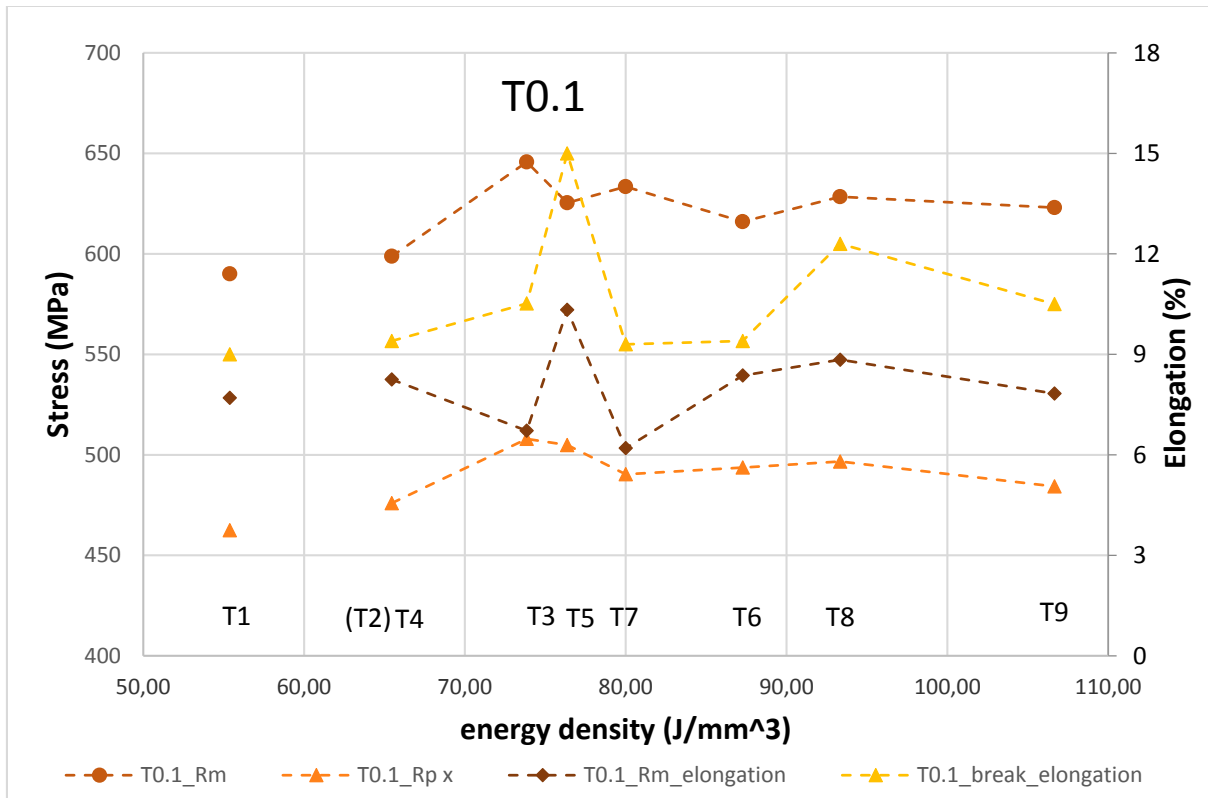
Graph 13 : Elongation at Rm per print direction per tensile piece set



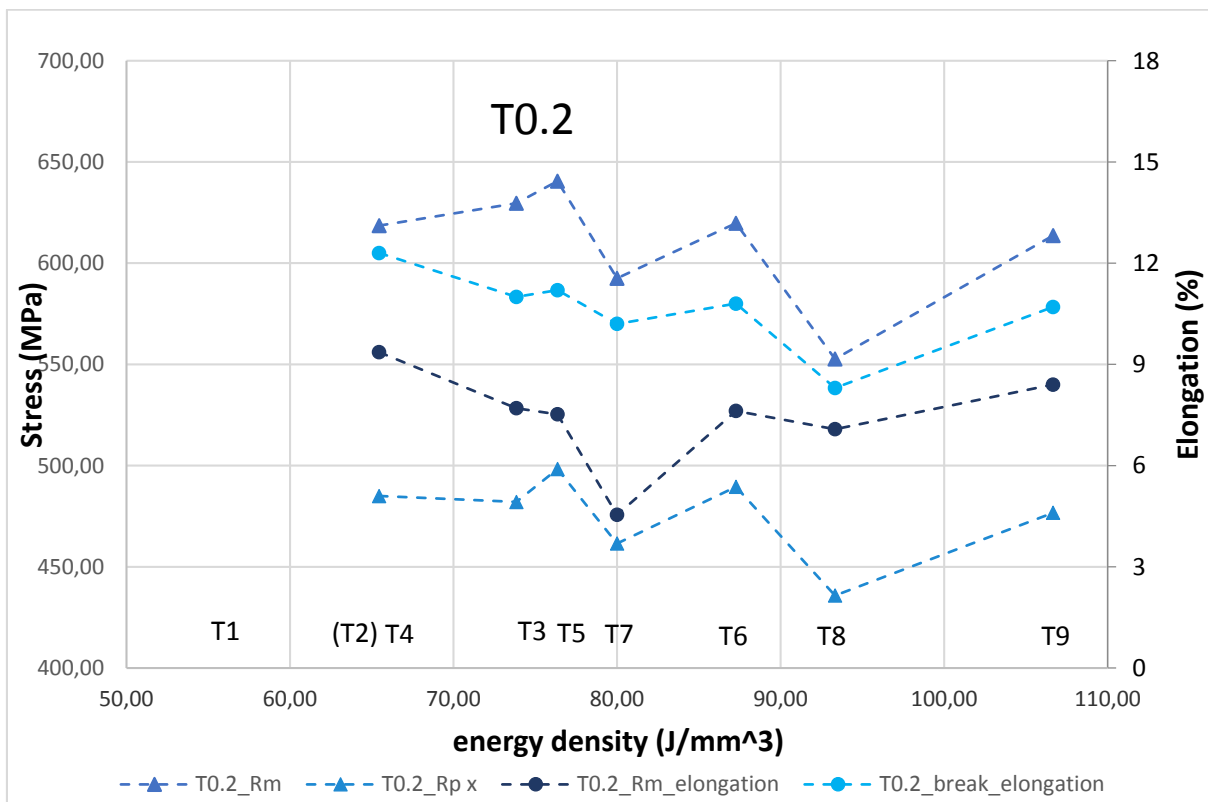
Graph 14 : Elongation at break per print direction per tensile piece set



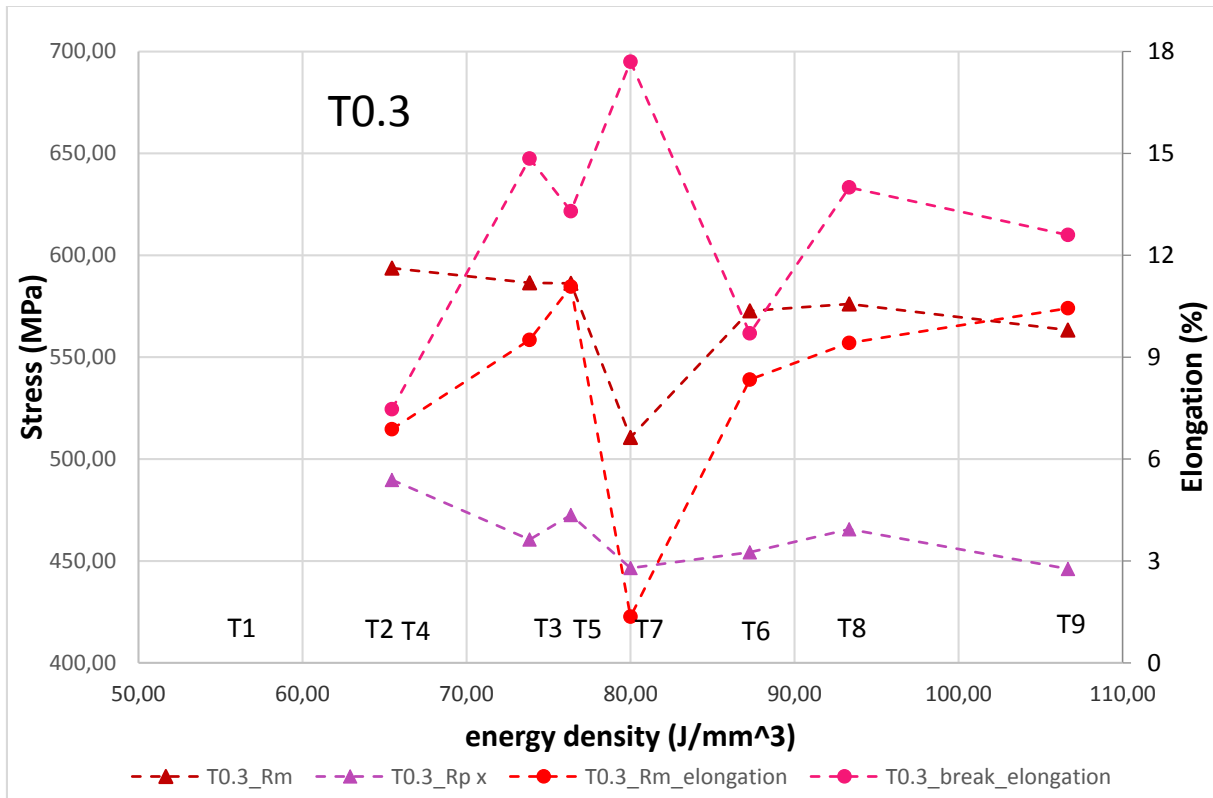
Graph 15 : The post uniform elongation per print direction



Graph 16 : The yield strength, ultimate tensile strength, elongation at Rm and elongation at break versus the energy density for the horizontal pieces perpendicular to the spreader directions. (T0.1)

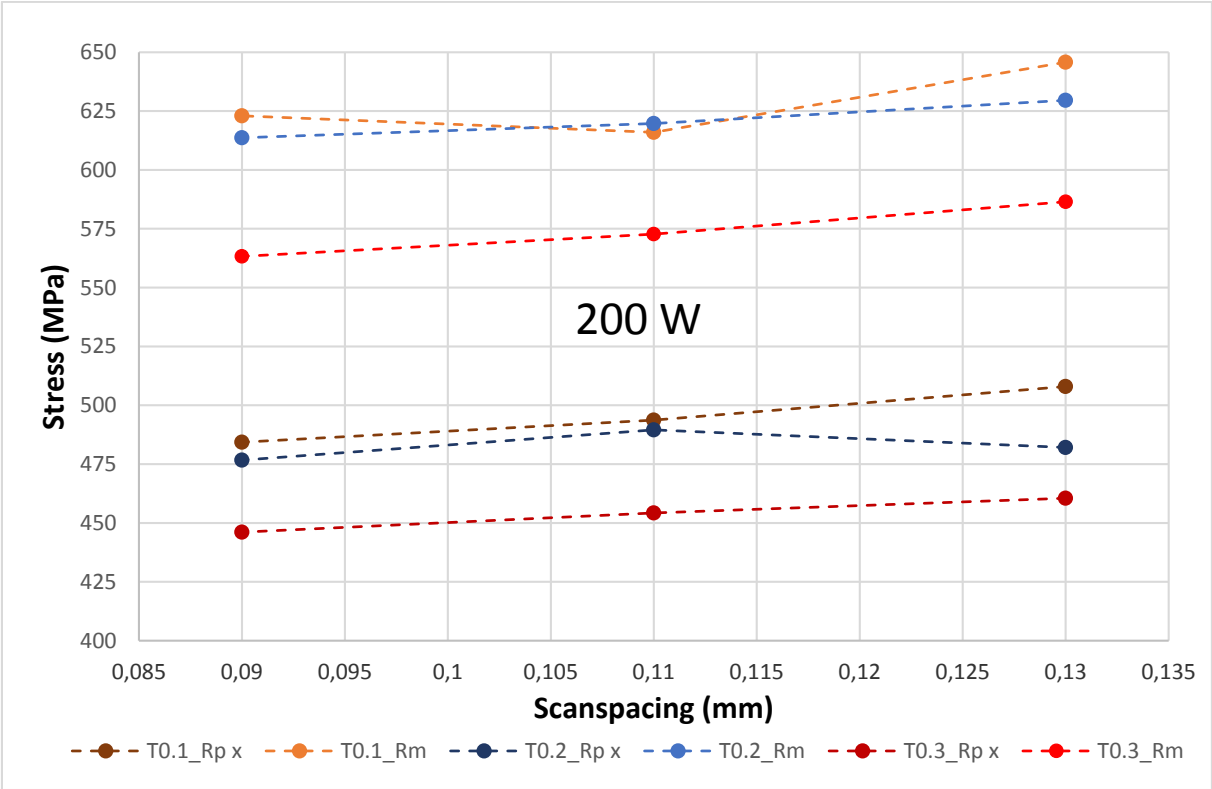


Graph 17 : The yield strength, ultimate tensile strength, elongation at Rm and elongation at break versus the energy density for the horizontal pieces parallel to the spreader directions. (T0.2)



Graph 18 : The yield strength, ultimate tensile strength, elongation at Rm and elongation at break versus the energy density for the vertical pieces (T0.3)

A plot (Graph 19) of the strength and the scan spacing for a laser power of 200W shows a clear relation. The yield strength and tensile strength rise slightly as the scan spacing increases but not enough to really make a difference, having a yield strength ranging between 475 to 510 MPa and a tensile strength of 615 to 650 for both horizontal directions (T0.1 and T0.2). For the vertical direction these values are 445 to 460 MPa and 560 to 585 MPa. The values for 175 W also stay mostly the same over the scan spacing and for 150 W there is much deviation between different directions. Since the elongation follows the same trend as the strength it is not needed to analyze it as I have analyzed the strength.



Graph 19 : Yield strength (Rp x) and ultimate tensile strength (Rm) versus scan spacing for a laser power of 200 W

4.4.3 **Conclusion**

It has been proven that generally the strength in the vertical print direction is less than in the horizontal print direction corresponding with the findings by I. Tolosa [15]. The cause is probably not delamination but some other cause within the microstructure. With a laser power of 200 W, the strength rises slightly as the scan spacing increases, thus with lower energy density. This goes against the theory that more energy density gives better bonding between the layers and between the scan tracks. There can be seen no overall trends in the effect of scan spacing or laser power on the strength and elongation. The overall strongest parameter set is T5 with 175 W laser power and 0,11 mm, this set also has the best elongation. There is a direct proportional relationship between elongation and strength. This goes against the normal decrease of elongation when strength increases.

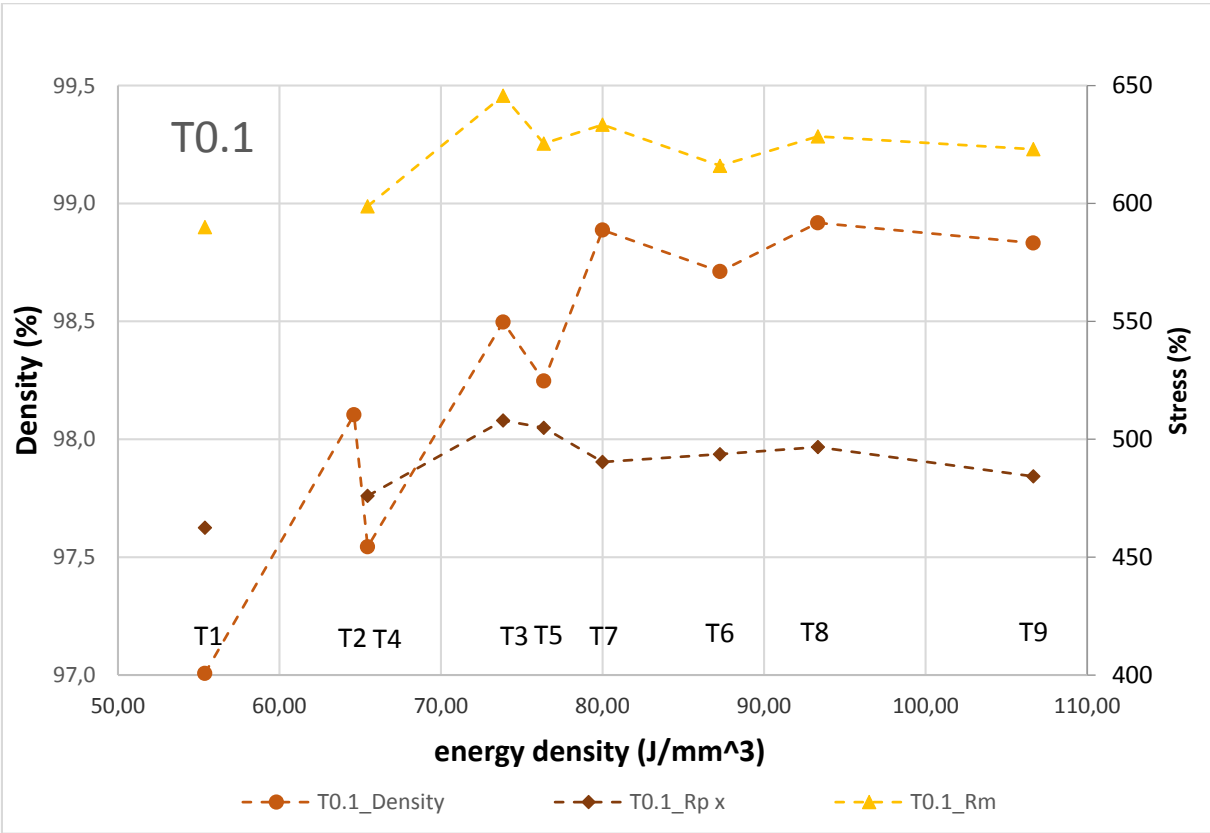
The results are further discussed in the overall discussion in chapter 4.5.

4.5 Overall Discussion

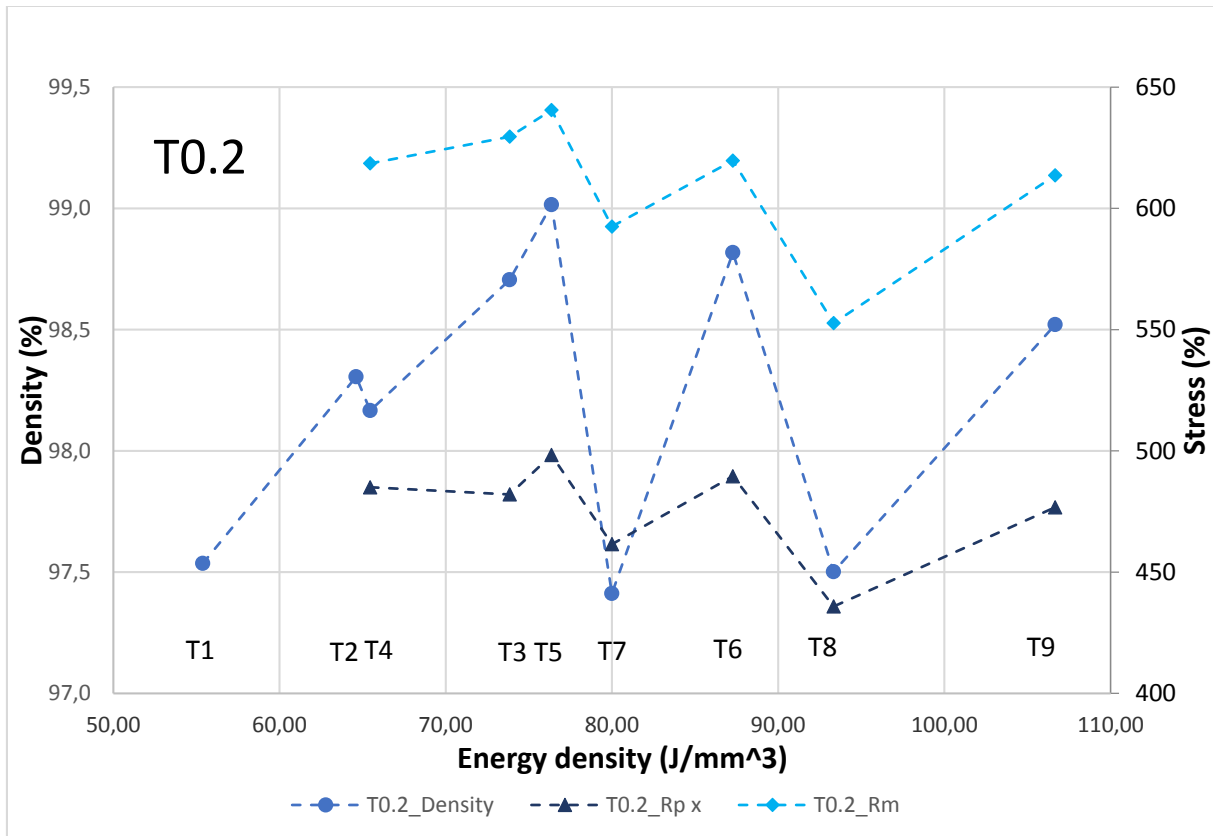
Geometries made with SLM are, for the most part, not dependent on slight changes in scan spacing or laser power. These changes seem to have much greater effect on the material properties. All of the vertical features, except the 0.5 mm hole and cylinder, are made without defects for all of the parameter sets. Horizontal circular tubes can be made with a diameter up from 2 mm to 9 mm. Though if a minimum wall thickness of 1 mm is used with a diameter of 9 mm the tube can only be 5 mm long, because of curling. It is impossible to create full horizontal overhangs with perfectly flat ceilings there will always be some stalactite forming beneath it, even with an overhang of 0,75 mm, as a matter of fact smaller horizontal overhangs beginning at 2 mm have a worse quality than the larger ones.

When comparing the results for the density tests and the tensile tests by plotting them both versus the energy density in the different directions as shown by Graph 20, Graph 21 and Graph 22, a similar trend for the strength as their respective density is found. This is noticeably more accurate for the ultimate tensile strength due to the fact that the ultimate tensile strength is more accurately measurable (the inaccurate values for T1 and T2 are excluded). Graph 22 also confirms the correctness of T8.3, which looked incorrect before.

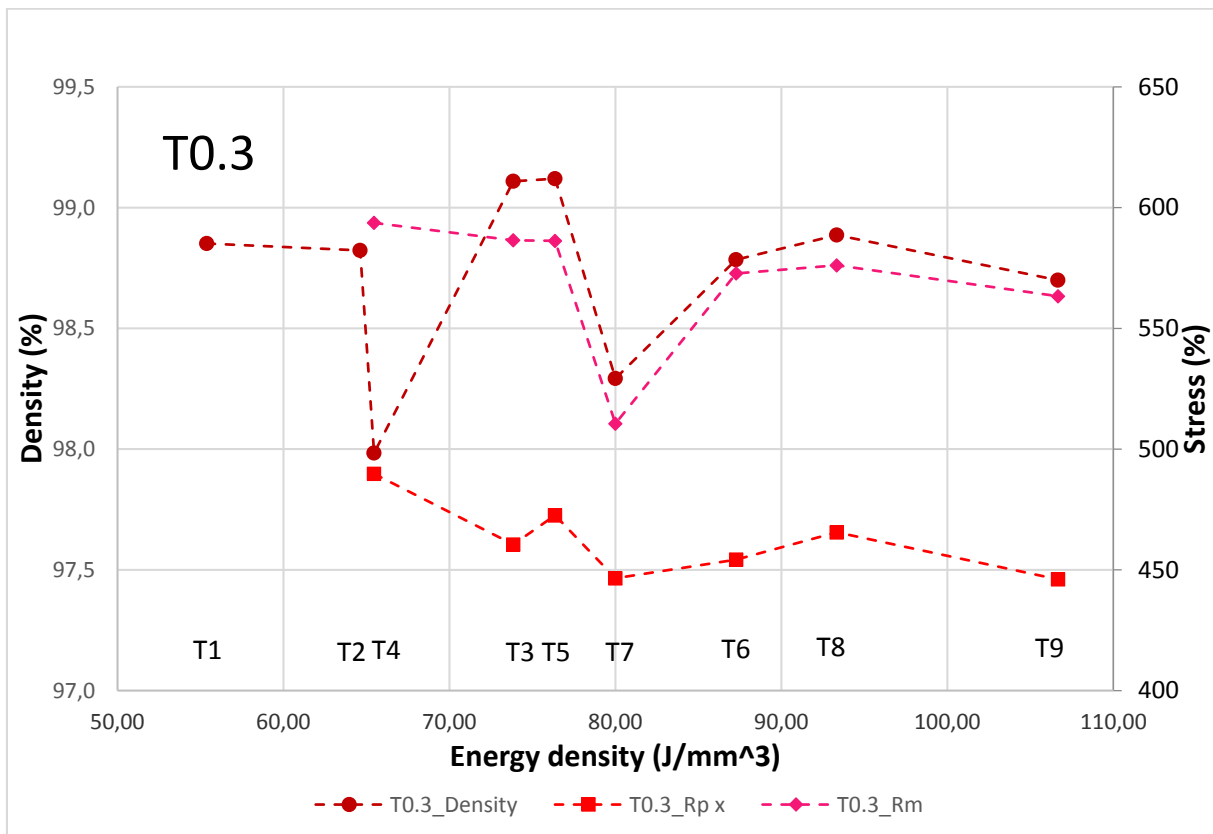
Graph 23 (p. 102) showing the strength versus the density indicates a direct relation between the strength and the density, with the strength increasing as the density increases.



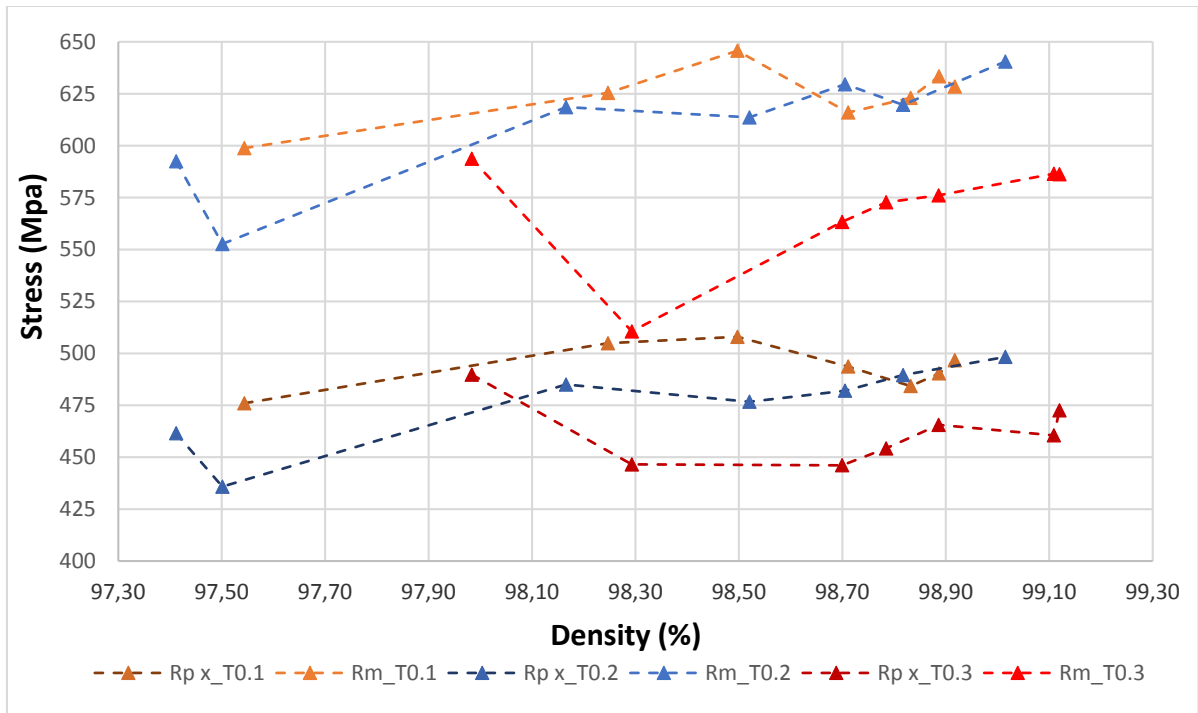
Graph 20 : The relative density, the yield strength (Rp x) and the ultimate tensile strength versus the energy density for the horizontal pieces perpendicular to the spreader directions (T0.1)



Graph 21 : The relative density, the yield strength (Rp x) and the ultimate tensile strength versus the energy density for the horizontal pieces parallel to the spreader directions (T0.2)



Graph 22 : The relative density, the yield strength (Rp x) and the ultimate tensile strength versus the energy density for the vertical pieces (T0.3)



Graph 23: Yield strength (Rp x) and ultimate tensile strength (Rm) versus Density

In the density tests there was concluded that the density values of the parameter set T6 (200W; 0,11 mm) has the most favorable density because of its consistence over the different directions. The most favorable strength and elongation however were found for the T5 (175W, 0,11 mm), the numbers are given in Table 20.

Table 20: The values to compare T5 and T6

Scan spacing (mm)	Laser power (W)	Energy density (W/mm ³)	code	Orientation	Rp x (N/mm ²)	Rm (N/mm ²)	Elongation at Rm (%)	Elongation at break (%)	Sample Relative density(%)
0,11	175	76,36	T5.1	Hor. Perpendicular	505	625	10,3	15,0	98,25 ± 0,07
			T5.2	Hor. Parallel	498	641	7,5	11,2	99,02 ± 0,13
			T5.3	Vertical	473	586	11,1	13,3	99,12 ± 0,09
0,11	200	87,27	T6.1	Hor. Perpendicular	494	616	8,4	9,4	98,71 ± 0,05
			T6.2	Hor. Parallel	490	620	7,6	10,8	98,82 ± 0,06
			T6.3	Vertical	454	573	8,3	9,7	98,78 ± 0,09
I. Tolosa [15]									
/	200	14,40		Horizontal	650,0	685		30,0	99,90
				Vertical	535,0	580		43,0	
B. Zhang [19]									
0.08	100	83.33		Horizontal		501			No preheat
						547			
						594			150 °c preheat

Parameter set T6 is the best choice because the differences in strength with T5 are small and it is most important to have little difference between the relative densities in both directions. This is because the porosity in the pieces will come to the surface when a mould is milled to the required dimensions, these pores will leave marks on the product. Trying to mill the pores away might uncover more pores and will have an effect on the product. The difference in yield strength between the horizontal and vertical pieces is only 40 MPa this is not enough to warrant a homogenizing heat treatment such as solution heat treatment.

Table 20 contains average results produce by I. Tolosa [15] in 2010 on a MTT equipment, model SLM 250 Realizer MCP (the predecessor of the Renishaw AM250). These tests were performed with 200 W laser power, 50 μm layer thickness and a build rate of $50 \text{ cm}^3\text{h}^{-1}$ resulting in an energy density of $14,4 \text{ J/mm}^3$ and using a 316L steel powder with particle size 10-45 μm . I. Tolosa claims that these parameters gave a density of 99.9%.

The table also contains results from B. Zhang [19] from 2013 on the same SLM 250 Realizer MCP at HEK Tooling GmbH Germany equipped with a continuous Nd:YAG laser source with wave length 1.054 μm but with a maximum output of 120 W. He used a 316L powder produced by gas-atomization spherical particles of 27 to 47 μm and printed on a mild steel baseplate. The parameters used were 100 W, layer thickness of 50 μm , a scan speed of 0,3 mm/s and an energy density of $83,33 \text{ W/mm}^3$.

Table 21 shows all the different parameters used in the articles and in my experiment

Table 21 : Parameters used in the literature and my experiment

	layer thickness (μm)	scan spacing (mm)	Power (W)	scanspeed (mm/s)	buildrate (cm^3/h)	buildrate (mm^3/s)	Energy density (J/mm^3)
I. Tolosa	0,05	/	200	/	50	13,88	14,40
B.zhang	0,05	0,08	100	300			83,33
C. Vanbergen	0,05	0,11	200	416,66			87,27

I. Tolosa [15] found a higher strength (the energy density is calculated from the build rate because the other build parameters were not mentioned). Unless his parameters perform very badly with other properties, it is peculiar that these are not the parameters used as standard. B. Zhang [19] used an energy equivalent to the energy used in the standard parameters yet the strength is far less. Both articles claim a density of around 99,9 which is around 1 % higher than the best density found in this project. In this project there was seen that the strength generally goes down as the laser power goes down but not enough to explain the small strength found by B. Zhang.

4.6 Conclusion

The goals of this SLM experiment was to expand the knowledge of producing 316L with SLM and produce a starting point for the production of injection moulds by looking at the geometry quality, density and strength of the test product with different geometries and overhangs. These goals were achieved by choosing parameters based on the standard Renishaw parameters and on literature, thereby choosing to vary the laser power and scan spacing around the standard parameters.

It was proven to be possible to print horizontal channels in different shapes (circular, triangular and square) with diameters up to 9 mm and overhang angles down to 45°. Upward turns of excellent quality can be printed. This means that there are possibilities of adding conformal cooling channels of different types to the mould design to create the optimal cooling and produce complex shapes of high quality using injection moulding.

The standard Renishaw parameters with 200 W laser power and 0,11 mm scan spacing were found to give the best characteristics, with a relative density of 98,87 %, a yield strength of 492 MPa and tensile strength of 618 MPa for horizontal printed pieces, a yield strength of 454 MPa and a tensile strength of 573 MPa for vertically printed pieces.

It has been proven that generally the strength in the vertical printed direction is less than in the horizontal printed direction, corresponding with the findings in other studies. The density was also found to be dependent on the printing direction. The opposite relation of that with strength was found, the vertical density is higher than the horizontal density. This does not apply to a laser power of 200 W where density is similar in all directions.

In the same printing direction a direct relation between the density and the strength was found, with strength rising as the density increases.

For a laser power of 200 Watt, the density is independent from scan spacing. The density increases as the laser power or the energy density rises. Overall the effect of the laser power and the scan spacing on the geometries is small. Density seems to be dependent on the position on the build plate yet more research is needed to confirm this because this was not the focus of this experiment.

Stainless 316L steel shows signs of corrosion when submerged into a sonar bath with deionized water. It might need a corrosion resistance enhancement treatment like solution annealing or passivation before usage in a mould cooled with deionized water. Parts produced with SLM seem to lose mass because of cavitation in pores just below the surface of the part when placed into a sonar bath, causing not fully melted powder particle to separate from the surface of the part.

Further research into the material properties such as hardness, microstructure, dimensional accuracy and roughness is necessary.

5 Mould design

5.1 Product design

The product chosen is a cup holder to hold coffee cups such as used in the coffee dispensing machine (at the Cell Kunststoffen). This cup holder was designed in such a way that conventional mould cooling and temperature control will produce parts with obvious defects, while with conformal cooling channels and variotherm temperature control these defects would be reduced as described in the literature in chapter 2.3. The final product and some of its dimensions (mm) are shown in Figure 52. The product was made with Creo Parametrics 3. The following features were included into the product:

- The walls of the product are 1 mm thick giving rise to high pressures in conventionally cooled moulds while variotherm temperature control should decrease the injection pressure. Conformal cooling causes an even shrinkage over the whole product giving less deformation and less failed products.
- The gap in the ring has the same function as with E. Sachs [4], indicating deformation in the product. Conformal cooling should enable better control over the size of the gap in the moulded product.
- The windows in the ring make pillars were the plastic flows merge, creating weld lines, these should be decreased by variotherm temperature control.
- The small space within the handle is a spot were conventional cooling cannot reach, conformal cooling should give better cooling in that area.
- The trapezium shaped gap on the bottom is to accommodate an optimal gate location.

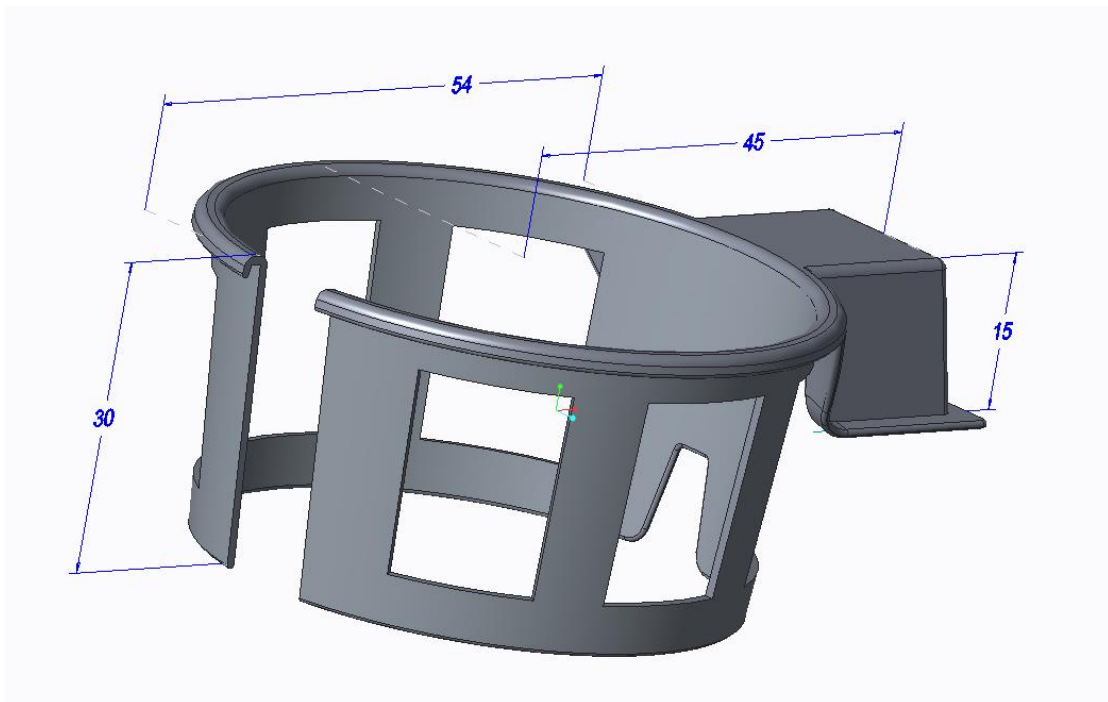


Figure 52 : The final product with some of its dimension in mm

PC-ABS blend was chosen as material to produce the product. This blend combines the heat-resistance and strength of a PC polymer with the good flow characteristics of an ABS polymer. The blend in particular is a Bay blend T65 by Bayer.

To optimize the design of the cup holder, the stresses and deformation in the product were simulated when the cup holder holds a cup full of coffee at a temperature of 100 °C. These simulation were performed with the add-on Creo Simulate in Creo Parametrics 3.

To simulate the product, changes in the model had to be made to reduce the simulation time while preventing singular points. These changes are shown in Table 22. The simulation design with mechanical data (left) and thermal data are shown in Figure 53 (P. 107). The setting used are shown in Table 23 (P. 107).

Table 22 : The changes made in the model for simulations

changes	reason	benefit
The product was cut in halve across the symmetry line. The cut surface is fixed only in the Z-direction. The mechanical force on the product is halved because the contact surface is halved in this instance.	When perfect symmetry exists both sides will take equal force inducing equal stress and deformation, this allows one half of the product to be deleted.	This method greatly reduces the amount of elements, decreasing the calculation time.
Outward rounded corners are deleted	Outward rounded corner are purely cosmetic and so do not contribute the mechanical strength.	Rounds, especially small rounds as used in this model, meshed with adaptive meshing will need small elements to follow the contour of the round, increasing the calculation time dramatically whilst giving no contribution to the actual calculations.
Rounds on all inward corners	The rounds that do not affect the thickness of the product can be added without changing the simulation results significantly	Sharp inward corners cause singular point where calculation go wrong and start to diverge to infinity, rounds on these corners negate these singular points.

Table 23 : Forces on the simulation model

Force/Fixture	Size/type of fixture	Surface	Directions	Indication	Comment
Mechanical simulations (Left picture, Figure 53)					
Mass of the water in the cup	Half of 0,2l cup water = 0,981 N (Symmetry)	inner surface of cup holder ring	Y-axis downwards	orange arrows	
Gravity force acting on the product			Y-axis downwards		Calculated from the density of the material
gripping of the hand	fixed	Underside of the handle	Y-direction	bleu arrows	Surfaces have to be fixed in the 3 directions separately to allow the product to expand and move as it would in reality. Fully fixing one surface in all direction would not allow this and induce large stresses around the edges of the fixtures.
	fixed	Back surface of the handle	X-direction	bleu arrows	
	fixed	Cut surface of the symmetry (Same fixture as necessary for the symmetry)	Z-direction	bleu arrows	
Thermal simulation (Right picture, Figure 53)					
The temperature of the coffee	a set temperature of 100°C	inner surface of cup holder ring	/	Green surface	
Convection in room temperature	$h = 10 \text{ W/m.K}$ bulk temperature = 20°C	All outward surfaces	/	bleu arrows	Normal room temperature values

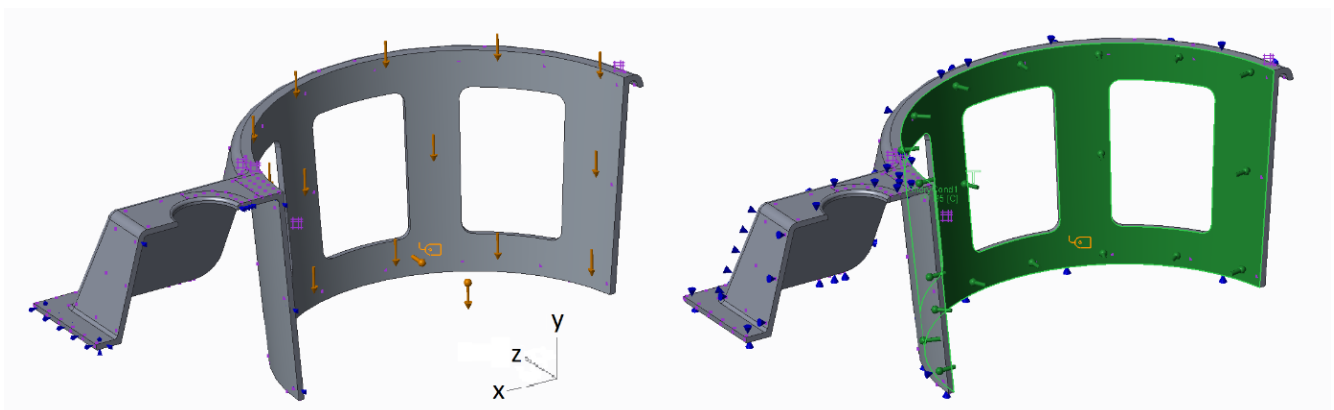


Figure 53 : The simulation setup: left : the mechanical forces and fixtures, right : the thermal forces and fixtures

The simulation was run with a multi-pass adaptive method using a maximum polynomial order of 9 and stopping when results lay 5 % from the previous results. The overall mesh size was 3 mm with refined areas of 1 mm mesh size where higher stresses were seen, this can be seen as closed grouped purple dots in Figure 53

NOTE: The product had to be free of any mathematical errors. Creo has a function called geometry check that indicates any mathematical errors in the product. The area where the downwards edge of the handle meets the top ring proved difficult to create without errors.

Simulations shown in Figure 54 show the largest stress for a 0,8 mm wall thickness in the handle going up to 20 MPa. This gives a good safety factor of 2,75 for the PC-ABS blend with a yield strength of 55 MPa at room temperature. Deformation in the Y-direction reaches a maximum in the outer part with a downward deformation of 6.27 mm, this would mean the cup would be sloped too much forward.

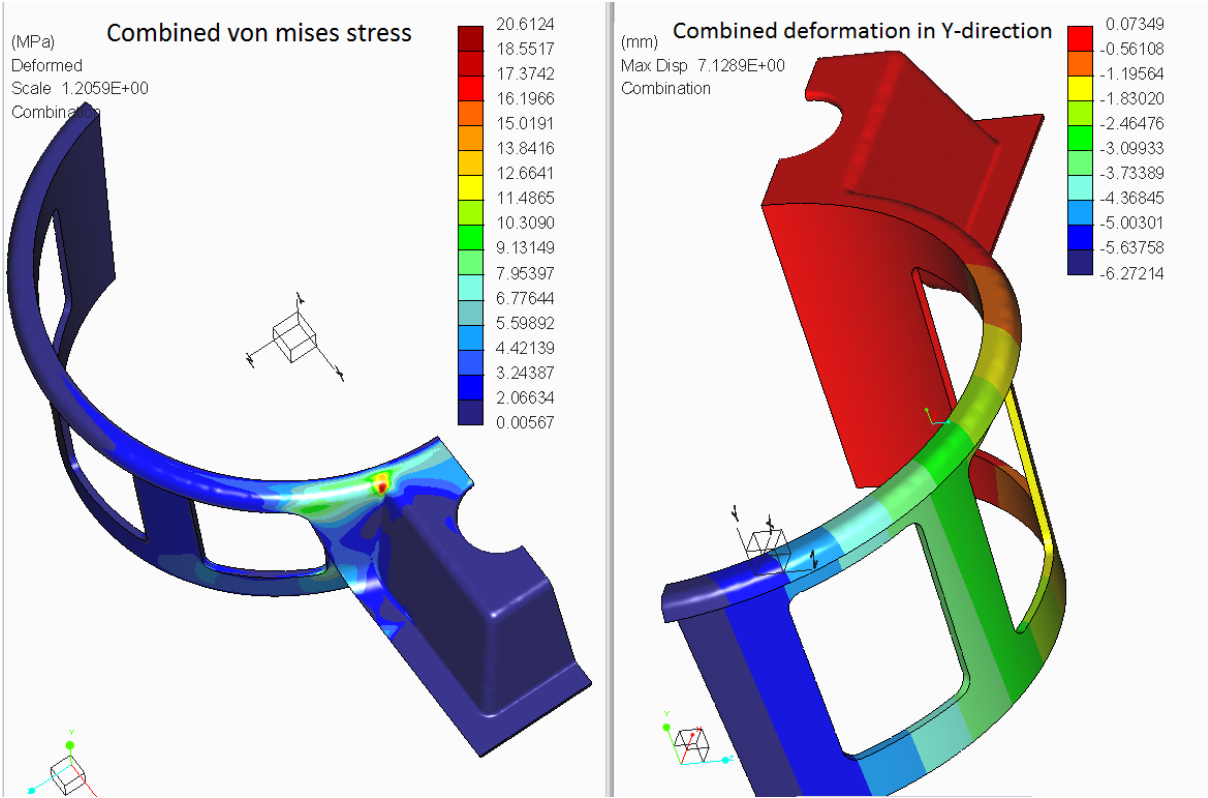
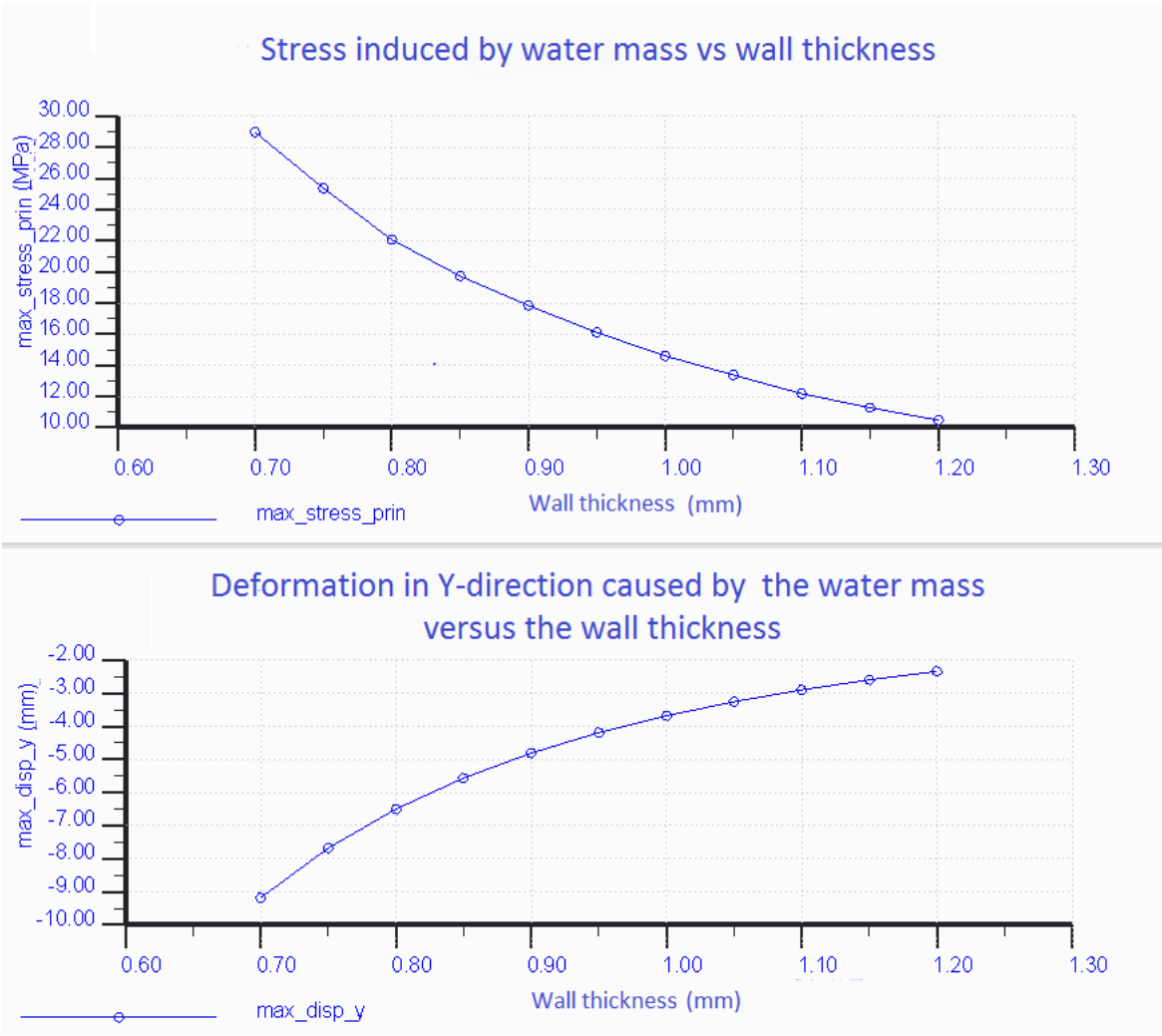


Figure 54 : Simulation results of the cup holder

To reduce the deformation in the Y-direction a sensitivity study was performed simulating the product with different wall thickness from 0,7 mm to 1,2 mm. The mass of the water had the most effect on the stress and deformation of the product. The relations with wall thickness are shown in Graph 24. Based on these results a wall thickness of 1 mm was chosen as sufficiently reducing the forward tilt of the cup, while keeping a sufficiently thin product to realize a reduction in injection pressure when using variotherm temperature control. The deformation in Y-direction caused by the water mass was reduced from 6,5 mm to 3,75 mm. The stress was also lowered from 20 MPa to 14,5 MPa further increasing the safety factor at 23°C to 3,8. This should certainly be enough to withstand any strength reduction due to the high temperatures.



Graph 24 : Top: relation between stresses caused by the water mass versus the wall thickness. Bottom: relation between the deformation in Y-direction caused by the water mass versus the wall thickness.

The ergonomics of the product were optimized by printing the product using 3D-printing process called fused deposition modeling. This process melts a solid plastic wire to build up the layers of the product. The machine used was an Ultimaker 2. An important consideration for printing with this procedure is placing the model in such a position that the number of supports is minimized. Another consideration is that model walls are not less than the diameter of the printing nozzle, being 0,4 mm. The standard parameters with a layer thickness of 0,1 mm were used to print the products. Overhangs were of a very good quality. Sanding was needed to remove some protruding bits.

In total three products were printed, the first one was printed in PLA and the next two were printed in ABS plastic. The first print was tested and found to have an insufficient diameter. An empty cup would stand out of it far too high as seen in the left of Figure 55. The bottom of the handle was too wide and long for a comfortable grip as seen in the middle of Figure 55. The right picture in Figure 55 shows the side view with a full cup, the ring splits open until it is pushed against the edge of the pattern in the cup. The handle is also slightly too high. The problem with the empty cup being so high in the holder is that the product would jump up as the cup gets emptied and the coffee cools down, possibly spilling coffee on the user. Next two models were printed with each a different, smaller ring diameter and smaller handle. They were analyzed in a similar fashion and the eventual dimensions seen in Figure 52 (P. 105) were based on these models.



Figure 55 : Ergonomic test of the first product; left: side view with empty cup, middle: top view with empty cup, right: side view with full cup

5.2 Printed mould design

The product was converted to a mould with the aid of a special type of model called mould cavity. This function allows a mould block to be defined around the product model. The program identifies the upper and under surfaces, creating a parting line along the edges of the product, without any undercuts. This works very well for simple products but was having difficulties with the transition between the ring and the handle. A mathematical error persists in the mould itself at that point, yet it is apparent that the error will not translate when converted to a step or other file type. Custom parting surfaces can be created within the program. The features that the program was unable to include were the gap in the ring and the ramp that is mentioned in the next chapter. This has to be carefully added after the generation of the mould parts giving particular attention to avoid undercuts.

The product was simulated in Autodesk Moldflow simulation software to find the optimal gate location. To keep the mould simple, only one gate was used. This is shown in the left picture of Figure 56 where the gate location analysis colours the best area for gate placement red and the worst area bleu. The right picture of Figure 56 shows the time it takes to fill every area of the product, with bleu as 0 sec and red as 0,4757 sec. The optimal position appeared to be right in the middle of the large inner surface ring below the handle. This could only be done by means of a ramp going into the core of the mould as indicated by the red arrows in Figure 57 (P. 112), resulting in the trapezium shaped gap in the final product. The mechanical simulation does not include this gap, but because the main forces are in the handle and the main deformations are further down the arms, this gap will not influence the results significantly.

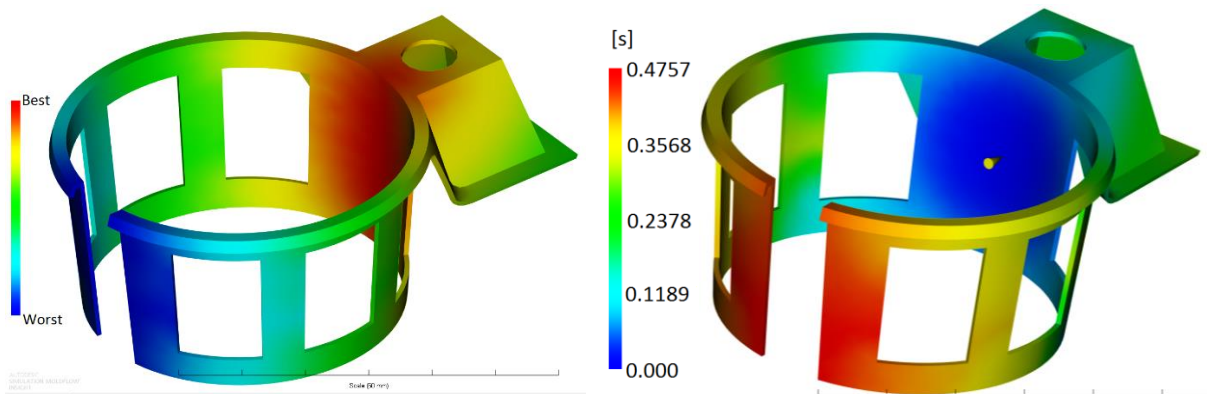


Figure 56 : Left: Results of the gate location analysis, Right: Filling times with the gate in the middle of the best gate location

The baseplate upon which the mould is printed is 120x140 mm (top surface), this is smaller than the normal 250x250 mm plates used in the Renishaw machine at the IISE. The reason is that milling will most certainly be necessary and if 5-axis milling is needed, then the plate cannot be too big to prevent the mill head from colliding with the base plate when milling in tight corners. For this purpose a reusable thick plate was going to be made with a set of holes at equal distance, the smaller blocks can be mounted on top of this large plate and can easily be removed after printing, reducing cost of baseplates.

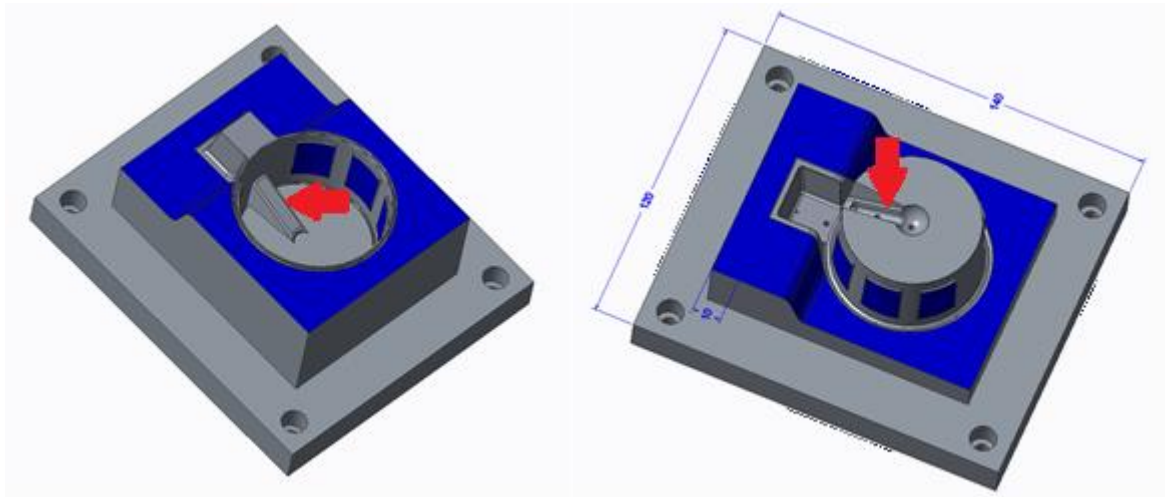


Figure 57 : Left: the cavity insert on the smaller base plate. Right: the core on the smaller base plate

The most efficient way of printing a mould is to restrict the bulk material around the cavity to provide enough room and strength to allow the placement of cooling channels. Milled blocks fitted around the mould will help to resist the pressure on the mould and prevent the printed mould from deforming outwards. Numerous attempts to calculate the size of the printed block through simulation of the forces in Creo Parametrics have failed due to the complexity of the mould and the placement of the fixtures, in all studies singular points with stress far exceeding the yield strength of the 316L stainless steel were observed. Based on conformal cooling dimensions given by S. Mayer [10]. A cooling channel of 4 mm diameter with a distance from cavity to channel centre of 6 mm, will give 2 mm of space when the printed block of steel ends 10 mm from the cavity, as indicated in Figure 57.

There are many different types of gates. One of the most frequently used is the diver gate, also called submarine gate [6]. This kind of gate leaves no trace on the moulded product, with the major advantage of needing no extra machining.

5.3 Milling

All of the outward surfaces have to be milled for a good surface quality of the product and to fit into the mould assembly.

The windows in the ring of the product are a difficult feature to incorporate in an injection mould. The first problem is that they tend to cause a slight undercut in the mould in which the product can become stuck during ejection, valuable production time is wasted with unjamming the injection moulding machine. This was solved by splitting this window into two, one on the core and one on the cavity as shown in Figure 58.

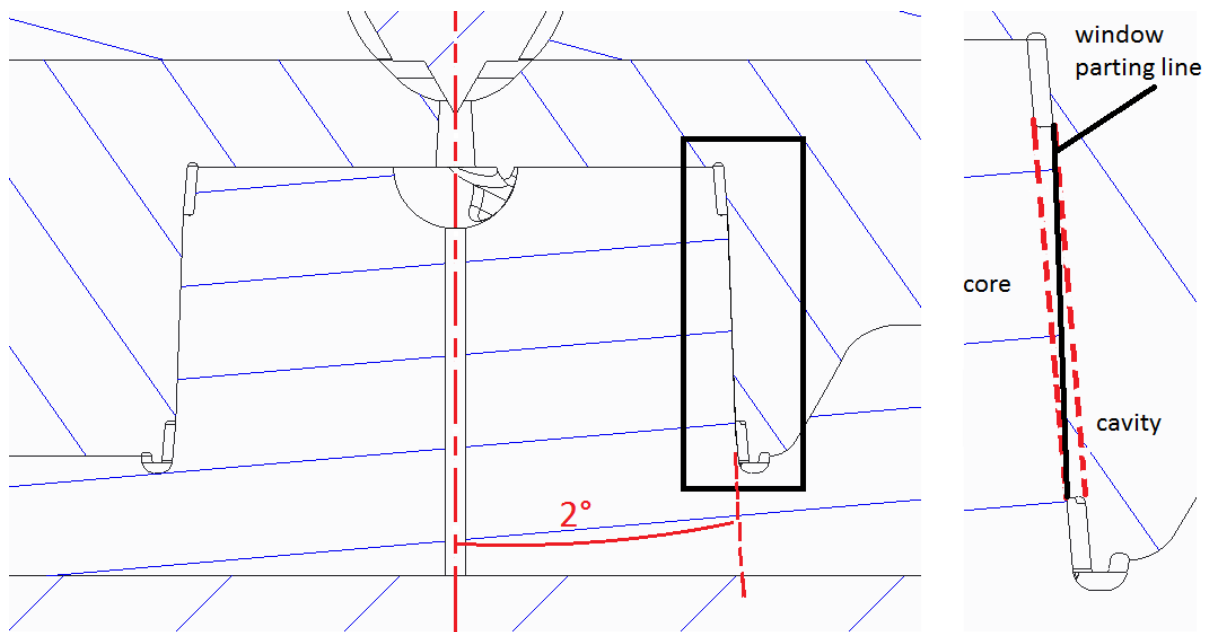


Figure 58 : Parting line of window feature

This solution however causes another problem. The contact surface between the two inserts, has an angle of 2° (Figure 58, Left) to the movement of the mould, causing surfaces of both moulds to slide over each other when closing. These surfaces have to be made with tight tolerances, if the surfaces touch too early the mould cannot close fully, if the surfaces do not touch at all, especially at the edges, polymer will penetrate between the surfaces and cause flash. When milling these surfaces, the limited stiffness of the mill bit will cause it to bend, resulting in dimensions that are larger than the defined dimensions in the milling program. The deviation is dependent on various parameters such as stiffness, quality and wear on the mill bit. It is impossible to compensate this effect without the risk of taking of too much material. Extra procedures are needed to fit the mould, first the mould is fitted together as tightly as possible, then the gap between the inserts is measured. The windows of both inserts are milled with compensated dimensions based on the gap between the inserts. This should reduce the largest part of the gap when fitting it back together without taking of too much material. After this procedure, a more accurate method known as blueing, also called Prussian Bleu fitting, is performed. This is a process where one of the surfaces

is coloured with a blue colour and when the core and the cavity are assembled and disassembled blue marks can be seen on the uncoloured side, this is where the cavity and core touch each other. If possible the cavity and core are slightly milled on those spots, if that is not possible they are polished by hand. The process is repeated iteratively until the mould closes perfectly. The amount of time this process takes is hard to predict.

5.4 Mould assembly design

The mould assembly is a quick change mould from manufacturer Meusburger, accepting inserts with dimension equal to 220x170x60 mm. All components from Meusburger are listed in appendix C. To allow the smaller, printed insert to be fitted into the mould, the base plate is bolted onto a mounting plate that fits into the mould assembly, with 2 positioning pins to hold the position. Four steel support blocks are milled to fit tightly around the printed inserts, positioned with one positioning pin and secured with 2 bolts each. The support blocks around the mould and the holes for the cavity insert are shown by Figure 59. The edge of the support blocks that protrude from the surface of the green block are chamfered to prevent collision with the core mould assembly during closing.

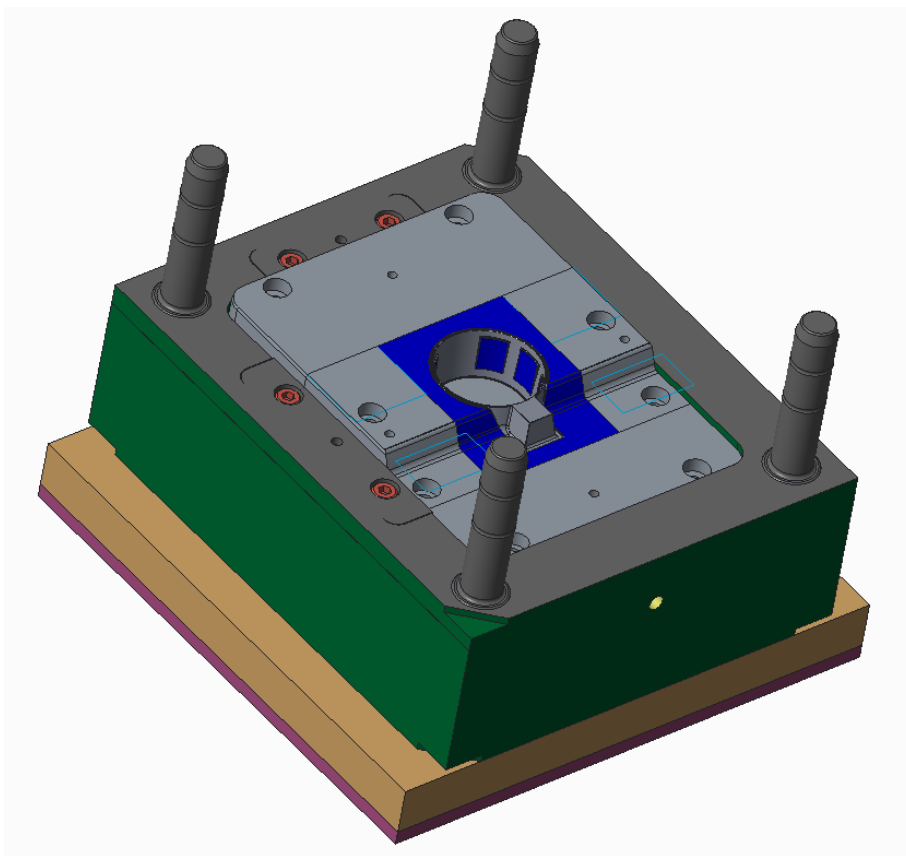


Figure 59 : The mould assembly for the cavity part (Stationary)

In many applications of injection moulding hot runners are used to improve productivity and reduce material waste, especially coupled with variotherm temperature control. This means that the polymer stays at a high temperature through the injection part of the cycle. The mould is fitted with a hot runner of the type 6DET50-G51 manufactured by Günther. The model was chosen based on the polymer. The length of the hot runner is 50 mm and was chosen to fit the mould, the nozzle has a diameter of 6 mm chosen because of the low shot weight in this mould. No insulating sleeve was used. The hole in which this hot runner is inserted has been designed to the guidelines by the manufacturer [35].

All ejectors in the mould are regular, round flat face models. The ejectors in the mould handle are positioned so that conformal cooling channels can be placed around them. On the top of the ring there is little flat surface to place flat face injector pins, for this reason a number of small pins were placed, to distribute the force so that traces of ejection on the final product are minimized. On the runner larger ejectors are used because imprints due to the ejector holes on the runner are not important. Only the ejector holes are visible in the top view of the mould in Figure 60.

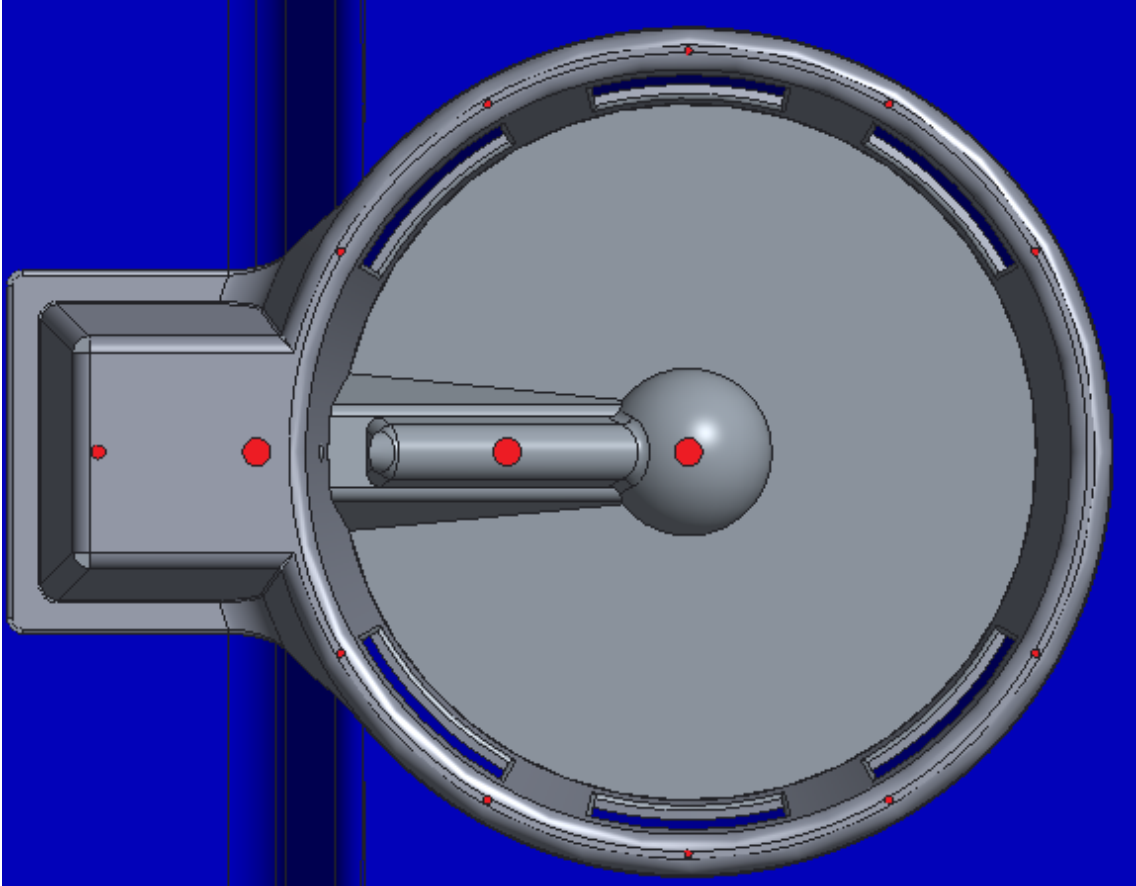


Figure 60 : Placement of ejectors in the core of the mould

A section of the mould with the parts indicated is shown in Figure 61.

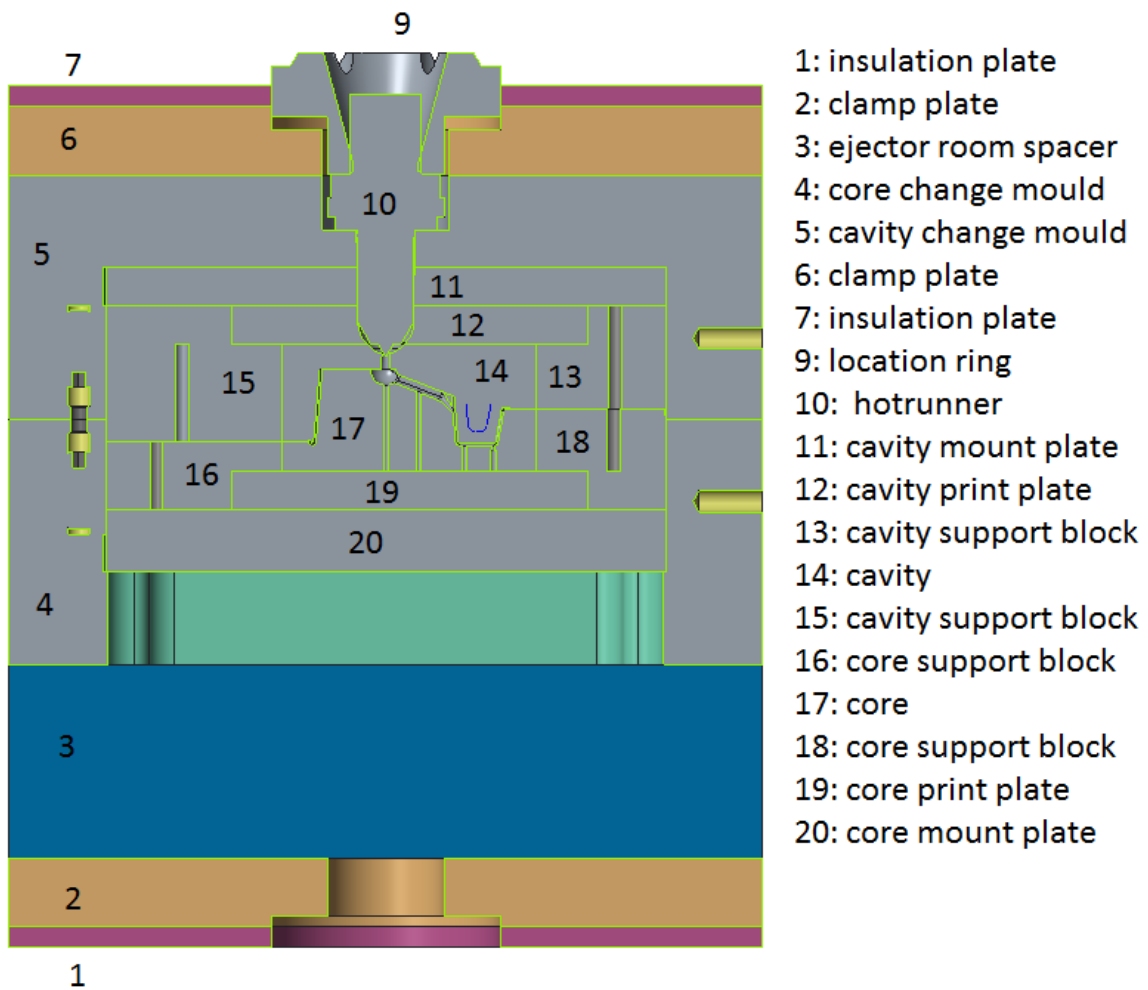


Figure 61: The section of the assembled mould

This mould design has all of the essential components, minor component have to add such as:

- Pens and bolts,
- Ejector pins,
- Electrical circuit slots,
- Cooling channels and connectors.

6 Conclusion

In this thesis an experiment with selective laser melting of 316L stainless steel was conducted. The effects of scan spacing and laser power on geometry, density and strength were examined. It was proven to be possible to print horizontal channels in different shapes (circular, triangular and square) with diameters up to 9 mm and overhang angles down to 45°. Upward turns of excellent quality can be printed. This means that there are possibilities of adding conformal cooling channels of different types to the mould design to create the optimal cooling and produce complex shapes of high quality using injection moulding.

The standard Renishaw parameters with 200 W laser power and 0,11 mm scan spacing were found to give the best characteristics, with a relative density of 98,87 %, a yield strength of 492 MPa and tensile strength of 618 MPa for horizontal printed pieces, a yield strength of 454 MPa and a tensile strength of 573 MPa for vertically printed pieces.

It has been proven that generally the strength in the vertical print direction is less than in the horizontal print direction, corresponding with the findings in other studies. The density was also found to be dependent on the printing direction. The opposite relation was found, the vertical density is higher than the horizontal density. This does not apply to a laser power of 200 W where density is similar in all directions.

In the same printing direction a direct relation between the density and the strength was found, with strength rising as the density increases.

For a laser power of 200 Watt, the density is independent from scan spacing. The density increases as the laser power or the energy density rises. Overall the effect of the laser power and the scan spacing on the geometries is small. Density seems to be dependent on the position on the baseplate, yet more research is needed to confirm this.

A test product and an injection mould to test the effects of conformal cooling and variotherm temperature control were designed, aided by 3D-printing of a prototype and numerical simulations.

Stainless 316L steel shows signs of corrosion when submerged into a sonar bath with deionized water. It might need a corrosion resistance enhancement treatment like solution annealing or passivation before usage in a mould cooled with deionized water.

Further research into the material properties such as hardness, microstructure, dimensional accuracy and roughness is necessary.

The missing components have to be added to the mould design and conformal cooling channels have be designed using numerical simulations. The mould has to be printed and tested on a injection moulding machine. A reference mould with conventional cooling channels has to produced and tested.

List of used sources

- [1] P. moulding, „History of plastic moulding,” [Online]. Available: <http://www.plasticmoulding.ca/history.htm>.
- [2] V. Goodship, ARBURG: Practical Guide to injection moulding, Shawbury, Shrewsbury, Shropshire, SY4 4NR, UK: Rapra Technology, 2004.
- [3] DME, „Mold bases and Plates catalog,” [Online]. Available: <http://www.dme.net/resources/pdf-catalogs>. [Geopend July 2015].
- [4] E. Sachs, „Production of Injection Molding Tooling with Conformal Cooling,” p. 1234, 1995.
- [5] L. Frick, „<http://machinedesign.com/3d-printing/difference-between-machined-and-3d-printed-metal-injection-molds>,” 2014. [Online]. Available: <http://machinedesign.com/3d-printing/difference-between-machined-and-3d-printed-metal-injection-molds>.
- [6] M. R. Kamal, A. Isayev en S.-J. Liu, Injection molding: Technology and Fundamentals, Munich/ Cincinnati: Hanser, 2012.
- [7] EOS, „Tooling: Injection moulding,” EOS, [Online]. Available: http://www.eos.info/industries_markets/tooling/injection_moulding. [Geopend July 2015].
- [8] A. Jacobs, E. Hooyberghs, E. Meynaerts en K. Vrancken, „Beste Beschikbare Technieken (BBT) voor kunststofverwerking,” Vlaamse BBT-Kenniscentrum, 2006.
- [9] O. Mohamed, „A Simulation Study of Conformal Cooling Channels in Plastic Injection,” Swinburne University of Technology, 2013.
- [10] S. Mayer, Optimised mould temperature control procedure using DMLS, Munich, Germany: EOS GmbH Electro Optical Systems, /.
- [11] Popular 3D printers, „selective laser melting (SLM),” 2013. [Online]. [Geopend november 2014].
- [12] V. Petrovic, J. V. H. Gonzalez, O. J. Ferrando, J. D. Gordillo, J. R. B. Puchades en L. P. Grinan, „Additive layered manufacturing: sectors of industrial application shown through case studies,” *International Journal of Production Research*, vol. 2011, p. 1063, 2009.
- [13] I. Yadroitsev, A. Gusarov, I. Yadroitsava en I. Smurov, „Single track formation in selective laser melting of metal powders,” *Journal of Materials Processing Technology*, pp. 1624-1631, 2010.
- [14] M. Van Elsen, „COMPLEXITY of SELECTIVE LASER MELTING:,” Catholic university of Leuven, 2007, pp. 101, 104, 116.
- [15] I. Tolosa, F. Garcíandía, F. Zubiri, F. Zapirain en A. Esnaola, „Study of mechanical properties of AISI 316 stainless steel processed by “selective laser melting”, following

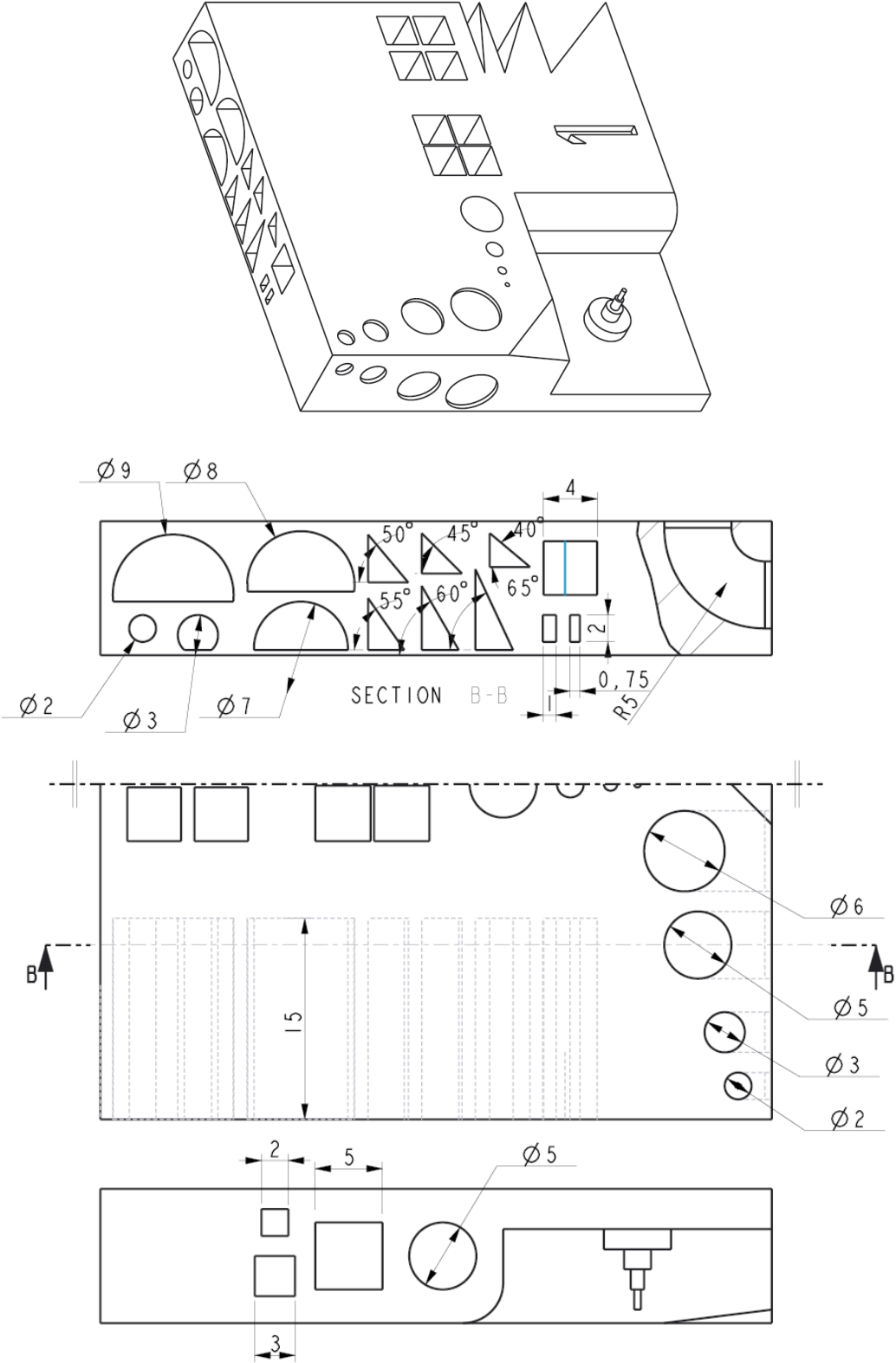
different manufacturing strategies,” *International Journal Advanced Manufacturing Technology*, vol. 2010, 2009.

- [16] Granta Design, *Edupack CES software*, Granta Design, 2014.
- [17] J. A. Cherry, H. M. Davies, S. Mehmood, . N. P. Lavery , S. G. R. Brown en J. Sienz, „Investigation into the effect of process parameters on microstructural and physical properties of 316L stainless steel parts by selective laser melting,” *International Journal for Advanced Manufacturing Technology*, p. 11, 2015.
- [18] J. P. Kruth, „BENCHMARKING OF DIFFERENT SLS/SLM PROCESSES AS RAPID MANUFACTURING TECHNIQUES,” Gent, Belgium, 2005.
- [19] B. Zhang, L. Dembinski en C. Coddet, „The study of the laser parameters and environment variables effect on mechanical properties of high compact parts elaborated by selective laser melting 316L powder,” *Materials Science & Engineering A*, pp. 27-28, 2013.
- [20] E. Yasa, K. Kempen, J.-P. Kruth, L. Thijs en J. Van Humbeeck, „MICROSTRUCTURE AND MECHANICAL PROPERTIES OF MARAGING STEEL 300 AFTER SELECTIVE LASER MELTING,” p. 393, 2010.
- [21] D. Thomas, „The development of design rules for Selective Laser Melting,” University of Wales Institute, Cardiff, United Kingdom, 2009.
- [22] K. Kempen, „LOWERING THERMAL GRADIENTS IN SELECTIVE LASER MELTING BY PRE-HEATING THE BASEPLATE,” 2013.
- [23] P. Mercelis en J.-P. Kruth, „Residual stresses in selective laser sintering and selective laser melting,” *Rapid Prototyping Journal*, Vol. 12 Iss 5, pp. 254 - 265, 2006.
- [24] R. D. Li, J. H. Liu, Y. S. Shi, L. Zhang en M. Z. Du, „Effects of processing parameters on rapid manufacturing 90W–7Ni–3Fe parts via selective laser melting,” vol. 2009, p. 9, 2009.
- [25] V. E. BEAL, P. ERASENTHIRAN, N. HOPKINSON, P. DICK en C. H. AHRENS, „Scanning strategies and spacing effect on laser fusion of H13 tool steel powder using high power Nd:YAG pulsed laser,” *International Journal of Production Research*,, p. 17, 2008.
- [26] J.-P. Kruth, M. Badrossamay, E. Yasa, J. Deckers, L. Thijs en J. Van Humbeeck, „Part and material properties in selective laser melting of metals,” /.
- [27] North American stainless, „Long products stainless steel grade sheet,” North American stainless, [Online]. Available: <http://www.northamericanstainless.com/wp-content/uploads/2010/10/Grade-316-316L1.pdf>. [Geopend July 2015].
- [28] American Metals Co., „316L Stainless Steel Technical Data Sheet,” American Metals Co., 2002-2014. [Online]. Available: <https://www.metalshims.com/t-316L-Stainless-Steel-technical-data-sheet.aspx>. [Geopend July 2015].




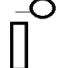
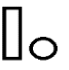
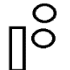
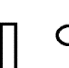
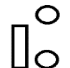
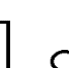
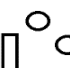

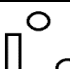

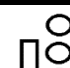


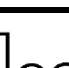
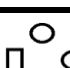
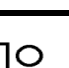
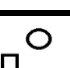
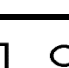
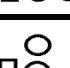
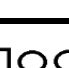
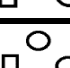
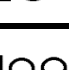
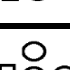
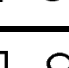
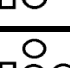

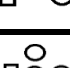
- [29] P. Atanda, A. Fatudimu en O. Oluwole, „Sensitisation Study of Normalized 316L Stainless Steel,” *Journal of Minerals & Materials Characterization & Engineering*, nr. Vol. 9, No.1, pp. pp.13-23, 2010.
- [30] K. Saeidi, X. Gao, F. Lofaj, L. Kvetková en Z. J. Shen, „Transformation of austenite to duplex austenite-ferrite assembly in annealed stainless steel 316L consolidated by laser melting,” *Journal of Alloys and Compounds*, p. 463–469, 2015.
- [31] Layerwise, *Powerpoint "Layerwise Metal Additive Manufacturing"*, 2015.
- [32] LPWtechnology, „LPWtechnology: iron based SLM powders,” LPWtechnology, 2015. [Online]. Available: <http://www.lpwtechnology.com/powder-finder/#>. [Geopend 2015].
- [33] B. A. Johnson, „corrosion of metals in deionized water at 38 °c,” *Nasa Technical Memorandum*, 1969.
- [34] Forum, „Deionized water - EngTips,” 2002. [Online]. Available: <http://www.EngTips.com/viewthread.cfm?qid=29596>.
- [35] Günther, „Hotrunner nozzle catalog,” [Online]. Available: http://www.guenther-heisskanal.de/uploads/pdf/Hot-runner-nozzles_2_EN_03-15_1_01.pdf. [Geopend August 2015].
- [36] (IISE) The insitute for innovation in sustainable engineering, „Research at derby: (IISE) The insitute for innovation in sustainable engineering,” The university of Derby. [Online]. [Geopend November 2014].
- [37] Cell Kunststoffen, „Expertise cell: Kunststoffen,” KULeuven, [Online]. Available: <http://www.khlim.be/expertise/cel-kunststoffen>. [Geopend November 2014].
- [38] Propolis, „Research at the KULeuven: Propolis,” [Online]. Available: <https://iiv.kuleuven.be/onderzoek/propolis/>. [Geopend November 2014].
- [39]
- [40] RP Photonics Encyclopedia, „Q-switching,” 2007. [Online]. Available: http://www.rp-photonics.com/q_switching.html. [Geopend July 2015].
- [41] AKSteel, „420 Stainless steel,” AKSteel, [Online]. Available: http://www.aksteel.com/pdf/markets_products/stainless/martensitic/420_data_sheet.pdf. [Geopend July 2015].

Appendix

Appendix A: Dimensions of the experimental design



Appendix B: Labels for tensile pieces

symbol	code	Scan spacing (mm)	Laser power (W)	Direction to spreader	symbol	code	Scan spacing (mm)	Laser power (W)	Direction to spreader
	T1.1	0,13	150	Horizontal Perpendicular		T6.1	0,11	200	Horizontal Perpendicular
	T1.2	0,13	150	Horizontal Parallell		T6.2	0,11	200	Horizontal Parallell
	T1.3	0,13	150	Vertical		T6.3	0,11	200	Vertical
	T2.1	0,13	175	Horizontal Perpendicular		T7.1	0,09	150	Horizontal Perpendicular
	T2.2	0,13	175	Horizontal Parallell		T7.2	0,09	150	Horizontal Parallell
	T2.3	0,13	175	Vertical		T7.3	0,09	150	Vertical
	T3.1	0,13	200	Horizontal Perpendicular		T8.1	0,09	175	Horizontal Perpendicular
	T3.2	0,13	200	Horizontal Parallell		T8.2	0,09	175	Horizontal Parallell
	T3.3	0,13	200	Vertical		T8.3	0,09	175	Vertical
	T4.1	0,11	150	Horizontal Perpendicular		T9.1	0,09	200	Horizontal Perpendicular
	T4.2	0,11	150	Horizontal Parallell		T9.2	0,09	200	Horizontal Parallell
	T4.3	0,11	150	Vertical		T9.3	0,09	200	Vertical
	T5.1	0,11	175	Horizontal Perpendicular		T10.1	0,11	200	Horizontal Perpendicular
	T5.2	0,11	175	Horizontal Parallell		T10.2	0,11	200	Horizontal Parallell
	T5.3	0,11	175	Vertical		T10.3	0,11	200	Vertical

Appendix C: Mould assembly components from Meusburger

Order		Date: 04.04.2015	http://www.meusburger.com			
Item	Designation	Description	pcs	EUR/1		Value in EUR
1	F 10/ 246 296/ 36/ 1730	Clamp plate	1	174		174
2	FW 54/ 246 296/ 96/ 60/ 2085	Change mould cavity plate	1	1.631,00		1.631,00
3	FW 56/ 246 296/ 96/ 60/ 2085	Change mould cavity plate	1	1.729,00		1.729,00
4	FW 70/ 246 296/ 58/ 76/ 1730	Riser	2	115		230
5	FW 90/ 246 296/ 100/ 1730	Ejector set	1	273		273
6	FW 10/ 246 296/ 27/ 1730	Clamp plate	1	166		166
7	E 1000/22- 96/ 95	Guide pillar	1	29,9		29,9
8	E 1000/24- 96/ 95	Guide pillar	3	29,9		89,7
9	E 1100/22- 96	Guide bush	1	28,4		28,4
10	E 1100/24- 96	Guide bush	3	28,4		85,2
11	E 1160/30 x 40	Centring bush	4	5,8		23,2
12	E 1200/12 x 45	Cylinder head screw	4	0,4		1,6
13	E 1200/12 x 110	Cylinder head screw	4	1,2		4,8
14	E 1402/296 296/198/170/248	Insulation board	1	62,1		62,1
15	E 1402/296 296/198/170/248	Insulation board	1	62,1		62,1
Total, VAT not included						4.590,00

Auteursrechtelijke overeenkomst

Ik/wij verlenen het wereldwijde auteursrecht voor de ingediende eindverhandeling:
Selective Laser Melting for production of injection moulds

Richting: **master in de industriële wetenschappen: elektromechanica**
Jaar: **2015**

in alle mogelijke mediaformaten, - bestaande en in de toekomst te ontwikkelen - , aan de Universiteit Hasselt.

Niet tegenstaand deze toekenning van het auteursrecht aan de Universiteit Hasselt behoud ik als auteur het recht om de eindverhandeling, - in zijn geheel of gedeeltelijk -, vrij te reproduceren, (her)publiceren of distribueren zonder de toelating te moeten verkrijgen van de Universiteit Hasselt.

Ik bevestig dat de eindverhandeling mijn origineel werk is, en dat ik het recht heb om de rechten te verlenen die in deze overeenkomst worden beschreven. Ik verklaar tevens dat de eindverhandeling, naar mijn weten, het auteursrecht van anderen niet overtreedt.

Ik verklaar tevens dat ik voor het materiaal in de eindverhandeling dat beschermd wordt door het auteursrecht, de nodige toelatingen heb verkregen zodat ik deze ook aan de Universiteit Hasselt kan overdragen en dat dit duidelijk in de tekst en inhoud van de eindverhandeling werd genotificeerd.

Universiteit Hasselt zal mij als auteur(s) van de eindverhandeling identificeren en zal geen wijzigingen aanbrengen aan de eindverhandeling, uitgezonderd deze toegelaten door deze overeenkomst.

Voor akkoord,

Vanbergen, Christiaan

Datum: **21/08/2015**